

Kinetics of subunit rotation of the ribosome during tRNA-mRNA translocation

Dissertation

for the award of the degree

“Doctor rerum naturalium” (Dr. rer. nat.)

of the Georg-August-Universität Göttingen

within the doctoral program IMPRS Molecular Biology
of the Georg-August University School of Science (GAUSS)



submitted by

Heena Sharma

from New Delhi, India

Göttingen, 2016

Thesis Committee

Prof. Dr. Marina V. Rodnina
Department of Physical Biochemistry
Max Planck Institute for Biophysical Chemistry
Göttingen, Germany

Prof. Dr. Kai Tittmann
Department of Molecular Enzymology
Georg August University Göttingen
Göttingen, Germany

Prof. Dr. Holger Stark
Department of Structural Dynamics
Max Planck Institute for Biophysical Chemistry
Göttingen, Germany

Members of the Examination Board

Prof. Dr. Marina V. Rodnina (Referee)
Department of Physical Biochemistry
Max Planck Institute for Biophysical Chemistry
Göttingen, Germany

Prof. Dr. Kai Tittmann (2nd Referee)
Department of Molecular Enzymology
Georg August University Göttingen
Göttingen, Germany

Further members of the Examination Board

Prof. Dr. Wolfgang Wintermeyer
Department of Physical Biochemistry
Max Planck Institute for Biophysical Chemistry
Göttingen, Germany

Prof. Dr. Patrick Cramer
Department of Molecular Biology
Max Planck Institute for Biophysical Chemistry
Göttingen, Germany

Prof. Dr. Ralf Ficner
Department of Molecular Structural Biology
Institute for Microbiology and Genetics
Göttingen, Germany

Date of the oral examination: November 7th, 2016

Affidavit

I hereby declare that the presented thesis entitled “Kinetics of subunit rotation of the ribosome during tRNA-mRNA translocation” has been written independently and with no other sources and aids than quoted.

Göttingen, September 29th, 2016

Heena Sharma

PUBLICATIONS

1. **Sharma, H.**, Adio, S., Senyushkina, T., Belardinelli, R., Peske, F., and Rodnina, M.V. (2016). Kinetics of Spontaneous and EF-G-Accelerated Rotation of Ribosomal Subunits. *Cell Rep.* *16*, 2187-2196.
2. Belardinelli, R., **Sharma, H.**, Caliskan, N., Cunha, C.E., Peske, F., Wintermeyer, W., and Rodnina, M.V. (2016). Choreography of molecular movements during ribosome progression along mRNA. *Nat. Struct. Mol. Biol.* *23*, 342-348.
3. Belardinelli, R., **Sharma, H.**, Peske, F., Wintermeyer, W., and Rodnina, M.V. (2016). Translocation as continuous movement through the ribosome. *RNA Biol.* *13*, 1197-1203.

TABLE OF CONTENTS

ABSTRACT.....	1
1. INTRODUCTION	3
1.1 The ribosome	3
1.2 Translation cycle.....	6
1.3 The elongation cycle.....	7
1.3.1 Decoding	7
1.3.2 Peptide bond formation.....	8
1.3.3 Translocation.....	9
1.4 Dynamic elements during translocation.....	10
1.4.1 Ribosome subunit rotation	10
1.4.2 L10–L7/L12–L11 stalk	13
1.4.3 L1 stalk	14
1.4.4 tRNA movement.....	15
1.4.5 Elongation factor G	16
1.5 Subunit rotation during translocation.....	18
1.6 Antibiotics inhibiting translocation	20
1.7 Subunit rotation during initiation and termination	22
1.8 Scope of the thesis	23
2. RESULTS.....	25
2.1 Experimental approach	25
2.2 Characterization of the double-labeled ribosome	27
2.3 Kinetics of spontaneous subunit rotation with different tRNAs in the P site.....	31
2.4 Kinetics of spontaneous subunit rotation with different tRNAs in the A site.....	35
2.5 Effect of EF-G on subunit rotation.....	40
2.6 Global-fitting of translocation kinetics	48
2.7 Effect of variants of EF-G on subunit rotation	52
2.8 Effect of magnesium ion (Mg^{2+}) concentration on subunit rotation.....	54
2.9 Effect of antibiotics on subunit rotation.....	57
2.9.1 Coupled inhibition of body rotation and head swiveling.....	57
2.9.2 Uncoupling of body rotation and head swiveling.....	59
2.9.3 Antibiotics effecting rotational states of the ribosome.....	62

3. DISCUSSION	65
3.1 Spontaneous rotation of ribosomal subunits	65
3.2 EF-G-induced ribosomal subunit rotation	67
3.3 Kinetic model of translocation.....	69
3.4 Effect of antibiotics on subunit dynamics	72
3.5 Ribosome as a Brownian machine	74
4. MATERIALS AND METHODS	77
4.1 Buffers	77
4.2 Cell culture media	80
4.3 Chemicals.....	80
4.4 Antibiotics.....	82
4.5 Fluorophores and Radioactive compounds	82
4.6 Nucleotides	83
4.7 Kits.....	83
4.8 Plasmids.....	83
4.9 Enzymes.....	83
4.10 Cell strains.....	83
4.11 Chromatographic columns.....	83
4.12 Other consumables	84
4.13 Instruments.....	84
4.14 Softwares	85
4.15 DNA primers.....	86
4.16 mRNAs	87
4.17 Preparation of fluorescence-labeled ribosomes.....	88
4.17.1 Development and verification of S6 and L9 knockout strains	88
4.17.2 Cloning and expression.....	90
4.17.3 Purification of protein S6	90
4.17.4 Purification of protein L9	91
4.17.5 Labeling of proteins	91
4.17.6 Reconstitution	92
4.18 Preparation of ribosome complexes	92
4.19 Rapid kinetics experiments.....	93
4.19.1 Characterization of the double-labeled ribosomes.....	93
4.19.2 Kinetics of spontaneous subunit rotation with different tRNAs in the P site	94

4.19.3 Kinetics of spontaneous subunit rotation with different tRNAs in the A site	94
4.19.4 Effect of EF-G on subunit rotation	95
4.19.5 Effect of Mg ²⁺ ion concentration on subunit rotation	95
4.19.6 Effect of antibiotics on subunit rotation	95
4.19.7 Time-resolved Pmn assay.....	96
4.19.8 Data analysis.....	96
4.19.9 smFRET experiments	97
5. REFERENCES.....	99
6. APPENDIX	109
6.1 Abbreviations.....	109
6.2 List of Figures	112
6.3 List of Tables	114
ACKNOWLEDGMENTS	115
CURRICULUM VITAE	117

ABSTRACT

Ribosome dynamics play an essential role in orchestrating all stages of protein synthesis. Recent biochemical, structural and computational studies have shown large-scale conformational changes of the ribosome, its tRNA substrates and translation factors during the elongation phase of protein synthesis. Dynamic movements of the ribosome not only govern the translation process but are also targeted by many antibiotics resulting in inhibition of protein synthesis. Therefore, complete understanding of conformational rearrangements in the ribosome will improve our knowledge about translation mechanism and its regulation which will also help to design novel antibiotics. One of the key dynamic processes important for ensuring forward movement of the tRNA-mRNA complex during translocation is the rotation of the small subunit (SSU) of the ribosome relative to the large subunit (LSU). Ribosomal subunits rotate spontaneously, i.e. in the absence of auxiliary translation factors, in the counterclockwise (CCW) direction upon the formation of deacylated tRNA in the P site of the ribosome as a result of peptide bond formation. Elongation factor G (EF-G) promotes the tRNA-mRNA translocation at the cost of GTP hydrolysis, which is accompanied by the clockwise (CW) rotation of the SSU. However, the exact role of subunit rotation in translocation is not properly understood.

In this thesis, I present the real time kinetics of spontaneous subunit rotation and show how EF-G promotes and coordinates the rotation of the subunits with the movement of the tRNA-mRNA complex along the ribosome. We used ribosomal subunits labeled with fluorescence reporters forming a FRET (Förster resonance energy transfer) pair and monitored the kinetics of subunit rotation relative to peptide bond formation and translocation using ensemble kinetics and single-molecule FRET (smFRET). We observed that spontaneous rotation of the SSU in CCW direction is rapid and reversible and is independent of the rate of preceding step of peptide bond formation. EF-G binding to the ribosome in the non-rotated state accelerates CCW rotation of the SSU by 5-fold. The transition back of the SSU body in clockwise (CW) direction to the non-rotated state starts early on the translocation pathway and precedes CW movement of the SSU head but overall coincides kinetically with the tRNA-mRNA translocation. The uncoupling of the movement of body and head of the SSU results in unlocking of the ribosome that allows translocation of the tRNA-mRNA complex. In addition, we show how the smooth synchronized motion of the SSU body and head can be perturbed by diverse antibiotics. Our work demonstrates how large-scale thermally driven movements of the ribosome are gated by its ligands such as EF-G, tRNAs and antibiotics.

1. INTRODUCTION

All living cells consist of myriad of proteins required to carry out essential functions for survival. Proteins are the polymers of amino acids and the genetic information for the synthesis of each protein is coded in the messenger RNA (mRNA) in the form of three nucleotide bases called codons. The ribosome, the so-called protein building factory, provides the platform to decode the information with the help of adaptor molecules called transfer RNAs (tRNAs) carrying amino acid and an anticodon for the recognition of their specific codon. In this way, the ribosome builds a protein with the amino acid sequence exactly as specified by the gene and this process of protein synthesis is termed as translation.

Understanding the bacterial ribosome is crucial not only because it has a fundamental function in gene expression, but also because the ribosome is a target for clinically important antibiotics. With the emergence of drug resistant bacteria, it has become necessary to intensify studies on translation and ribosome mechanism in order to find new targets for drug development. A more detailed knowledge will facilitate the design of new antimicrobials to combat infections.

1.1 The ribosome

The ribosome is a complex molecular machine that synthesizes proteins in all living cells. The ribosome is composed of ribosomal (r) RNAs and several different proteins (r-proteins). The key components of the ribosome are conserved across the three kingdoms of life: bacteria, archaea and eukarya (Korobeinikova et al., 2012). The bacterial ribosome consists of two unequal subunits: the large 50S subunit (LSU) and the small 30S subunit (SSU) that reversibly associate to form complete 70S ribosomes (where S, Svedberg unit, is defined as the sedimentation rate of the particle of a given size and shape and one unit is 10^{-13} s) with a molecular mass of approximately 2.5 MDa (**Figure 1.1**). The eukaryotic ribosome is 4 MDa in size with 60S and 40S as small and large subunits respectively, together forming an 80S complex. With two-thirds RNA and one-third protein, the functional centers of both subunits (the decoding site and the peptidyl transferase center (PTC)) and the subunit interface are largely composed of RNA. rRNA forms the structural core whereas r-proteins are located at the surface of the subunits. This makes the ribosome an essentially RNA-based machine where RNA, in its compact form, carries out all the fundamental reactions of protein synthesis (Ban et al., 2000; Nissen et al., 2000; Noller et al., 1992; Ramakrishnan, 2014). Moreover, high resolution structures showed that several antibiotics interact with special and distinct sites on rRNA emphasizing the functional relevance of rRNAs in the ribosome (Carter et al., 2000; Hansen et al., 2003). On the other hand, r-proteins play a

structural role and act like a scaffold, controlling and stabilizing three-dimensional folds of rRNAs. They hold the rRNAs in a conformation which brings the distant parts of the rRNAs together to form active centers. As a functional role, r-proteins interact with many ligands such as translational GTPase that are important at different stages of translation (Ban et al., 2000; Harms et al., 2001; Schluenzen et al., 2000; Wimberly et al., 2000).

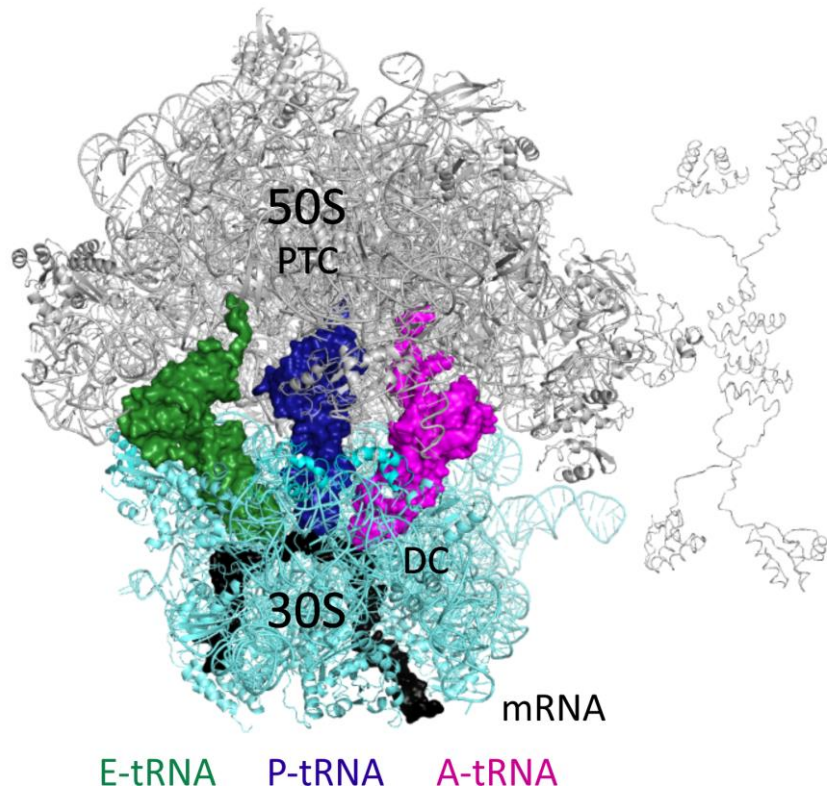


Figure 1.1 The prokaryotic ribosome.

Bacterial ribosome is composed of two subunits: large 50S subunit (LSU) (grey) and small 30S subunit (SSU) (light blue). LSU contains peptidyl transferase center (PTC), while SSU carries the decoding center (DC) and the mRNA (black) binding channel. Together, the two subunits form three tRNA binding sites; A site, P site and E site. The image is produced from structures with Protein Data Bank (PDB) accessions 3J4V, 3J52, 2QA4 and 3AIY (Bock et al., 2013; Kavran and Steitz, 2007; Naganuma et al., 2010). The colour code for different components will remain the same throughout the thesis.

Solving the high-resolution atomic structure of the ribosome was a great challenge because of its huge size and asymmetry. A milestone was set in the ribosome and RNA field when the atomic structure of each subunit was solved in 2000, followed by the structures of functional 70S complex (Ban et al., 2000; Harms et al., 2001; Schluenzen et al., 2000; Wimberly et al., 2000; Yusupov et al., 2001). Since then, the high resolution X-ray crystal structures and 3-D cryo-electron microscopy (cryo-EM) reconstructions have provided beautiful insight into the interaction of functional ligands and factors with the ribosome (Agirrezabala and Frank, 2010; Ramakrishnan, 2014; Schmeing and Ramakrishnan, 2009; Steitz, 2008; Voorhees and Ramakrishnan, 2013).

The SSU is composed of the 16S rRNA (1500 nucleotides) and about 20 different proteins, whereas the LSU comprises the 23S rRNA (2900 nucleotides), 5S rRNA (120 nucleotides), and more than 30 different proteins (Ban et al., 2000; Harms et al., 2001; Schluenzen et al., 2000; Wimberly et al., 2000). The SSU engages with the mRNA and decodes the genetic information by monitoring the base pairing between mRNA codon and tRNA anticodon at the decoding center. The decoding center is composed of 16S rRNA and contributes to tRNA recruitment and the fidelity of translation. The entire SSU is divided into four domains: the head, the body, the platform and the spur. The mRNA binds at the cleft between the head and the body. In the vicinity of decoding center, the mRNA channel makes two kinks along the mRNA allowing two tRNA molecules to bind simultaneously and move with the mRNA chain (Schluenzen et al., 2000).

The LSU homes the PTC composed of the 23S rRNA that catalyzes essentially two chemical reactions during translation, the formation of the peptide bond between aminoacyl-tRNA (aa-tRNA) and peptidyl-tRNA during elongation of the polypeptide chain and the hydrolysis of the synthesized peptide during termination of protein synthesis. PTC opens into the peptide exit tunnel through which the growing polypeptide chain passes as it is synthesized. The tunnel provides the environment for co-translation folding of the nascent peptides and can interact with the growing polypeptide chain. LSU recruits the translational GTPases that assist in different stages of translation and plays a key role in the GTPase activity (Rodnina and Wintermeyer, 2010). Additionally, the LSU also provides docking sites for many accessory factors that are important for processing of peptides, their folding and sorting them to different cellular compartments.

The ribosome forms three stable tRNA binding sites: the A site that accepts the incoming tRNA loaded with an amino acid (aa-tRNA) for decoding, the P site that holds the tRNA carrying the growing polypeptide chain (peptidyl-tRNA) and maintains correct reading frame when the A site is vacant, and the E site that binds the deacylated tRNA after peptide bond formation and directs its way out of the ribosome (**Figure 1.1**).

The high-resolution structures of the ribosome along with the advanced biochemical and genetic studies have helped characterizing different steps of translation. The application of bulk and single-molecule fluorescence studies for pre-steady state and steady state kinetics have provided deeper insights into the dynamics and mechanism of ribosome function. With these methods it is possible to observe conformation changes and ligand binding in real time which has resulted in detailed kinetic models of translation. Combined together, the structural and functional studies have dissected the path of protein synthesis and have led to the understanding of complex mechanism underlying the process of translation.

In the following sections, I will discuss the mechanism of translation with the emphasis on the elongation cycle (sections 1.2 and 1.3). In the later sections, I will focus on the dynamic

elements important during translocation and on antibiotics inhibiting translocation (sections 1.4, 1.5 and 1.6).

1.2 Translation cycle

Translation is highly dynamic in nature and can broadly be divided into four stages: initiation, elongation, termination and ribosome recycling (Dunkle and Cate, 2010; Schmeing and Ramakrishnan, 2009). Different factors, namely initiation factors (IFs), elongation factors (EFs), release factors (RFs) and ribosome recycling factor (RRF) facilitate each stage of translation.

During initiation, the SSU binds to an mRNA by base pairing between the 3' end of the 16S RNA and the complimentary sequence called Shine-Dalgarno sequence present at the upstream of the start codon (usually AUG). The initiator tRNA (fMet-tRNA^{fMet}) is placed at the start codon in the P site along with three initiation factors IF1, IF2 and IF3 forming the 30S pre-initiation complex. IF1 and IF3 guide the correct assembly of mRNA and initiator tRNA at the start codon. Upon binding of the LSU, IF2 hydrolyses GTP and all initiation factors are released leading to the formation of the active 70S complex ready to enter the elongation cycle. The process of initiation is different in all kingdoms of life and is more complex in eukaryotes compared to bacteria. Initiation in eukaryotes involves many different proteins some of which are multi-protein complexes. The high degree of complexity reflects the high degree of regulation and control of the process in multicellular organisms.

Elongation of protein synthesis is a process which involves repeated cycles of decoding, peptide bond formation and translocation. At the beginning of elongation cycle the ribosome has peptidyl-tRNA in the P site carrying a growing polypeptide chain and a vacant A site. During decoding, the next amino acid is delivered in a ternary complex with elongation factor Tu (EF-Tu), GTP and aa-tRNA followed by the formation of the peptide bond which results in the elongation of the polypeptide chain by one amino acid. Elongation factor G (EF-G) then promotes the translocation of the tRNA-mRNA complex and the ribosome moves by one codon along the mRNA for the next round of elongation. The process of elongation is discussed in detail in the next section.

The elongation cycle continues until a stop codon is presented in the A site that signals the termination of protein synthesis. In bacteria there are three stop codons: UAG, UGA and UAA. Release factors (RFs) recognize these stop codons and stimulate the hydrolysis of the peptide chain from the P-site tRNA resulting in the release of newly synthesized protein from the ribosome. There are two different classes of RFs: class I and class II. Class I RFs namely RF1 and RF2, recognize the UAG and UGA stop codon, respectively, whereas the UAA codon is recognized by both factors. The signature PXT amino acid sequence motif in RF1 and the SPF motif in RF2

confer the specificity for the respective stop codons. The universally conserved GAQ motif, that points into the PTC, catalyze the hydrolysis of the peptides. The class II release factor RF3 assists in the dissociation of class I factors from the ribosomes after peptide hydrolysis. Binding of RF3 in the GTP form induces a conformational change in the ribosome that destabilizes the interaction of class I release factors leading to their dissociation followed by GTP hydrolysis and the release of RF3.

As RF3 dissociates from the ribosome, it leaves mRNA and a deacylated tRNA in the P site. The ribosomal subunits must be recycled to take part in the next round of translation, also releasing mRNA and tRNA. This essential function is performed by ribosome recycling factor (RRF) along with EF-G and IF3. RRF together with EF-G perturbs the inter-subunit interactions. Subsequent hydrolysis of GTP causes the dissociation of 70S into the LSU and a complex of the SSU with mRNA and tRNA. The separation of the SSU from mRNA and tRNA is then enhanced by IF3 binding to the complex.

1.3 The elongation cycle

The cyclic process of elongation encompasses three steps: decoding, peptide bond formation and translocation that follow universally conserved mechanisms (**Figure 1.2**).

1.3.1 Decoding

Decoding is the process in which the ribosome selects the aa-tRNA from the pool of total aa-tRNAs based on its ability to base pair correctly with the codon in the A site (the cognate aa-tRNA). It rejects the near cognate and non-cognate aa-tRNAs either during initial selection or subsequent proofreading phases, which ensures the high fidelity protein synthesis (Pape et al., 1999; Rodnina and Wintermeyer, 2001). The delivery of cognate tRNA is facilitated by EF-Tu that hydrolysis GTP in the process. In the first step, a stable ternary complex is formed between EF-Tu, GTP and aa-tRNA (EF-Tu–GTP–aa-tRNA) that binds to the ribosome initially through L7/L12 stalk (Diaconu et al., 2005; Kothe et al., 2004). In the second step, the formation of the cognate codon and anti-codon duplex induces local conformational changes in the universally conserved residues A1492, A1493 and G530 of the 16S rRNA such that they interact with the minor groove of the first two base pairs of the codon-anti-codon duplex (Ogle et al., 2001). The tertiary interactions made by A1492 and A1493 are termed A-minor motifs and are specific for Watson-Crick base pair geometry, but are independent of the sequence. The codon-recognition complex is stabilized by purines present at the 37th position of the anti-codon loop of the tRNAs, mainly by strong stacking interaction and by binding to additional Mg²⁺ ions (Konevega et al., 2004). The local rearrangements of the decoding center are accompanied by the rotation of the SSU head and shoulder domains towards the subunit interface, collectively described as domain closure (Ogle et

al., 2002). These conformational changes distort the tRNA molecule forcing its anticodon stem-loops (ASL) into the accommodated orientation while the acceptor arm still maintains contacts with EF-Tu (Schmeing and Ramakrishnan, 2009; Schuette et al., 2009; Villa et al., 2009). All these conformational changes enhance the GTPase activity of EF-Tu by four orders of magnitude (Rodnina and Wintermeyer, 2001). GTP hydrolysis and the subsequent release of EF-Tu-GDP allows the accommodation of the 3' end of the aa-tRNA in the PTC where it takes part in peptide bond formation.

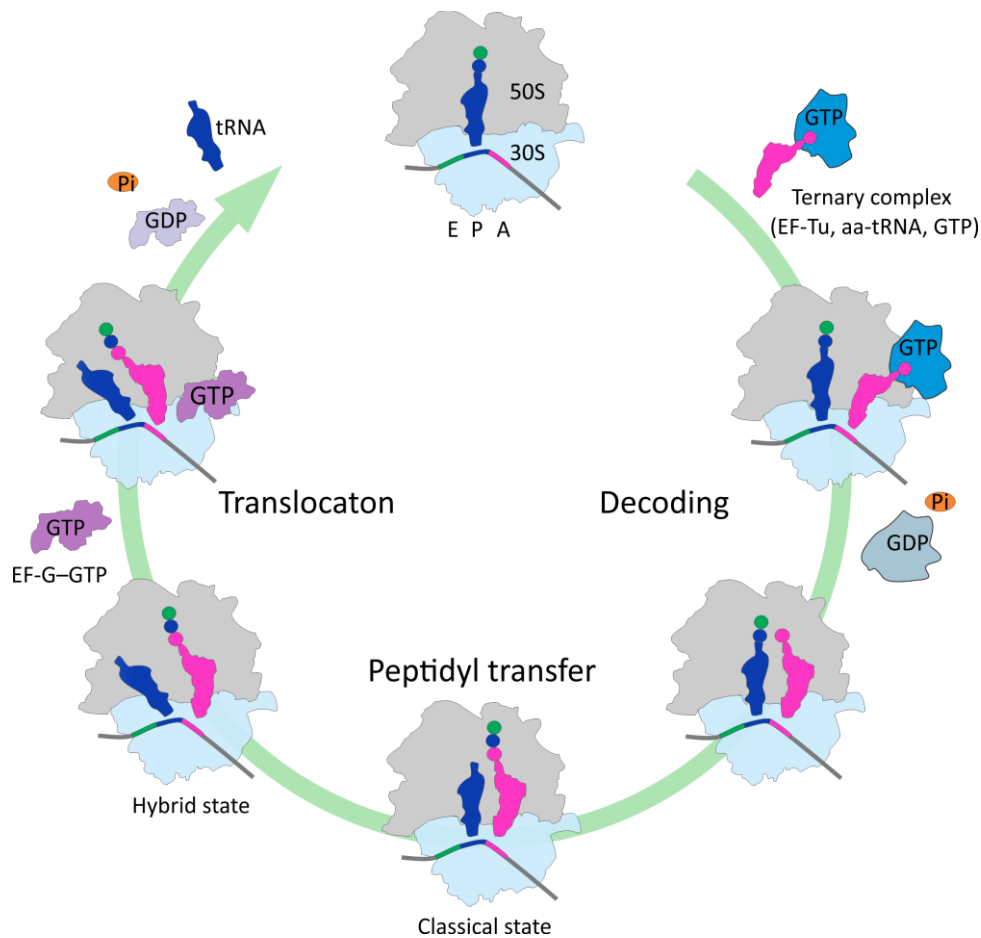


Figure 1.2 Overview of the elongation cycle.

The process of elongation entails repetitive cycles of decoding, peptidyl transfer and translocation. During decoding, the aa-tRNA (pink) is delivered to the A site in the ternary complex with EF-Tu (marine blue) and GTP. This is followed by the formation of a peptide bond between the newly delivered amino acid and polypeptide chain attached to the P-site tRNA (blue). The tRNAs move spontaneously with respect to the LSU but not with respect to the SSU forming the hybrid (H) state. EF-G (purple) then promotes complete translocation of the tRNA-mRNA complex leading to release of the deacylated tRNA from the E site and making the A site vacant for the next round of elongation. The colour codes will remain the same throughout the thesis.

1.3.2 Peptide bond formation

The peptide bond is formed in the PTC located on the LSU where the nucleophilic α -amino group of aa-tRNA in the A site attacks the carbonyl group of peptidyl-tRNA in the P site. The nascent chain is transferred to the A-site tRNA leaving a one amino acid longer peptidyl-tRNA in the A site

and deacylated tRNA in the P site. The catalysis by the peptidyl center is intrinsically independent of the pH indicating that ionizing groups of the ribosome are not involved in catalysis and that the ribosome does not utilize general acid-base catalysis (Beringer et al., 2005; Bieling et al., 2006). These findings were corroborated with extensive mutational analysis of the catalytic core of the ribosome (Beringer et al., 2003; Youngman et al., 2004). It is suggested that the peptidyl transfer reaction proceeds through two steps via transition states (Satterthwait and Jencks, 1974). The first step is the rate limiting step and consists of the formation of a zwitterionic tetrahedral intermediate and the transfer of proton from the attacking nitrogen. The second step is rapid and involves the breakdown of the tetrahedral intermediate into the reaction products (Hiller et al., 2011). The attack of α -amino group on the ester carbonyl carbon – a rate limiting step – results in the formation of an eight-membered transition state in which the α -amino group receives a proton from the 2'OH of A76 of the P-site tRNA, which at the same time donates a proton to the carbonyl oxygen via an adjacent water molecule (Kuhlenkoetter et al., 2011). Protonation of the 3'OH group then would be an independent rapid step (Hiller et al., 2011). Therefore, peptidyl transfer reaction utilizes a proton shuttle mechanism and the rRNA functions as an entropy trap, bringing reactants close enough to each other to allow the reaction to occur (Sievers et al., 2004).

1.3.3 Translocation

After the formation of the peptide bond, the tRNAs are present in the classical (C) state with the peptidyl-tRNA in the A site and the deacylated tRNA in the P site (P/P and A/A). Ribosome and tRNAs now form the pre-translocation complex (PRE). During translocation, the mRNA together with the two tRNAs must advance unidirectionally, such that the deacylated tRNA and peptidyl-tRNA move to the E and P site, respectively, and the next codon on the mRNA is presented in the A site of the SSU forming the post-translocation complex (POST) (Aitken et al., 2010; Dunkle and Cate, 2010; Rodnina and Wintermeyer, 2011).

The movement of tRNAs during translocation takes place in two major phases: First the 3' end or acceptor arm of the tRNAs moves with respect to the LSU where they interact with the P and E site while their ASL still resides in the A and P site of the SSU, respectively (Agirrezabala et al., 2008; Blanchard et al., 2004b; Julian et al., 2008; Moazed and Noller, 1989). This intermediate state of tRNA translocation is called hybrid state (H) and is denoted as P/E and A/P configuration. This configuration is different from the initial classical (C) P/P and A/A state where the peptidyl-tRNA and deacylated tRNA resides in the A and P site, respectively, with respect to both subunits just after peptide bond formation. The formation of H state is spontaneous and reversible, mainly driven by thermal energy. In fact, the PRE complex is highly dynamic and

fluctuates spontaneously between the C and the H state (Adio et al., 2015; Blanchard et al., 2004b; Chen et al., 2011; Kim et al., 2007; Munro et al., 2010a).

The second step involves EF-G which utilizes the energy of GTP hydrolysis and promotes the movement of the mRNA and the ASL of the tRNAs with respect to the SSU leaving a vacant A site (Moazed and Noller, 1989; Rodnina et al., 1997). Translocation is the inherent property of the ribosome and can take place spontaneously albeit very slowly - in both forward and backward direction (Fredrick and Noller, 2003; Gavrilova et al., 1976; Konevega et al., 2007; Shoji et al., 2006). It was proposed that differences in the affinities of the tRNA for the A, P and E site of the ribosome might act as the driving force for their spontaneous movement (Semenkov et al., 2000) EF-G provides the unidirectionality to the process and accelerates translocation by several orders of magnitude making it relevant under cellular conditions. In following sections, I will focus on the mechanism of translocation and will discuss important aspects of the process.

1.4 Dynamic elements during translocation

Translocation requires the interplay of many ligands orchestrated by conformational flexibility of the ribosome. Several dynamic elements of the ribosome work together with the translational machinery to carry out the important task of protein synthesis. Here, I will discuss some of the essential motions of the ribosome coordinated with the tRNA movement and EF-G dynamics that together lead to translocation.

1.4.1 Ribosome subunit rotation

The universal architecture of the ribosome, built of two unequal subunits that are easily separable but associate and carry out the function of protein synthesis, has always pointed towards coordinated movements between the two subunits. Central to the mechanism of ribosome action is the rotation of two subunits of the ribosome relative to each other. In the rotated state (R), the SSU body rotates about 7° - 8° , viewed from the solvent side of the SSU, in counterclockwise (CCW) direction with respect to the LSU (Agirrezabala et al., 2008; Ermolenko et al., 2007a; Frank and Agrawal, 2000; Julian et al., 2008; Schuwirth et al., 2005). In addition, the head of the SSU acts as an autonomous domain and rotates about 18° - 21° around an axis nearly orthogonal to the axis of body rotation (**Figure 1.3**). The rotation of the head is often termed as head swiveling. It takes place in the same direction as tRNA movement on the ribosome (Guo and Noller, 2012; Ramrath et al., 2013; Ratje et al., 2010; Schuwirth et al., 2005; Zhou et al., 2013, 2014).

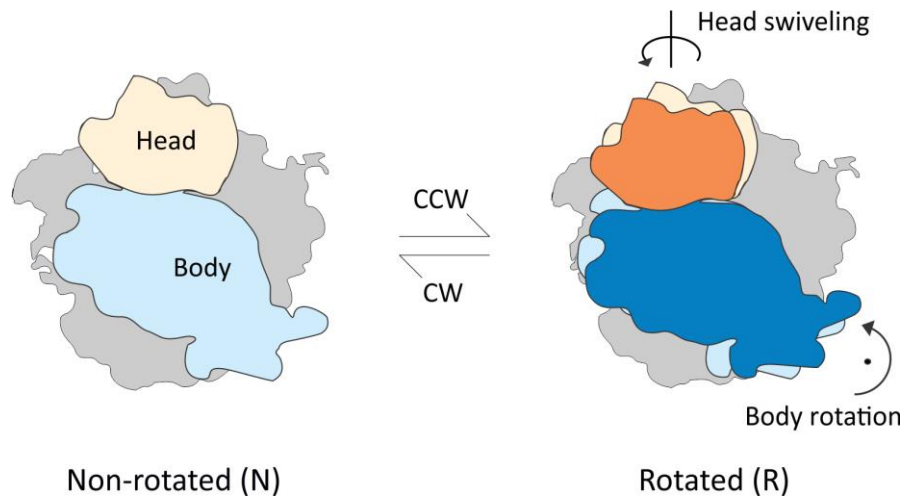


Figure 1.3 Movements of the SSU of the ribosome.

Ribosomal subunit rotation from the N state to the R state involves the CCW rotation of the SSU body (light blue to dark blue) with respect to the LSU and CCW swivelling motion of the SSU head (light yellow to orange) around the axis nearly orthogonal to the axis of SSU body rotation. The ribosome subunit rotation is a spontaneous and reversible process. Arrows indicate the direction of rotation.

Ribosome subunit rotation is an inherent property of the ribosome and can take place spontaneously and reversibly (Agirrezabala et al., 2008; Cornish et al., 2008; Schuwirth et al., 2005; Wasserman et al., 2016; Zhang et al., 2009). The ribosome exists in equilibrium between the non-rotated (N) and the R state and the movement of the SSU is loosely coupled to the movement of the tRNAs (Fischer et al., 2010). The presence of deacylated tRNA in the P site favours the formation of the R-H state (ribosome in the rotated state and tRNAs in the hybrid state) in contrast to the P-site peptidyl-tRNA where the N-C conformation (ribosome in the non-rotated state and tRNAs in the classical state) is predominant (Cornish et al., 2008; Valle et al., 2003). Each time a peptide bond is formed; the subunits rotate relative to each other and permit the tRNAs to move from the C to the H state (R-H state). From the R-H state the tRNA-mRNA complex is rapidly translocated by the action of EF-G, which brings back the ribosome and the tRNAs into the N-C conformation (Aitken et al., 2010; Voorhees and Ramakrishnan, 2013).

Subunits rotation assists in the movement of tRNAs within the ribosome. The swiveling motion of the head domain allows the SSU to maintain partial contacts with the tRNA at any given time during translocation and also helps to position tRNAs properly within the ribosome (Ratje et al., 2010; Zhang et al., 2009; Zhou et al., 2014). Moreover, the path of the tRNA ASL is blocked between P and E site by a constriction of head and platform of the SSU that inhibits translocation (Schuwirth et al., 2005; Zhou et al., 2013). Head swiveling widens the tRNA binding groove giving sufficient room for the ASL to move from the P to E site.

Subunit rotation: A Brief History

The relative motion of the two subunits with respect to each other was first suggested by Brestcher (1968) and Spirin (1968) who independently proposed two different models for inter-subunit movements during translocation of tRNAs and mRNA through the ribosome (Bretscher, 1968; Spirin, 1968). Bretscher predicted the hybrid structure model and proposed that the translocation is a two-step process with the formation of intermediate hybrid state where the peptidyl-tRNA is bound to different sites of the ribosomal subunits and involves inter-subunit movement in order to achieve that configuration.

*Nearly two decades later, the first experimental evidence was published which reported the existence of hybrid state by chemical footprinting studies (Moazed and Noller, 1989) which again emphasized on the existence of relative movements within the two subunits. Another ten years later, the first cryo-EM reconstruction showed a large conformational rearrangement in the ribosome in the presence of EF-G–GMPP(CH₂)P (non-hydrolysable GTP analogue) where the SSU was rotated by about 6° in CCW direction, viewed from the solvent side, with respect to the LSU and the tRNAs being in the hybrid state (Frank and Agrawal, 2000). This conformation of the ribosome was different from structures solved at the time by crystallography (Yusupov et al., 2001) (N-C state) and the phenomena was termed as ribosome **ratcheting**. Soon it was shown that the ribosome can spontaneously adopt ratcheted conformations in the absence of any translation factor, with tRNAs in the hybrid state indicating that the rotated state of the ribosome is linked to the hybrid state of the tRNAs (R-H state). Biochemical and ensemble kinetics experiments demonstrated that the R-H state is an authentic translocation intermediates that serves to accelerate tRNA movement through the ribosome (Dorner et al., 2006; Semenov et al., 2000). Crosslinking the two ribosomal subunits by a disulfide bond to prevent subunit rotation specifically abolished EF-G dependent translocation, suggesting that subunit rotation is essential for the tRNA-mRNA translocation (Horan and Noller, 2007). Now, with the advancement of structural and biophysical studies, it becomes clear that subunit rotation is essential at all stages of translation. In addition, it was demonstrated that the head of the SSU swivels as an independent domain, crucial for tRNA translocation, and the movements of the SSU body and head are loosely coupled (Fischer et al., 2010; Schuwirth et al., 2005). Subunit rotation, which is the intrinsic property of the ribosome, can take place spontaneously and reversibly and is different from ratcheting and therefore, the term ratcheting is no longer used.*

Additionally, it is speculated that the site for the helicase activity, required to unwind mRNA secondary structures during translocation, is at the subunit interface between head and body of the SSU; the opposite strands of the mRNA helix could bind to head and body, respectively. Movement of head with respect to body would result in the disruption of the mRNA helix. Thus, the head swiveling may contribute to the intrinsic helicase activity of the ribosome in unwinding mRNA secondary structures (Horan and Noller, 2007; Takyar et al., 2005; Zhou et al., 2014). Distinct intermediate structures (R1 and R2) with different degrees of rotation have been identified through structural studies (Pulk and Cate, 2013; Zhang et al., 2009). These intermediates are found on the path of ribosome ratcheting from the N (R_0) to the R state (R_f) and they direct the tRNAs from the C to the H state. Overall, three different motions of the SSU: overall rotation of the SSU relative to the LSU, head swiveling and opening of the tRNA binding groove to allow the tRNA to pass from the P site to the E site are required for tRNA-mRNA translocation (Schuwirth et al., 2005).

The interactions at the subunit interface are mainly RNA based and relatively labile. The central RNA-RNA bridges changes little during subunit rotation and have been suggested to be responsible for maintaining 70S stability. The bridge B2a of the ribosome is formed by the interaction between the conserved 23S rRNA helix-loop 69 (H69) and the tip of the 16S rRNA helix 44 (h44), adjacent to mRNA decoding center of the SSU and undergoes large conformational change during rotation. Additionally, proteins S13, S19, L5 and regions of 16S and 23S rRNAs are mainly involved in the interactions occurring at the subunit interface as subunit rotation takes place (Agirrezabala et al., 2008; Bock et al., 2013; Bock et al., 2015; Schuwirth et al., 2005; Zhang et al., 2009).

1.4.2 L10–L7/L12–L11 stalk

Together with the proteins L10 and L11, protein L7/L12 builds a lateral protrusion on the LSU termed as L7/L12 stalk (or L12 stalk) (**Figure 1.4**). L7 is the N-acylated form of protein L12. L7/L12 forms a dimer and exists in four copies in *E. coli*, in other species of bacteria it can also be in six to eight copies (Davydov et al., 2013). The L12 stalk is located on the opposite side of the L1 stalk near the A site entrance and has been shown to play a crucial role in factor recruitment and GTPase activation (Diaconu et al., 2005; Kothe et al., 2004; Mohr et al., 2002). The L12 stalk is remarkably dynamic; it may “fish” for translational factors and places them on their ribosomal binding site (Diaconu et al., 2005).

The protein L11, which forms a part of the base of the L12 stalk, with the 23S rRNA is referred to as the L11-RNA complex (Wimberly et al., 1999). The C-terminal domain (CTD) of L11 contacts the 23S rRNA whereas the N-terminal domain (NTD) is loosely folded and highly dynamic.

The NTD makes contact with translational GTPases or incoming aa-tRNA (Agrawal et al., 2001). As EF-G binds, the L11 stalk moves away from the A site towards the SSU body (about 7-12 Å) in order to maintain contacts with EF-G during translocation as the latter rotates around the sarcin-ricin loop (SRL) for GTP hydrolysis. Additionally, after GTP hydrolysis by EF-G, L11 rotates and changes its position to form an arc-like connection (ALC) with the G' domain of EF-G. It was suggested that this connection might promote the dissociation of the factor from the ribosome (Brilot et al., 2013; Zhou et al., 2013).

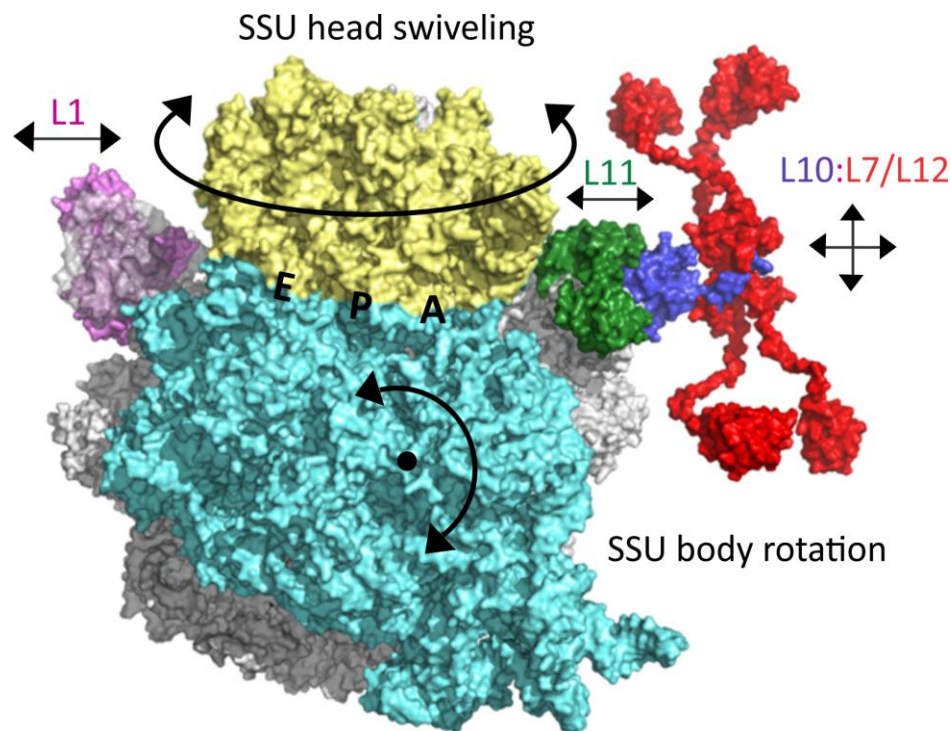


Figure 1.4 Motions in the ribosome during translocation.

The ribosome is remarkably dynamic with two large scale movements, SSU body rotation and SSU head swiveling. The L10-L12 stalk (purple:red) and the L1 stalk (pink) are two highly flexible arms of the ribosome present on opposite sides of the ribosome and assist in translocation. The L10-L12 stalk facilitates factor recruitment whereas the L1 stalk helps in the dissociation of deacylated tRNA from the E site. The L11 stalk (green) is also highly flexible and assists in factor recruitment and dissociation. The image is produced from structures with Protein Data Bank (PDB) accessions 3J4V, 3J52, 2QA4 and 3AIY (Bock et al., 2013; Kavran and Steitz, 2007; Naganuma et al., 2010).

1.4.3 L1 stalk

The L1 stalk is another highly dynamic element of the ribosome located near the E site and consists of helices H76-78 from the 23S rRNA and protein L1 (**Figure 1.4**) (Yusupov et al., 2001). The stalk alters between the open conformation, where the exit path for the movement of the E-site tRNA is free, and a closed conformation, where the exit path for the movement of the E-site tRNA is blocked (Cornish et al., 2009; Valle et al., 2003). Besides acting as a tRNA exit gate, the L1 stalk actively removes the E-site tRNA from the ribosome during translocation. The movement of tRNAs between the C and H state is loosely coupled to the movement of the L1 stalk (Brilot et al.,

2013; Fischer et al., 2010). As the deacylated P-site tRNA moves to the hybrid P/E state, the L1 stalk (open conformation, L1_{open}) moves about 30-40 Å into the inter-subunit space towards the tRNA binding site and interacts with the elbow region of the P/E hybrid tRNA (closed conformation, L1_{closed}) (Chen et al., 2013b; Fu et al., 2011; Tourigny et al., 2013). This interaction is repetitively formed and disrupted as the tRNA fluctuates between the C and H state accompanied by the movement of the L1 stalk in an open (L1_{open}) and closed conformation (L1_{closed}), respectively (Fei et al., 2009; Fei et al., 2008; Munro et al., 2010a). As EF-G binds and hydrolyzes GTP, the L1 stalk actively pulls the tRNA from P/E to the E/E classical state moving away from the subunit interface to the half-open conformation followed by further opening of the stalk to the open conformation and releases the E-site tRNA (Bock et al., 2013; Cornish et al., 2009).

1.4.4 tRNA movement

The movement of tRNAs during translocation from PRE to POST state takes place via the formation of the H state – a major intermediate state of tRNA translocation. With the advancement of structural and biophysical techniques, several intermediates of tRNA movement in the translocation pathway have been identified that are either formed spontaneously or are induced during EF-G-promoted translocation. These intermediates differ in the orientation, the position of different regions of tRNAs (3'end, elbow and ASL), their pattern of interaction with the ribosome and their ability to react with the a drug puromycin – a diagnostic tool to identify complete translocation on LSU (Adio et al., 2015; Brilot et al., 2013; Fischer et al., 2010; Holtkamp et al., 2014a; Ramrath et al., 2013; Ratje et al., 2010; Zhou et al., 2014).

Recently, a spontaneously formed intermediate state has been observed where only deacylated P-site tRNA enters the H state but the A-site tRNA maintains its C configuration (P/E and A/A) demonstrating that the movement of two tRNAs can be uncoupled (Fischer et al., 2010; Munro et al., 2007). Many other EF-G-induced chimeric intermediates (CHI) have also been identified (Adio et al., 2015; Brilot et al., 2013; Fischer et al., 2010; Holtkamp et al., 2014a; Ramrath et al., 2013; Ratje et al., 2010; Zhou et al., 2014). The CHI states differ in the position of the tRNAs not only with respect to the two subunits but also with respect to different domains of the SSU. All CHI states are reversibly formed and occur in the trajectory of the tRNAs as they move from the PRE to POST state.

It should be noted that in the H state the tRNAs are not fully translocated and are not located in the authentic POST state with respect to the LSU, because peptidyl-tRNA reacts very slowly with puromycin (Sharma et al., 2004). They represent an important intermediate on the path of tRNA translocation. By promoting tRNA movement on the SSU, EF-G synchronizes the

translocation of tRNAs on both subunits to achieve the final authentic POST state (Holtkamp et al., 2014a).

1.4.5 Elongation factor G

EF-G promotes translocation by accelerating the process by 50-folds while consuming one molecule of GTP at each round and undergoing extensive conformational changes. EF-G consists of five domains: domain I (or G domain containing a long insertion, the subdomain G') is the GTP/GDP binding domain. G domain contains three highly conserved and mobile functional elements: the phosphate-binding loop (P-loop), which binds the GTP at its α - and β -phosphates; and the switch 1 and switch 2 motifs, which coordinate the γ -phosphate (Wittinghofer and Vetter, 2011). It is suggested that switch regions convert the free energy of GTP hydrolysis in the G domain into the unidirectional movement of the tRNA-mRNA complex on the ribosome and also assist in rapid recycling of EF-G during protein synthesis. Domain II of EF-G interacts with the 16S RNA of the SSU (Rodnina and Wintermeyer, 1998). Domains I and II are conserved in all translational GTPases. Domains III to V are specific to EF-G and structurally resemble the tRNA part of ternary complex formed by EF-Tu, GTP and aa-tRNA (Agrawal et al., 1998; Nissen et al., 1995). Binding of EF-G to the ribosome mainly occurs through the ribosomal protein L7/L12 and the SRL which activates the GTP hydrolysis by the factor. Domain I and V of EF-G primarily contact the LSU, while domains II, III and IV mainly contact the SSU (Brilot et al., 2013; Pulk and Cate, 2013; Zhou et al., 2013).

EF-G forms two super-domains composed of domains I-II and domains III-V, respectively, connected through a flexible hinge. This makes EF-G highly dynamic and allows it to sample between two major conformations: compact and elongated (**Figure 1.5**) (Lin et al., 2015; Salsi et al., 2015). In the compact conformation, domains I-II are in close proximity to domains III-V, in contrast to extended conformation where domain IV is in elongated form pointing away from domains I-II. Because most of the structural studies were performed with a vacant A site, they show EF-G bound to the ribosome in an extended conformation with its domain IV projecting into the decoding site of the SSU where the anticodon end of the A-site tRNA would be bound in a PRE complex. How EF-G binds to the ribosome in the PRE complex and what the position of domain IV before translocation is puzzling. A study with an A-site tRNA blocked in the A site by the antibiotic viomycin has shown that the tip of domain IV of EF-G is located outside the decoding center 20 Å away from the A site (Brilot et al., 2013). By binding the ribosome in the compact conformation transiently, EF-G avoids steric clash with the ASL of A-site tRNA. However, the compact conformation is less stable and EF-G undergoes an essential structural rearrangements from compact to extended state on the ribosome with domain IV moving into the A site promoting

translocation of peptidyl-tRNA from the A to the P site (Chen et al., 2013b; Peske et al., 2000; Savelsbergh et al., 2003; Tourigny et al., 2013).

In addition to the movement of domain IV, EF-G as a whole rotates around the SRL which interacts with the GTP binding domain of EF-G. This rotation of EF-G promotes the movement of domain IV on the ribosome. Also, the switch I and switch II regions of the GTPase domain become highly ordered upon binding to the ribosome leading to the activation of GTPase activity of EF-G. Upon GTP hydrolysis, the Switch regions become highly disordered that promotes EF-G dissociation (Zhou et al., 2013).

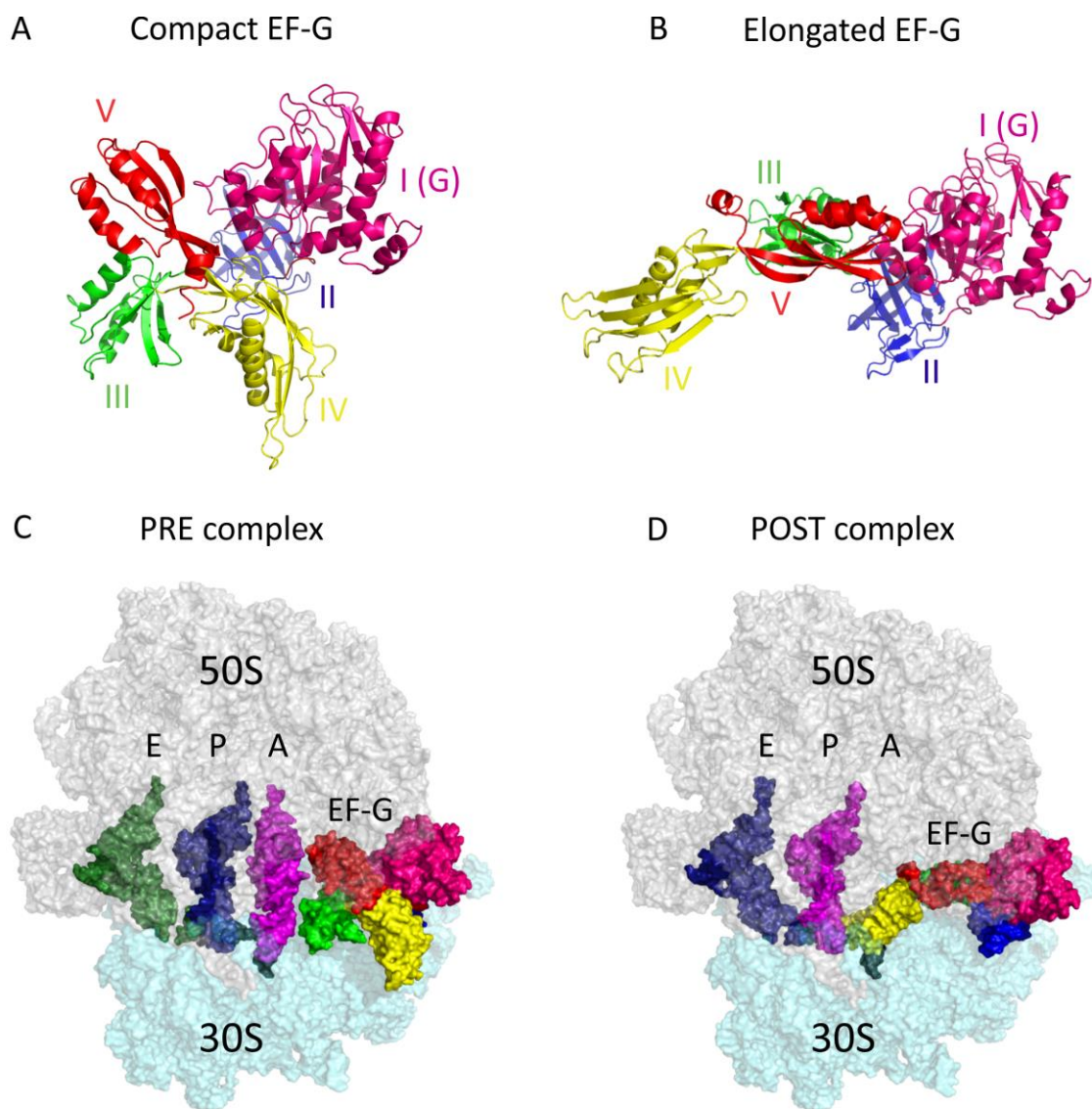


Figure 1.5 Different conformations of EF-G.

EF-G, a five domain protein, exists in two different conformations, (A) the compact form and (B) the elongated form. (C) In the PRE complex where the ribosome is in the N state and the tRNAs are in the C state, EF-G binds to the ribosome in the compact form. (D) On binding, EF-G changes the conformation from compact to elongated form, thereby projecting its domain IV (yellow) into the A site and facilitating the unidirectional translocation process of tRNA movement. The five different domains of EF-G are represented in different colours. Image modified from PDB files 4WPO and 4WQY (Lin et al., 2015).

All structural rearrangements of EF-G make energetic contributions to promote tRNA-mRNA translocation. EF-G drives the directional movement of the tRNA-mRNA complex on the ribosome by three distinct mechanisms. First, binding of EF-G stabilizes the R-H-L1_{closed} state (the ribosome in the rotated state, tRNAs in the hybrid state and L1 in closed conformation) of the ribosome and therefore, promotes the partial movement of the tRNAs on the LSU (Cornish et al., 2008; Dorner et al., 2006; Fei et al., 2008; Munro et al., 2010b; Spiegel et al., 2007; Wasserman et al., 2016). Second, EF-G utilizes the energy of GTP and brings about conformational rearrangement of the ribosome including changes at the decoding site, which unlock the ribosome for translocation (Rodnina et al., 1997; Savelsbergh et al., 2003). Third, domain IV of EF-G occupies the A site on the SSU and blocks the backward movement of peptidyl-tRNA making translocation essentially a unidirectional process (Gao et al., 2009; Pulk and Cate, 2013; Savelsbergh et al., 2009).

1.5 Subunit rotation during translocation

Translocation can be viewed as a series of multiple conformational changes with three types of major fluctuations – $N \leftrightarrow R$, $C \leftrightarrow H$, and $L1_{open} \leftrightarrow L1_{closed}$, which are loosely coupled (**Figure 1.6**) (Fei et al., 2008; Fischer et al., 2010; Munro et al., 2010b) and have different fluctuation kinetics (Munro et al., 2010a; Wasserman et al., 2016). The initiation or POST complex starts in the N conformation with the tRNAs in the C state (P/P, A/A) and L1 in the open conformation (N-C-L1_{open}). After accommodation of aa-tRNA and peptide bond formation, the P-site tRNA is deacylated leading to CCW rotation of the SSU body (7°-8°) and swiveling of the SSU head (6°-7°) (Brilot et al., 2013; Tourigny et al., 2013). The tRNAs move from the C to the H state, the L1 stalk establishes contacts with the tRNA in the P/E hybrid state and changes its conformation from open to the closed state. The PRE complex is highly dynamic and fluctuates spontaneously between the N-C-L1_{open} \leftrightarrow R-H-L1_{closed} conformations.

EF-G in the GTP bound form is recruited to the ribosome by the L12 stalk and stabilizes the R-H-L1_{closed} state, hence drives the equilibrium towards the R-H-L1_{closed} conformation. The hydrolysis of GTP induces the CW rotation of the SSU with respect to the LSU. At this point, the motion and rotation kinetics of the SSU domains, body and head are uncoupled. As the SSU body starts rotating backward in CW direction (3°-5°), the CCW swiveling motion of the head continuous and reaches as much as 18°-21° (Ramrath et al., 2013; Ratje et al., 2010; Zhou et al., 2013, 2014). Because the two opposite movements within the SSU (CCW swiveling of the head and CW rotation of the body) occur at the same time, the P-site tRNA interacts simultaneously with the P site component of the SSU head (p), the E site component of the SSU platform (e) while the tRNA on the LSU interacts with the E site (E) and acquires an intermediate intra-subunit state

termed as pe/E hybrid state (Ramrath et al., 2013). In a similar way, the A-site tRNA acquires the ap/ap followed by ap/P hybrid state (Ramrath et al., 2013; Zhou et al., 2014). The presence of intermediates provide an essential mechanism in which the CW rotation of the body along with a high degree of head swiveling is coupled to the translocation of tRNAs and mRNA with respect to the SSU. In this conformation the interaction between the tRNA-mRNA complex and the SSU might loosen and hence the ribosome is unlocked for translocation. Ultimately, the tRNA-mRNA complex is translocated by one codon, the SSU body and the head comes back to the N state. The L1 stalk acquires an open conformation after escorting the tRNA to the E site and EF-G dissociates subsequently in a GDP-bound form. With the peptidyl-tRNA in the P site and a vacant A site, the ribosome is back in the N-C-L1_{open} conformation ready for the next round of the elongation.

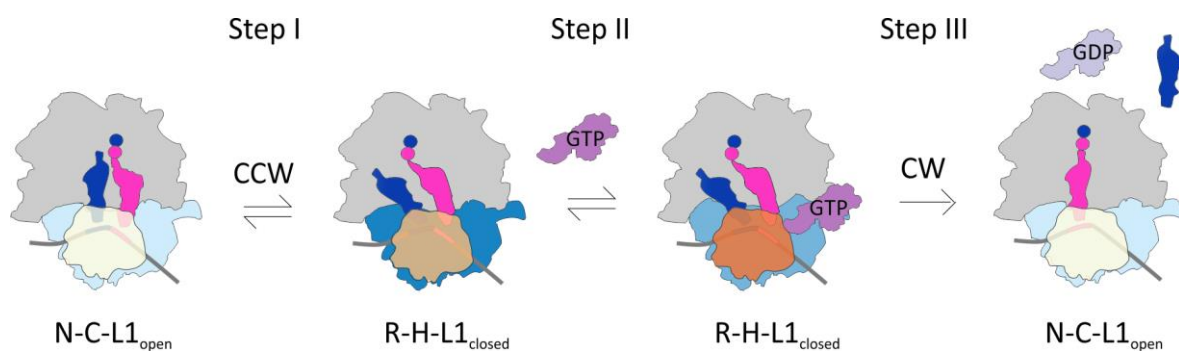


Figure 1.6 Schematic depicting subunit rotation during translocation.

Following peptide bond formation, the nascent peptide is attached to the A-site tRNA and the P-site tRNA is deacylated. This drives the spontaneous CCW rotation of the SSU body and the swiveling motion of the SSU head with respect to the LSU and movement of tRNAs from the C to H state, resulting in a dynamic equilibrium between the PRE (N-C-L1_{open}) and PRE (R-H-L1_{closed}) state (step I). Binding of EF-G-GTP stabilizes the PRE (R-H-L1_{closed}) state and induces an intermediate state of SSU rotation with a small scale rotation of the SSU body but large scale swiveling of the SSU head (step II). GTP hydrolysis by EF-G promotes translocation of the tRNA-mRNA complex by one codon, which is accompanied by a CW rotation of both SSU body and head back to the POST (N-C-L1_{open}) state followed by dissociation of EF-G-GDP and the deacylated tRNA (step III). The gradients in the colour of the SSU body and head represent different degrees of rotation with darkest having the highest degree of rotation.

Surprisingly, although peptide bond formation was proposed to drive CCW subunit rotation, no experiments have been reported that compared the relative rates of two reactions. Moreover, major unresolved questions are whether the spontaneous N-to-R transition of the ribosome defines the global rate of the tRNA-mRNA translocation and whether EF-G can bind to the ribosome in the N state and accelerates the N-to-R transition such that subunit rotation does not limit translocation. In addition, several translocation intermediates have been identified through structural studies but the exact sequence of occurrence of these intermediates is not clearly defined. The precise timing of CCW and CW rotation of the body and the head are unknown as body and head move as independent domains of the SSU. Additionally, how

movement of the tRNA-mRNA complex is coordinated with the CW rotation of the SSU is unclear. These questions will be addressed in this thesis.

1.6 Antibiotics inhibiting translocation

A broad array of chemically distinct antibiotics inhibits protein synthesis by targeting functional centers of the ribosome. Several of these antibiotics directly affect different stages of translocation. Structural, biochemical and kinetics studies have shed light on their mechanism of action, and have in turn provided essential clues about the molecular workings of the ribosome and its ligands. Here, I will focus on those antibiotics that target the ribosome complex and inhibit the translocation step of elongation. Most of these antibiotics are aminoglycosides (hygromycin B, kanamycin, paromomycin, streptomycin and neomycin); spectinomycin and viomycin are aminocyclitol and peptide antibiotics, respectively (Shoji et al., 2009).

Hygromycin B: Hygromycin B binds to h44 of the 16S rRNA between the A and P site near the decoding center. It stabilizes the bases A1492 and A1493 in a flipped-out conformation in a way that the unique orientation of A1493 stabilizes the A-site tRNA and sterically blocks its movement from the A to P site (Borovinskaya et al., 2008; Peske et al., 2004). Additionally, Hygromycin B contacts the mRNA codons in the P and A site and confines the mRNA to its position (Borovinskaya et al., 2008). Kinetic studies show that the antibiotic stabilizes an intermediate state during stepwise movement of peptidyl-tRNA on the LSU from C (A/A) to H (A/P) to C state (Holtkamp et al., 2014a).

Spectinomycin: Spectinomycin is an antibiotic that binds to h34, a hinge point between the head and shoulder of the SSU. It inhibits head swiveling and traps the head domain in a distinct state that is slow in translocation (Borovinskaya et al., 2007b; Carter et al., 2000; Peske et al., 2004). Kinetic studies report that spectinomycin increases the rate of LSU translocation and uncouples it from SSU translocation, which becomes very slow (Holtkamp et al., 2014a).

Kanamycin: Kanamycin interacts with h44 of the 16S rRNA and binds at the decoding center. Binding of the antibiotic to h44 decoding site favors an extra-helical conformation of residues A1492-A1493 which stabilizes the interaction between the mRNA codon and the tRNA anticodon at the A-site tRNA (Llano-Sotelo et al., 2002; Voorhees and Ramakrishnan, 2013). This results in stabilization of the C state of the tRNAs and inhibition of translocation (Feldman et al., 2010).

Paromomycin: Like kanamycin, paromomycin also binds to h44 of the 16S and stabilizes the A-site tRNA binding (Carter et al., 2000). Thus, the antibiotic inhibits translocation by stabilizing the N-C state of the ribosome (Tsai et al., 2013; Wasserman et al., 2015). The major effect of

paromomycin has been seen on miscoding. It causes bases A1492 and A1493 of the 16S rRNA to flip out and interact with the codon-anticodon helix. Paromomycin significantly reduces the rate of dissociation of near-cognate tRNA and increases the rate of GTP hydrolysis by EF-Tu by one order of magnitude (Pape et al., 2000).

Streptomycin: Streptomycin binds to the backbone of the 16S rRNA (h44) and makes contact with protein S12. The antibiotic destabilizes the binding of cognate tRNA but stabilizes binding of near-cognate tRNA in the A-site (Demirci et al., 2013). Streptomycin alters the rate of GTP hydrolysis by EF-Tu on cognate and near-cognate codons resulting in almost identical rates of GTP hydrolysis and in complete loss of selectivity (Gromadski and Rodnina, 2004). In addition, the antibiotic might trap the SSU head in a conformation which is error prone but facilitates rapid translocation (Carter et al., 2000; Peske et al., 2004).

Viomycin: Viomycin is a cyclic peptide antibiotic that interacts with h44 of the 16S rRNA and H69 of the 23S rRNA and binds at the subunit interface. The antibiotic strongly stabilizes the A-site tRNA and blocks translocation completely (Modolell and Vazquez, 1977; Peske et al., 2004; Rodnina et al., 1997). Viomycin also enhances subunit association and inhibits ribosome recycling (Shoji et al., 2009). The antibiotic locks the ribosome in an intermediate conformation where the tRNAs occupy either the H1 or the H2 state (Pan et al., 2007).

Neomycin: Neomycin has two binding sites and exhibits bimodal effect. At lower concentrations (<0.1 μM), neomycin binds to h44 of the 16S rRNA and inhibits translocation by stabilizing the A-site tRNA and N-C state of the ribosome. At the higher concentrations (>0.1 μM), the antibiotic also interacts with H69 of the 23S rRNA and blocks the subunit rotation by stabilizing an intermediate state of rotation (Wang et al., 2012; Wasserman et al., 2015).

Fusidic acid: Fusidic acid binds to EF-G on the ribosome and inhibits the dissociation of EF-G–GDP complex from the ribosome once translocation has occurred. The antibiotic does not interfere with the primary function of EF-G in promoting the tRNA–mRNA translocation coupled to GTP hydrolysis. However, formation of EF-G–GDP–FA on the ribosome blocks the subsequent rounds of the elongation cycle and inhibits protein synthesis (Bodley et al., 1969; Cox et al., 2012; Savelsbergh et al., 2009; Tanaka et al., 1968).

1.7 Subunit rotation during initiation and termination

Subunit rotation is involved in all stages of translation. Here, I will introduce the role of subunit rotation during initiation and termination. The detailed description of the mechanisms of the two translation steps is beyond the scope of this thesis.

Initiation: IF2–GTP along with the other initiation factors (IF1 and IF3) facilitates the assembly of the SSU and the LSU in the R conformation (Julian et al., 2011; Marshall et al., 2009; Shoji et al., 2009). At this point the initiator tRNA is present in an intermediate site between the classical P/P site and the hybrid P/E site called P/I site (Allen et al., 2005; Julian et al., 2011). Upon GTP hydrolysis and subsequent dissociation of the initiation factors, the SSU rotates back in CW direction along with the accommodation of the initiator tRNA in the PTC of the LSU attaining the classical P/P state. This process acts as a checkpoint before the ribosome enters the elongation cycle.

Termination: Class I release factors bind to the pre-termination complex with the peptidyl-tRNA in the P site and stabilize the N conformation of the ribosome. Subsequent hydrolysis of the polypeptide chain and binding of RF3 in the GTP bound form drives the CCW rotation of the SSU (Zhou et al., 2012). In the R form of the ribosome there are steric clashes between domain II and IV of RF2 with h18 of the SSU and domain I of RF2 with L11 region of the LSU leading to its dissociation from the ribosome. Hydrolysis of GTP followed by dissociation of RF3 from the ribosome prepares the post-termination complex for recycling (Dunkle et al., 2011).

After the peptide hydrolysis, the ribosome, with deacylated tRNA in the P site, is very dynamic and fluctuates between the N and R conformation (Cornish et al., 2008; Fei et al., 2011). RRF binds and stabilizes the R-H conformation of the ribosome. EF-G along with IF3 then dissociates entire post-termination complex into its components (Dunkle et al., 2011).

1.8 Scope of the thesis

In this work, we used fluorescence labeled ribosomal subunits to monitor the kinetics of subunit rotation in real time and determined the rates of peptide bond formation and spontaneous subunit rotation for different tRNA pairs using rapid kinetic approaches (Sharma et al., 2016). We also monitored the effect of EF-G on subunit rotation and examined the coupling between tRNA-mRNA translocation and subunit rotation at different temperature and buffer conditions using ensemble kinetics and smFRET approach (Sharma et al., 2016). To know the exact sequence of events during translocation, we used nine different fluorescence reporters placed on ribosomal subunits, tRNA, mRNA and EF-G and reconstructed the choreography of molecular movements during translocation that placed translocation intermediates along a time axis (Belardinelli et al., 2016). To better understand the role of EF-G in facilitating subunit rotation, we also monitored SSU rotation in the presence of different variants of EF-G which are either slow in translocating the tRNA-mRNA complex or are defective in GTP hydrolysis. In addition, we utilized a collection of antibiotics that impair translocation and monitored their effect on subunit dynamics. Our results provide estimations for the subunit rotation rates at physiologically relevant conditions and show how early on-pathway conformation rearrangement in the ribosome contributes to the energetics of translocation.

2. RESULTS

2.1 Experimental approach

Translocation of the tRNA-mRNA complex is a multi-step process which involves consecutive steps of binding, GTP hydrolysis, conformational rearrangements and dissociation accompanied by different motions in the ribosome. Most of these events take place on a millisecond to seconds time scale and can be monitored by rapid kinetic techniques. Rapid kinetic approaches exploit the biochemical and biophysical properties of the reactant and enable to monitor reactions in real time. The pre-steady state kinetics allow for the detection of transient intermediates. Following the kinetics of formation and consumption of these intermediates provides reaction rate constant which help in deducing the sequence of events.

To study the kinetics of rotation of the SSU relative to LSU, we utilized the FRET assay developed and validated by Noller and colleagues (Cornish et al., 2008; Ermolenko et al., 2007a; Hickerson et al., 2005; Majumdar et al., 2005). We introduced fluorescence reporters on ribosomal proteins bS6 and bL9 at cysteine residues introduced by site-directed mutagenesis at position 41 replacing aspartic acid (D41C) in protein bS6 and at position 11 replacing asparagine (N11C) in bL9. SSU and LSU carrying labeled bS6 and bL9 were prepared by *in vitro* reconstitution by mixing subunits prepared from strains lacking bS6 (Δ S6) or bL9 (Δ L9) with excess of fluorescence-labeled protein bS6 or bL9, respectively (**Figure 2.1**) (Methods). For ensemble kinetics, bS6 was labeled with Alexa 488, serving as a FRET donor (S6Alx488), and bL9 was labeled with Alexa 568 serving as a FRET acceptor (L9Alx568). For smFRET experiments, bS6 was labeled with Cy5 (FRET acceptor) and bL9 was labeled with Cy3 (FRET donor). The two proteins are located far from the ligand (such as EF-G or EF-Tu) binding site on the ribosome and their labeling does not affect the interaction between the ligands and the ribosome, nor the fluorophore properties of the dyes are affected by the presence of the ligands on the ribosome (Ermolenko et al., 2007a).

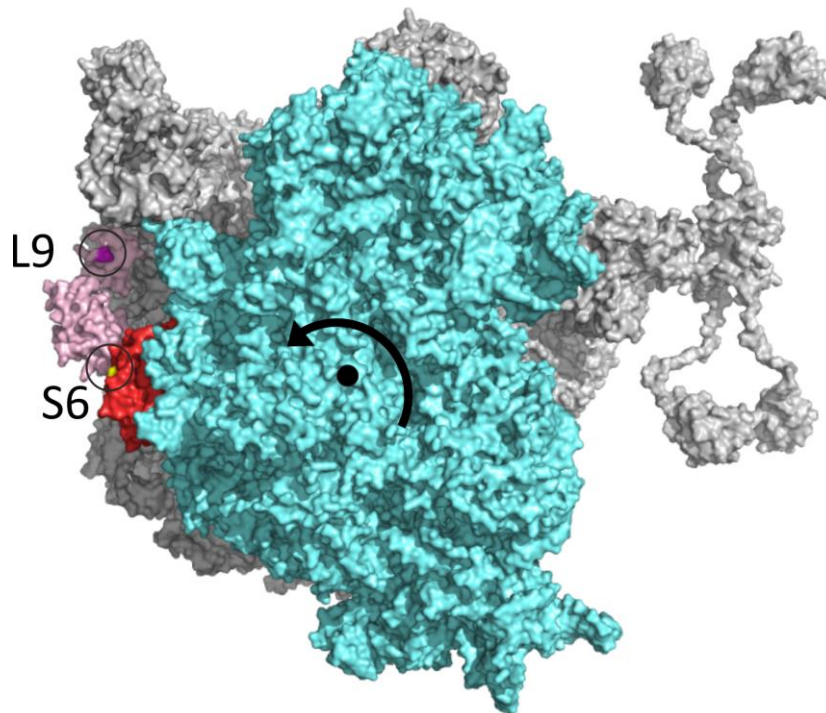


Figure 2.1 Position of the fluorescence reporters on ribosomal subunits used for FRET measurements. Protein bS6 (red) of the SSU was labeled at position D41C (yellow) and protein bL9 (light pink) of the LSU was labeled at position N11C (magenta) with either donor or acceptor forming a FRET pair (labeling positions marked in circles). The arrow indicates the direction of rotation of the SSU relative to the LSU.

All ensemble kinetic experiments were performed in TAKM_7 buffer (subscript indicates the concentration of magnesium ions in mM) at 37°C unless specified differently (Methods). Double-labeled ribosomes (S6Alx488–L9Alx568) were excited at 470 nm (excitation wavelength for Alexa 488) and the change of acceptor and donor fluorescence were observed in two different channel of a stopped-flow apparatus after passing through cut-off filter OG590 and KV500, respectively. For simplicity, only the change in the acceptor fluorescence is reported for all experiments representing the change in the FRET signal. The biochemical assays and HPLC outputs were analyzed by radioactivity counting of the peptides. All concentrations reported are the final concentration of the reactant after rapid mixing in either quench-flow or stopped-flow apparatus.

2.2 Characterization of the double-labeled ribosome

We assessed the rates of translocation of the double-labeled ribosomes and compared it with the wild type ribosome (WT) (prepared from standard *E. coli* strain MRE 100 in our laboratory) to verify that the functional activity of the ribosome is not affected by labeling. To measure the rate of translocation, we performed a time-resolved puromycin (Pmn) assay. High Pmn reactivity is indicative of a position of the peptidyl-tRNA in the P site in a POST complex whereas low Pmn reactivity is evidence of position of the peptidyl-tRNA in the A site either in the C or H state (Sharma et al., 2004). We prepared PRE complex with deacylated tRNA^{fMet} in the P site and fMetPhe-tRNA^{Phe} in the A site, PRE(fMF) and rapidly mixed it with saturating concentrations of EF-G-GTP and Pmn in a quench-flow apparatus (**Figure 2.2A**). The reaction of Pmn is completed on a millisecond time scale, which is comparable to the rate of translocation. Single-exponential fitting of the time course of formation of fMetPhe-Pmn gave the apparent rate constants for translocation. The apparent rate of translocation for S6Alx488–L9Alx568 and S6Cy5–L9Cy3 were 28 s^{-1} and 30 s^{-1} , respectively, which were comparable to the translocation rate of WT ribosomes (25 s^{-1}). Therefore, the kinetics of translocation of double-labeled ribosomes was unaffected in addition to their unaltered ability to bind to tRNA. About 80-90% of ribosomes were active in translocation when compared to the WT ribosome (**Figure 2.2A**).

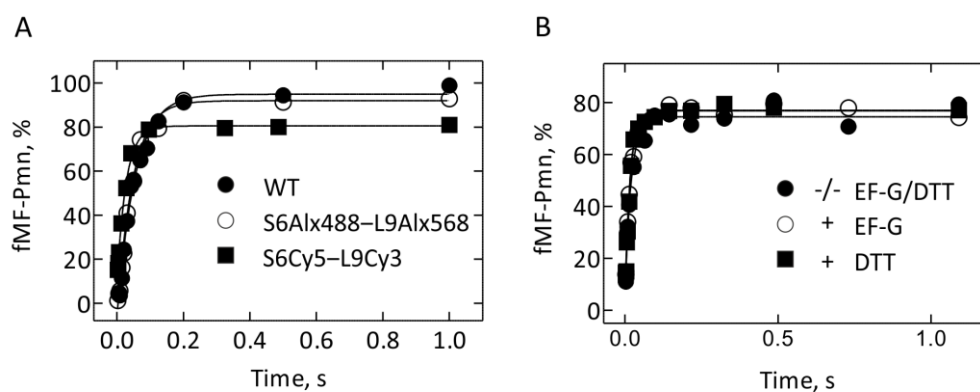


Figure 2.2 Time-resolved Pmn assay for S6–L9 double-labeled ribosomes.

(A) Time-resolved Pmn assay for WT (closed circles), S6Alx488–L9Alx568-labeled (open circles) or S6Cy5–L9Cy3-labeled ribosomes (closed squares). PRE complexes ($0.1\ \mu\text{M}$) were rapidly mixed with EF-G ($4\ \mu\text{M}$) and Pmn ($10\ \text{mM}$) in a quench-flow and the time course of fMetPhe-Pmn formation was measured. (B) POST complexes ($0.1\ \mu\text{M}$) were rapidly mixed with Pmn ($10\ \text{mM}$) in the absence of EF-G and DTT (closed circles), in the presence of EF-G ($4\ \mu\text{M}$) (open circles) or in the presence of DTT ($1\ \text{mM}$) (closed squares).

The rate of translocation was measured upon addition of a saturating concentration of EF-G that leads to Pmn reaction of the resulting POST complex. Because of the high concentration of EF-G used for rapid translocation of the the tRNAs, we wanted to make sure that the kinetics of the Pmn reaction with resulting POST complex was not affected by the presence of EF-G. In addition, we tested the effect of DTT on the reaction of POST complex with Pmn. Traditionally,

DTT is often used in buffers, which was shown to be required as a reducing agent needed for the activity of some tRNA-synthetases in a non-purified *in vitro* translation system. DTT also maintains the reduced form of cysteines present in r-proteins to prevent inter-molecular disulfide bonds which would otherwise influence their activities. We do not use DTT in our purified *in vitro* translation system and therefore wanted to check if DTT has any influence on the activity of the ribosome. We prepared POST complex with fMetPhe-tRNA^{Phe} in the P site and rapidly mixed it with Pmn in the absence or presence of EF-G–GTP or DTT. The rate constant estimated from the single-exponential fitting of time courses were about 60 s⁻¹ for all three conditions. Therefore, neither EF-G nor DTT has any effect on the kinetics of the Pmn reaction (**Figure 2.2B**).

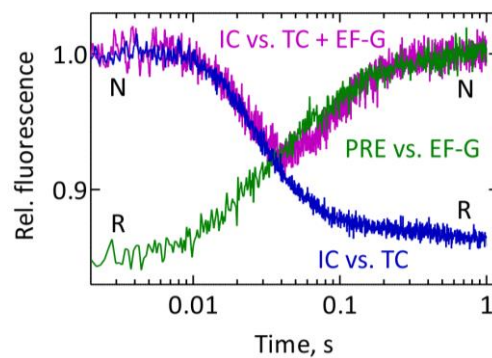


Figure 2.3 Subunit rotation monitored with S6–L9 FRET pair.

Subunit rotation monitored by FRET changes using stopped-flow apparatus. Initiation complex (IC) (0.05 μM), in the N state, was rapidly mixed with ternary complex (TC) (10 μM) to form PRE complex resulting in the R state formation (blue). Addition of EF-G–GTP (4 μM) to the PRE complex formed POST complex resulting in rotation from the R to the N state (green). IC (0.05 μM) was rapidly mixed with TC (10 μM) and EF-G–GTP (4 μM) together to observe both CCW and CW subunit rotation (pink). N and R indicate the non-rotated and rotated conformations of the ribosome.

Next, to verify that the double-labeled ribosomes report on subunit rotation, we measured the FRET between the labeled ribosomal subunits using a stopped-flow apparatus. As shown previously, rotation of the subunits relative to each other results in a FRET change between bS6-labeled SSU and bL9-labeled LSU (Cornish et al., 2008; Ermolenko et al., 2007a; Ermolenko and Noller, 2011). CCW rotation of the SSU relative to the LSU moves the fluorophores apart resulting in a decrease in FRET and CW rotation of the subunit brings the labels closer resulting in an increase in FRET. The acceptor fluorescence decreased upon reaction of ternary complex EF-Tu–GTP–Phe-tRNA^{Phe} with double-labeled initiation complex, 70S–mRNA–fMet-tRNA^{fMet}, indicating CCW rotation of the SSU with respect to the LSU upon formation of deacylated tRNA in the P site (**Figure 2.3**). On addition of EF-G–GTP to the PRE complex, the acceptor fluorescence increased to the initial value reporting on the CW rotation of the subunits accompanied by translocation of the tRNAs.

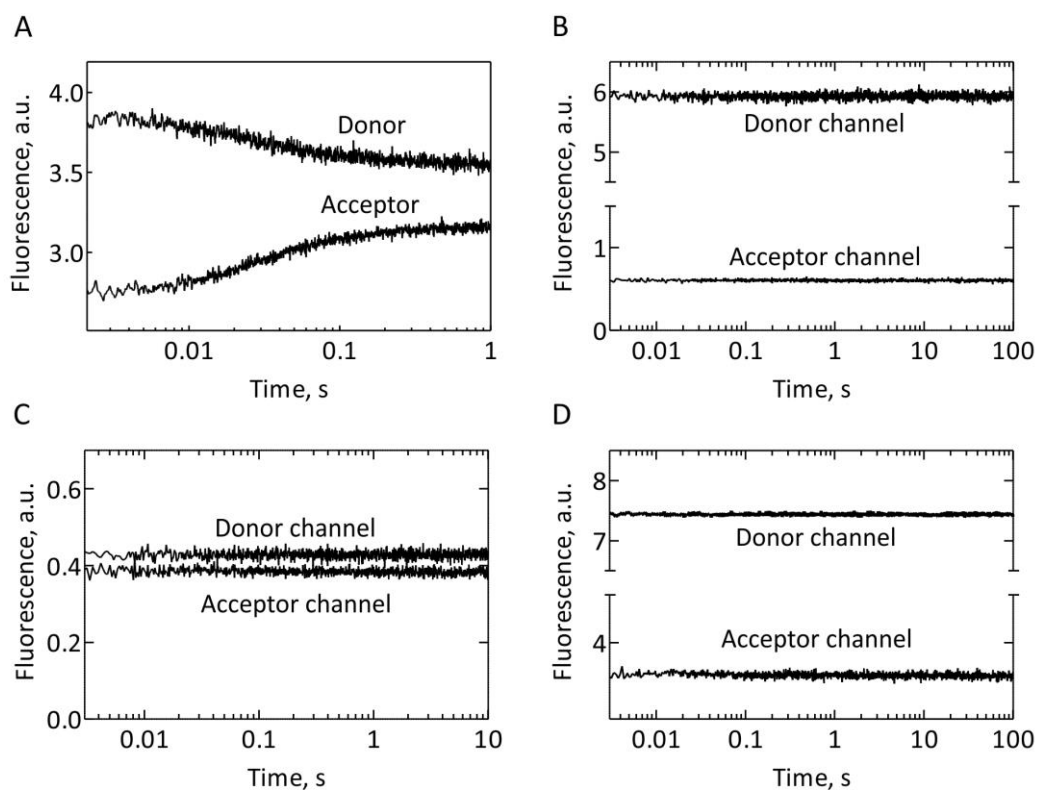


Figure 2.4 Controls for subunit rotation monitored with S6-L9 FRET pair.

FRET changes monitored upon rapid mixing of PRE complex (0.05 μM) with EF-G-GTP (4 μM). (A) Double-labeled 70S, S6Alx488-L9Alx568 showed a counter signal change of acceptor and donor. No fluorescence signal change was observed in both acceptor and donor channels upon rapid mixing of single-labeled 70S (B) S6Alx488 or (C) L9Alx568, with EF-G-GTP (excitation wavelength at 470 nm). (D) Excitation of single-labeled L9Alx568 at 550 nm upon rapid mixing with EF-G-GTP also did not show any change in the fluorescence signal in either donor or acceptor channel.

For all ensemble kinetic experiments, the fluorescence change of the donor was monitored as a control which showed counter change in the fluorescence signal compared to the acceptor fluorescence change. An example trace is shown in **Figure 2.4A**, where rapid mixing of PRE complex with EF-G-GTP resulted in translocation of the tRNA-mRNA complex and CW subunit rotation. The decrease in the fluorescence signal of the donor was attenuated as compared to the counter-increase in the fluorescence signal of the acceptor due to the use of a cut-off filter (KV500). The cut-off filter KV500 allows visible light greater than 500 nm to pass through and to be detected by the instrument. That means in addition to the donor fluorescence, the acceptor fluorescence (emission maxima is at 603 nm) was also detected in the donor channel which resulted in the attenuated decrease in the signal of the donor fluorescence. On contrary, the use of the cut-off filter OG590 in the acceptor channel did not allow the light from the donor fluorescence (emission maxima is at 519 nm) to pass through leading to a clearer signal for the acceptor. For this reason, the acceptor signal change is reported in all experiments. As control experiments, PRE complex with single-labeled ribosome; 70S-Alx488 or 70S-Alx568 were rapidly mixed with EF-G-GTP and were excited at 470 nm to monitor the background change in the

RESULTS

fluorescence in both the acceptor and donor channel (**Figure 2.4B and C**). No change in the fluorescence of either donor or acceptor was observed in either channel when single-labeled ribosomes were used. Similarly, no signal change was observed when single-labeled 70S-Alex568 was excited at 550 nm, the excitation wavelength for Alexa 568 (**Figure 2.4D**). These relevant controls confirmed that the double-labeled ribosomes report on the dynamics of subunit rotation.

2.3 Kinetics of spontaneous subunit rotation with different tRNAs in the P site

The ribosome rotates spontaneously and reversibly in the absence of any auxiliary factor which establishes equilibrium between the N and R state. In PRE complex, the SSU rotates spontaneously with respect to the LSU in CCW direction upon the formation of deacylated tRNA in the P site as a result of peptide bond formation (Blanchard et al., 2004b; Cornish et al., 2008; Julian et al., 2011; Kim et al., 2007). In order to determine the kinetics of the CCW subunit rotation upon peptide bond formation, we measured the rate of peptide bond formation by quench-flow and followed the spontaneous CCW rotation by stopped-flow (**Figure 2.5A**). We prepared POST complexes with different dipeptidyl-tRNAs in the P site (fMetX-tRNA^X, where X is Lys, Val, Phe or Pro, denoted as fMX) and rapidly mixed them with a high concentration of Pmn. Pmn was used as an A site substrate instead of a native aa-tRNA because unlike native aa-tRNA, binding and accommodation of Pmn are not limiting for the peptidyl transfer reaction (Sievers et al., 2004). Thus, the kinetics of peptide bond formation and presumably subunit rotation depends solely on the identity of P-site peptidyl-tRNA.

The time courses of the formation of fMX–Pmn were evaluated by single-exponential fitting. We observed that the Pmn reaction was rapid with fMK, fMF and fMV, decreasing in this order, but very slow with fMP in agreement with previously published report (**Figure 2.5B**) (Wohlgemuth et al., 2008). The CCW rotation of the ribosomal subunits was monitored as a decrease in the acceptor fluorescence that followed a delay phase due to the preceding Pmn reaction (**Figure 2.5C**). Time courses for the CCW rotation were evaluated by one (fMV) or two (fMK, fMF) exponential fitting with a preceding delay (**Figure 2.5D**). For fMK and fMF, an additional minor downward phase was observed which constituted 12% and 20% of the total signal, respectively. As an exception, time courses with fMP did not show the delay and were evaluated by two-exponential fitting with the two phases constituting 55% and 45% of the total amplitude change. The apparent rates (k_{app}) of the major phase of CCW rotation were rapid for fMK, fMV and fMF and very slow for fMP showing the same trend as the Pmn reaction but were in general slower than those of peptide bond formation (**Figure 2.5D**). Hence, the chemical step of peptide bond formation was limiting the subsequent CCW rotation and to determine the elemental rate constant of CCW rotation (k_{CCW}) the two subsequent reactions of peptide bond formation and subunit rotation needed to be deconvoluted.

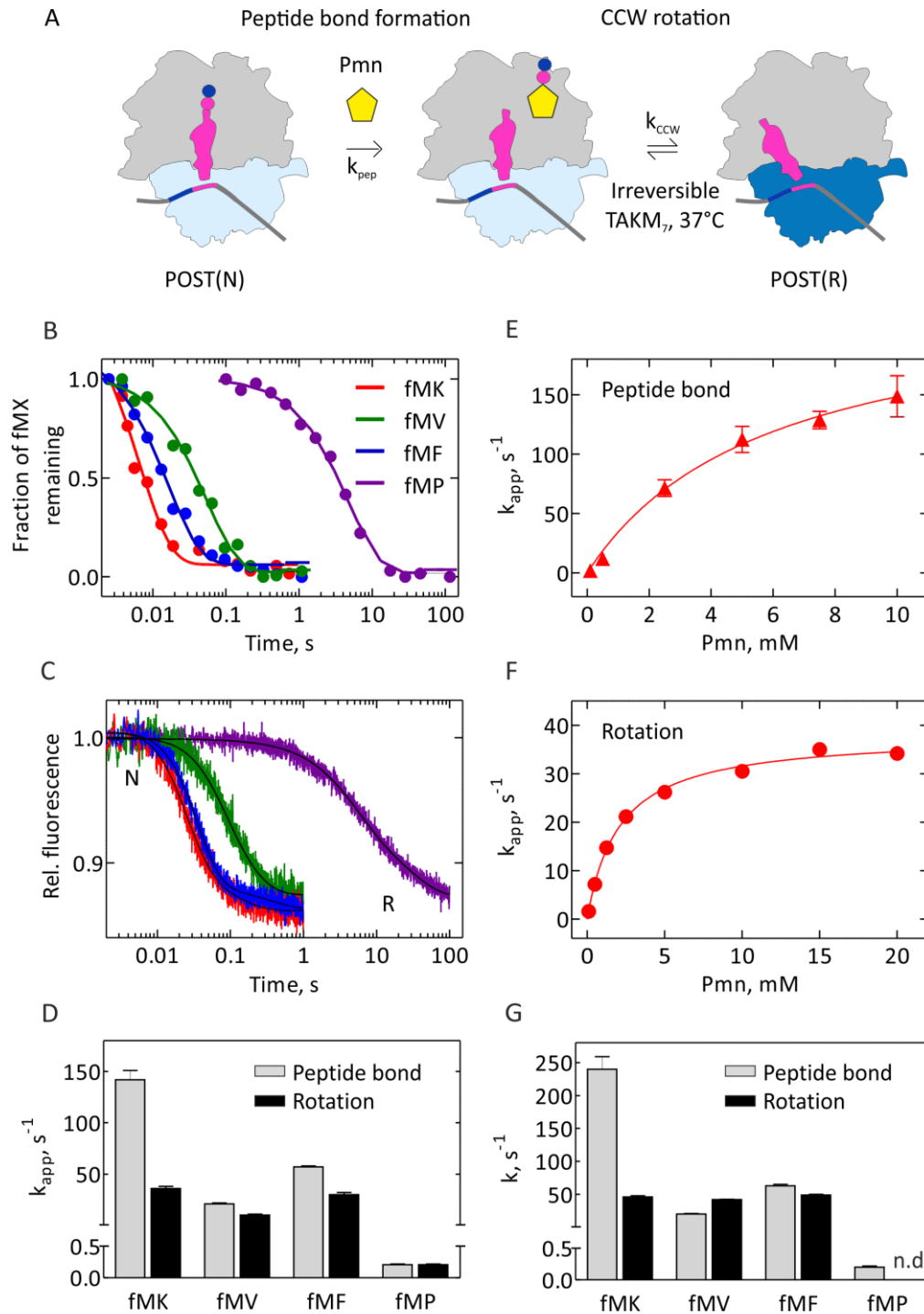


Figure 2.5 Peptide bond formation and spontaneous CCW subunit rotation with different P-site tRNAs.

(A) Schematic representing the two consecutive steps of peptide bond formation and spontaneous CCW rotation of ribosomal subunit. The POST complex in the N state spontaneously rotates to the R state upon formation of the peptide bond. (B) Time courses of Pmn reaction measured as the formation of fMetX–Pmn upon rapid mixing of fMX (0.1 μM) with Pmn (10 mM) in a quench-flow apparatus. (C) Time courses of CCW subunit rotation observed as a decrease in acceptor fluorescence upon rapid mixing of fMX (0.1 μM) with Pmn (10 mM) in a stopped-flow apparatus. Colour codes are the same as in (B). (D) The apparent rate constants (k_{app}) of peptide bond formation and CCW subunit rotation obtained by exponential fitting of the data from (B) and (C). (E and F) Pmn concentration dependence of k_{app} of (E) peptide bond formation and (F) CCW subunit rotation for fMK complex. For CCW subunit rotation, k_{app} values of the major step (>80% of the total amplitude) are plotted. (G) Elemental rate constants of peptide bond formation (k_{pep}) and CCW subunit rotation (k_{CCW}) estimated from numerical integration analysis of the data shown in (B) and (C).

Values are mean \pm s.d. ($n = 3$ independent kinetic experiments). Smooth lines in (B) and (C) represent the global fit. X is Lys, Val, Phe or Pro; N is non-rotated and R is rotated ribosomal state; n.d. is not defined.

For fMK, the K_M value for Pmn is very high such that the concentration of 10 mM is not saturating and the maximum rate of peptide bond formation was not achieved. Therefore, as a first approach to deconvolute the steps of peptide bond formation and CCW rotation, we determined rates of two reactions at increasing concentration of Pmn (**Figure 2.5E and F**). The rate of peptide bond formation (k_{pep}) and CCW rotation (k_{rot}) obtained from hyperbolic fitting of the Pmn concentration dependence curve were $240 \pm 20 \text{ s}^{-1}$ and $40 \pm 2 \text{ s}^{-1}$ with K_M value $6 \pm 1 \text{ mM}$ and $2.0 \pm 0.5 \text{ mM}$, respectively. From these rate constants, we calculated $48 \pm 5 \text{ s}^{-1}$ as an elemental rate of CCW rotation (k_{CCW}) using a mathematical expression $k_{\text{CCW}} = k_{\text{pep}} \times k_{\text{rot}} / (k_{\text{pep}} - k_{\text{rot}})$. The K_M value of Pmn for fMV, fMF and fMP is lower than fMK and near maximum velocity is reached at 10 mM Pmn concentration (Wohlgemuth et al., 2008). Therefore, the rates of peptide bond formation obtained at this concentration were considered as elemental rates (k_{pep}) for these complexes. From the analyses we assumed that the CCW subunit rotation upon deacylation of the P-site tRNA with Pmn is quasi-irreversible in TAKM₇ at 37°C, as (i) from the Pmn concentration dependence of subunit rotation, we observed that experiments at low concentrations of Pmn (<2.5 mM) were in the linear range of the curve and gave the apparent rate constant of Pmn binding. The Y-intercept of such curve yields the rate of reverse reaction of the step monitored i.e subunit rotation in our case. Since, the Y-intercept is close to zero we assumed that the subunit rotation is quasi-irreversible in our condition (**Figure 2.5F**). (ii) Spontaneous reversible SSU rotation sets different equilibrium between the N and R state depending on the identity of the tRNAs present in the ribosome (Cornish et al., 2008). This means that the reaction of different fMX complex with Pmn that leads to spontaneous N-to-R transition should result in different amplitude due to different proportions of the R state formed at the end of the reaction. But on contrary, no difference in the end levels of fluorescence signals was observed with different P-site tRNA indicating that spontaneous CW rotation is extremely slow and the reaction of fMX with Pmn could be considered quasi-irreversible (**Figure 2.5C**).

As a second approach, we performed numerical integration analysis of the data shown in **Figure 2.5B and C** to calculate the k_{CCW} values for different complexes. Such analysis resolved the delay observed in stopped-flow traces (**Figure 2.5C**) and provided reliable fitting for determination of k_{CCW} . For analysis, we assumed a two-step sequential model with irreversible steps of peptide bond formation followed by CCW subunit rotation (**Figure 2.5A**). Wherever necessary, a third step was included to account for a minor decrease in the fluorescence at the end of stopped-flow traces (see above). The value of k_{CCW} obtained for fMK from such analysis was $46 \pm 2 \text{ s}^{-1}$, identical to the value calculated from Pmn titration. For fMV and fMF, numerical

integration analysis also yielded similar values for k_{CCW} which were in the range of 40-50 s^{-1} , although the rate of peptide bond formation varied with the different P-site tRNA (**Figure 2.5G**). For fMP, the Pmn reaction is extremely slow and completely limits the following CCW rotation. The rates obtained for the two-step model were $0.22 \pm 0.01 \text{ s}^{-1}$ and $0.037 \pm 0.002 \text{ s}^{-1}$ which were identical to the apparent rates obtained by exponential fitting (**Figure 2.5D**); therefore, the accurate value for k_{CCW} could not be determined.

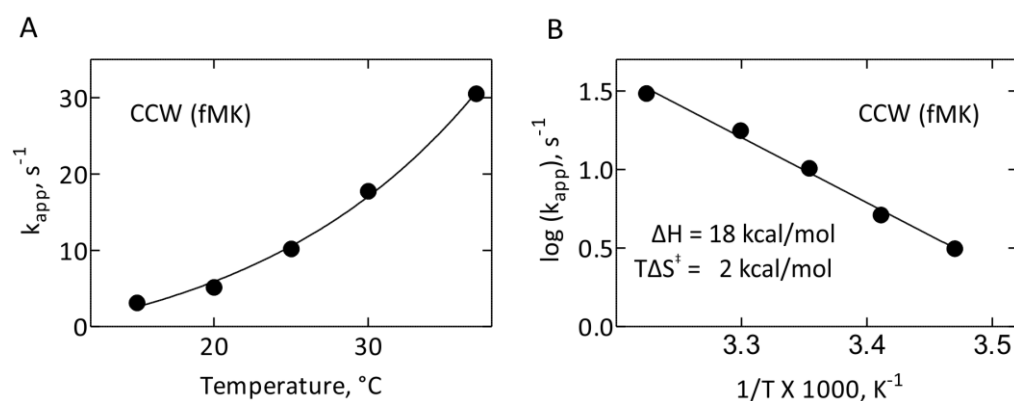


Figure 2.6 Temperature dependence of spontaneous CCW subunit rotation.

POST(fMK) (0.1 μM) were rapidly mixed with saturating concentration of Pmn (10 mM) in a stopped-flow apparatus at different temperatures (15 $^{\circ}\text{C}$ -37 $^{\circ}\text{C}$). (A) The apparent rates of spontaneous CCW subunit rotation (k_{app}) plotted against increasing temperature. (B) The Arrhenius plot of data in (A) showing linear dependence.

The rate constants of spontaneous CCW rotation (k_{CCW}) reported here are rapid and about 10 times faster than the values reported in the literature (Cornish et al., 2009; Qin et al., 2014; Wasserman et al., 2016). Most of these studies were performed at smFRET conditions and hence at lower temperature. For better comparison we determined the apparent rate of CCW rotation (k_{app}) at different temperature (15 $^{\circ}\text{C}$, 20 $^{\circ}\text{C}$, 25 $^{\circ}\text{C}$, 30 $^{\circ}\text{C}$ and 37 $^{\circ}\text{C}$) for fMK by rapidly mixing POST complex with Pmn (**Figure 2.6A**). We chose fMK for temperature dependence experiment because peptide bond formation was much faster and not limiting for the subsequent CCW subunit rotation with this complex. The Arrhenius plot of the reaction of fMK with Pmn was linear indicating that a single elemental reaction was observed (**Figure 2.6B**). The apparent rate constant of CCW rotation obtained at 22 $^{\circ}\text{C}$ was about 8 s^{-1} . The value measured here is faster than the value reported for CCW subunit rotation obtained from spontaneous transition between two rotational states of the ribosome with the same S6–L9 FRET positions but using tRNA^{fMet} in P site and synthetic N-Ac-Phe-tRNA^{Phe} in the A site or only tRNA^{Tyr} in P site ($\sim 2 \text{ s}^{-1}$) (Cornish et al., 2008; Qin et al., 2014). However, the rate is comparable to the rate reported for PRE(fMF) using S13–L5 positions for FRET couple (5 s^{-1}) and in the same range of our smFRET data (**Table 1**) (Wasserman et al., 2016).

2.4 Kinetics of spontaneous subunit rotation with different tRNAs in the A site

We next monitored the kinetics of peptide bond formation and CCW subunit rotation with different A-site tRNAs, native substrates of the ribosome, using quench-flow and stopped-flow, respectively (**Figure 2.7A**). We prepared different initiation complexes with mRNAs differing in second codon and rapidly mixed them with saturating concentration of ternary complex EF-Tu-GTP-X-tRNA^X where X is Lys, Val, Phe or Pro (denoted as fMX).

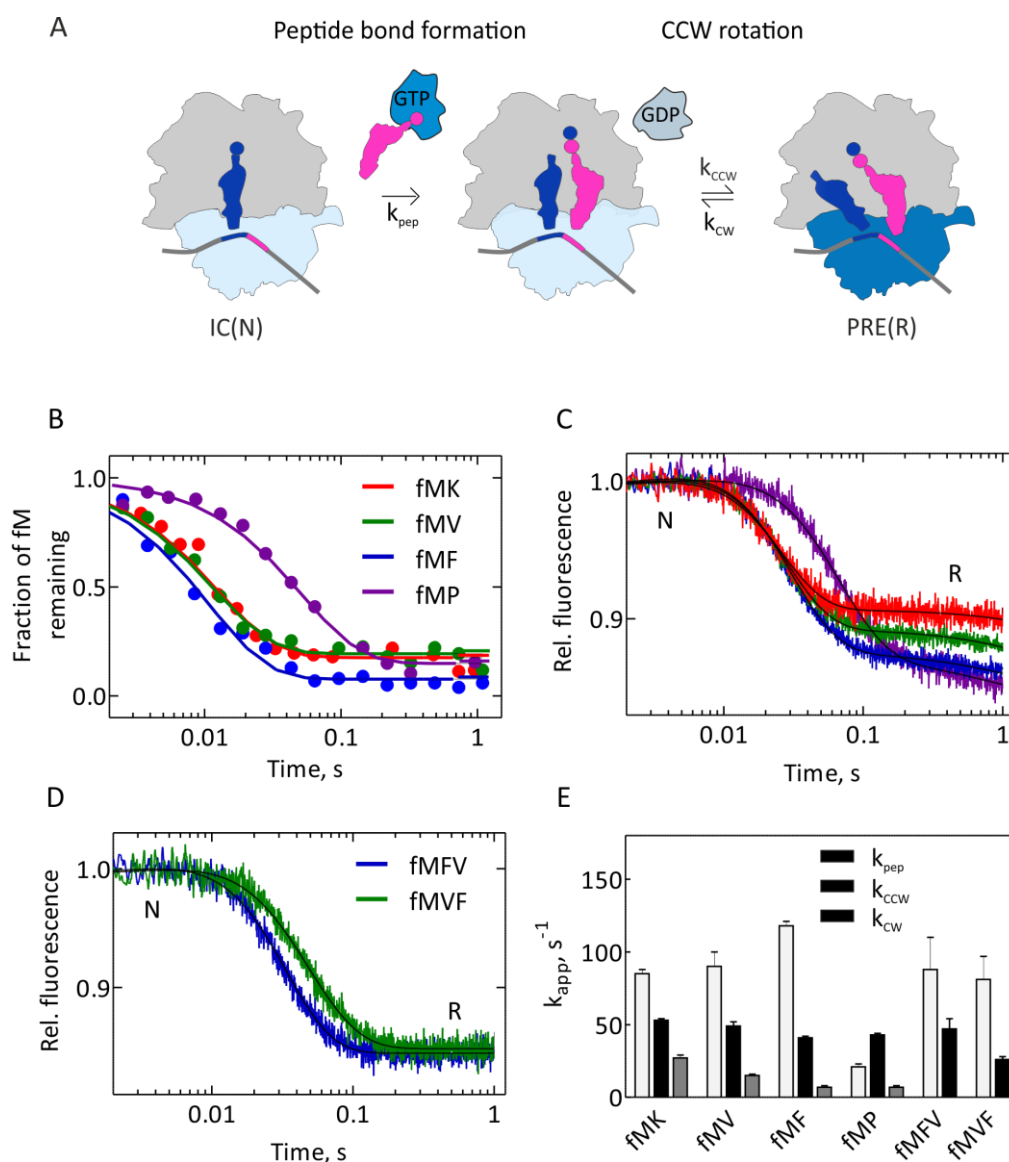


Figure 2.7 Spontaneous CCW subunit rotation with different tRNAs in the A site.

(A) Schematic representing the two consecutive steps of peptide bond formation and spontaneous CCW rotation of ribosomal subunit. Ternary complex EF-Tu-GTP-aa-tRNA binds to the initiation complex in the N state. Upon peptide bond formation, the PRE complex rotates spontaneously and reversibly from the N to R state. (B) Time course of peptide bond formation upon rapid mixing of initiation complex (0.1 μM) with saturating concentration of ternary complex (10 mM) EF-Tu-GTP-X-tRNA^X, where X is Lys, Val, Phe or Pro. (C) Time course of CCW subunit rotation observed as a decrease in fluorescence upon rapid mixing of initiation complex (0.1 μM) with saturating concentrations of ternary complex (10 μM) in a stopped-flow apparatus. Colour codes are the same as in (B). (D) Time course of CCW subunit rotation upon reaction of POST(fMF) or POST(fMV) complexes (0.1 μM) with saturating concentration of ternary complex (10 μM)

EF-Tu-GTP-Val-tRNA^{Val} or EF-Tu-GTP-Phe-tRNA^{Phe}, respectively. (E) Elemental rate constants of peptide bond formation (k_{pep}), spontaneous CCW (k_{CCW}) and CW (k_{CW}) subunit rotation determined by numerical integration analysis of the data shown in (B), (C) and (D). Values are mean \pm s.d. ($n = 3$ independent kinetic experiments). Smooth lines in (B), (C) and (D) represent the global fit. N is non-rotated and R is rotated ribosomal state.

The rates of peptidyl transfer reaction determined by single-exponential fitting were rapid and similar for fMK, fMV and fMF ($\sim 90 \text{ s}^{-1}$). fMP was formed more slowly ($\sim 20 \text{ s}^{-1}$) (**Figure 2.7B**). The similar apparent rates (k_{app}) of peptide bond formation for different complexes are in line with the notion that the rate of peptide bond formation is generally limited by the preceding step of accommodation of aa-tRNA unless the peptidyl transfer reaction is very slow as in the case of fMP (Wohlgemuth et al., 2008; Wohlgemuth et al., 2011). The CCW rotation was monitored as a decrease in fluorescence upon mixing of initiation complex with ternary complex in a stopped-flow experiment (**Figure 2.7C**). Although the kinetics of CCW rotation (apparent rates of the major step with $>80\%$ of the amplitude change, estimated by two-exponential fitting preceded by a delay) was similar in fMK, fMV and fMF except fMP which is slower, the amplitude change or the end level differed depending on the identity of the A-site tRNA (**Figure 2.7C**). The differences in the amplitudes were not due to different yields of dipeptides as the end levels of the peptidyl transfer reaction were similar (**Figure 2.7B**). For comparison, we also monitored the CCW rotation upon rapidly mixing of POST(fMV) or POST(fMF) complex with ternary complex EF-Tu-GTP-Phe-tRNA^{Phe} or EF-Tu-GTP-Val-tRNA^{Val}, respectively. The decrease in the fluorescence was observed with the maximum change in the amplitude for these complexes (**Figure 2.7D**).

Different end levels of reaction of initiation complex with ternary complex might reflect different proportions of spontaneously formed N and R state or the presence of intermediate rotational states depending on the identity of the A-site tRNA (**Figure 2.7C**). To distinguish between these two alternatives, we performed smFRET experiments and observed only two sub-populations with FRET efficiencies 0.7 and 0.5 in all cases (Adio et al., 2015). These FRET efficiencies represented the N (0.7) and R (0.5) states of the ribosome. On calculating the population distribution of these two states, we noted that the ratio of the two sub-population were different for different complexes depending on the A-site tRNA (**Figure 2.8**). As expected, initiation complex was predominantly present in the N state while the R state was favored in the PRE(fMF) (**Figure 2.8C**). In contrast, the majority of PRE(fMK) and PRE(fMV) complexes were present in the N state explaining the lower amplitude change observed for fMK or fMV compared to fMF (**Figure 2.8 compared to Figure 2.7C**). Addition of EF-G-GTP to PRE complexes resulted in translocation and the formation of a POST complex in the N state. The proportion of N state was identical for all POST complexes, independent of the identity of tRNA in the P site (**Figure 2.8**). The rates of CCW and CW subunit rotation calculated from spontaneous transition of PRE complex

were in agreement with previously reported values (**Table 1**) (Cornish et al., 2008; Qin et al., 2014; Wasserman et al., 2016). An example trace for spontaneous transition between the N and R state for PRE(fMK) and POST(fMK) is shown in **Figure 2.9**. High fluctuations in the FRET signals were observed for PRE(fMK) indicating that the PRE complex is highly dynamic in contrast to POST(fMK) complex in which the FRET signal was stable.

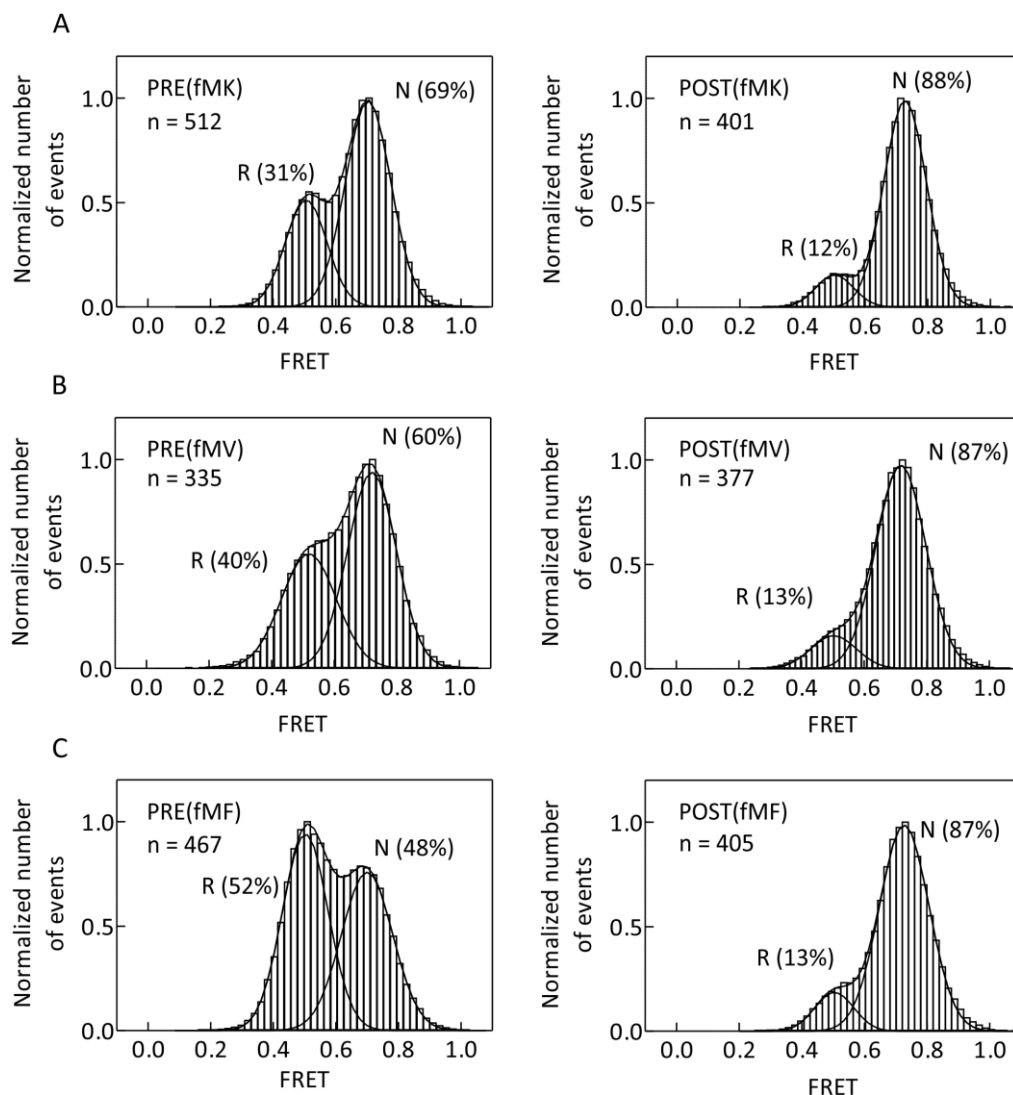


Figure 2.8 Population distribution of N and R state measured by smFRET.

PRE complexes formed with tRNA^{fMet} in the P site and fMetX-tRNA^X in the A site (left panel). Addition of EF-G-GTP to the PRE complex formed POST complex (right panel), where X is (A) Lys, (B) Val and (C) Phe. n is the number of traces analyzed. N is the non-rotated and R is rotated ribosomal state and numbers in brackets corresponds to their percentage in each complex. smFRET experiments were performed and analyzed by Dr. Sarah Adio and Dr. Tamara Senyushkina, respectively.

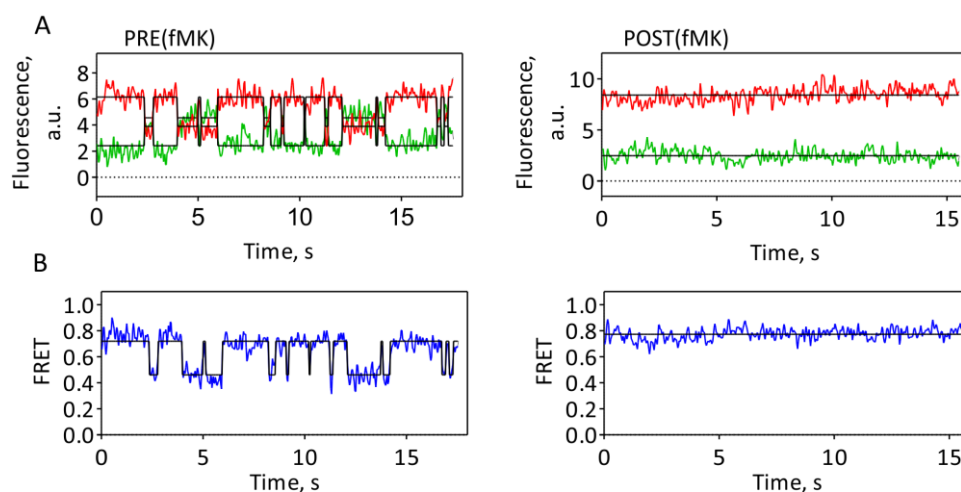


Figure 2.9 Spontaneous transition of CCW and CW subunit rotation observed by smFRET.

Representative example of single molecule fluorescence intensity trajectories (top panels) for the donor dye, Cy3 (red) and the acceptor dye, Cy5 (green) and the trajectory of smFRET (blue, lower panel) observed over time for (A) PRE(fMK) and (B) POST(fMK). smFRET experiments were performed and analyzed by Dr. Sarah Adio and Dr. Tamara Senyushkina, respectively.

Table 2.1 Rates of spontaneous N-to-R and R-to-N transitions determined by smFRET and ensemble kinetics

PRE	Experimental conditions			
	smFRET, 22°C ^a		TAKM ₇ , 37°C ^b	
	k_{CCW}, s^{-1} N → R	k_{CW}, s^{-1} R → N	k_{CCW}, s^{-1} N → R	k_{CW}, s^{-1} R → N
fMK (320) ^c	2.1 ± 0.1 (3557) ^d	3.7 ± 0.1 (3561) ^d	53 ± 1	27 ± 2
fMV (141) ^c	3.2 ± 0.3 (1153) ^d	3.9 ± 0.4 (1168) ^d	49 ± 3	15 ± 1
fMF (196) ^c	4.1 ± 0.2 (1768) ^d	3.0 ± 0.2 (1757) ^d	41 ± 1	7 ± 1

^aN is the population in high-FRET state (FRET efficiency = 0.7); R is the population in low-FRET state (FRET efficiency = 0.5).

^bRates calculated from numerical integration analysis of Figure 2.7.

^cThe number of dynamic traces used to calculate the transition rates between the two populations in smFRET experiments.

^dThe number of transitions observed in smFRET experiments.

All values are mean ± s.d. from 3 independent data sets.

Because the differences in the amplitudes of fluorescence signal in **Figure 2.7C** were due to different equilibria of spontaneously formed N and R state in different PRE complexes, we sought to determine the elemental rates of spontaneous CCW (k_{CCW}) along with CW (k_{CW}) rotation for PRE complexes by numerical integration analysis. We assumed a three-step model, with the first irreversible step of peptide bond formation, a second reversible step for CCW and CW subunit rotation and a third irreversible step that account for a minor decrease in fluorescence (<10% of the total amplitude change) observed towards the end of each stopped-flow trace. Numerical integration analysis gave the information about the absolute value of intrinsic fluorescence intensity (IFI) of the FRET reporter at each step during the course of the reaction (Belardinelli et al., 2016). We noted that the amplitude change for POST(fMF) complex after reacting with the ternary complex EF-Tu-GTP-Val-tRNA^{Val} (fMFV) was the highest and the absolute value of IFI at the end of the reaction was minimum (as decrease in the fluorescence was observed) in comparison to other complexes (**Figure 2.7C**). Because of two-state equilibrium between the N and R state of the ribosome, in a simplest model we assumed that the decrease in fluorescence is due to N to R transition and the difference in the end levels reflect different proportions of the R state of the ribosomes after the reaction is complete. Hence, POST(fMF) with the highest amplitude change assumed the highest percentage of the R state at the end of the reaction and a minimum IFI value. From differences in values of the IFI at the end of each reaction, one could estimate the elemental rate of CW rotation (k_{CW}). Therefore, we fixed the IFI value for the final rotated state to that of POST(fMF) and performed a numerical integration analysis of data for peptide bond formation and rotation for all different A-site tRNAs together. The elemental rates of CCW subunit rotation, k_{CCW} , for different A-site tRNA were in the range of 40-50 s⁻¹ while the elemental rates of CW subunit rotation, k_{CW} , varied from 7-27 s⁻¹ depending on the identity of the A-site tRNA (**Figure 2.7E and Table 1**). Thus, we concluded that the formation of the peptide bond, which results in decaylation of the P-site tRNA, drives rapid spontaneous CCW subunit rotation, however, differences in the rates of spontaneous CW rotation results in different equilibria of the N and R state for different A-site tRNAs.

2.5 Effect of EF-G on subunit rotation

It is often suggested that EF-G binding is restricted to the R state and that the rate of conversion from the N to R state determines the rate of EF-G-promoted translocation (Fei et al., 2008; Spiegel et al., 2007; Wasserman et al., 2016). On contrary, there are several studies that demonstrate that binding of EF-G is independent of the conformational state of the ribosome (Adio et al., 2015; Chen et al., 2011; Holtkamp et al., 2014a). Whether EF-G binds to ribosome in both N and R state and – if it does – how the kinetics of CCW subunit rotation is affected by EF-G are some of the questions which are currently unclear and controversial. To understand how EF-G affects subunit rotation, we prepared PRE complexes with deacylated tRNA^{fMet} in the P site and fMetX-tRNA^X in the A site (where X is Lys, Val, Phe and Pro (denoted as PRE(fMX)) and rapidly mixed them with saturating concentration of EF-G–GTP in a stopped-flow apparatus.

For PRE(fMK) and PRE(fMV), a biphasic change in the acceptor fluorescence was observed with an initial small downward phase reflecting CCW subunit rotation followed by a large upward phase that reported on the CW rotation upon translocation of the tRNA-mRNA complex promoted by EF-G (**Figure 2.10A**). For PRE(fMF) and PRE(fMP), the initial downward phase had a very small amplitude change (~2%) and the upward phase was preceded by a delay. The analysis of PRE(fMF) by numerical integration indicated that the delay actually comprised of small downward phase followed by an upward phase which cancels out each other (Belardinelli et al., 2016). Therefore, the analysis by exponential fitting was difficult in this case. In contrast, the FRET signal change in case of PRE(fMK) and PRE(fMV) could be analyzed by two-exponential fitting that yielded apparent rate constants for CCW (k_{app1}) and CW (k_{app2}) subunit rotation. We performed time courses of subunit rotation at increasing concentration of EF-G and the hyperbolic fit of the apparent rates of CCW (k_{app1}) and CW (k_{app2}) rotation yielded the rate constant of the CCW rotation (k_{CCW}) of $200 \pm 20 \text{ s}^{-1}$ or $210 \pm 10 \text{ s}^{-1}$ with K_M of $1.2 \pm 0.3 \text{ }\mu\text{M}$ or $1.5 \pm 0.2 \text{ }\mu\text{M}$ for PRE(fMK) or PRE(fMV), respectively. Similarly, the rate of CW rotation (k_{CW}) from the hyperbolic fit was $15 \pm 1 \text{ s}^{-1}$ or $11 \pm 1 \text{ s}^{-1}$ with K_M of $0.5 \pm 0.1 \text{ }\mu\text{M}$ or $0.7 \pm 0.1 \text{ }\mu\text{M}$ for PRE(fMK) or PRE(fMV), respectively (**Figure 2.10B and D**). Therefore, k_{CCW} in the presence of EF-G was about five-times faster than the spontaneous rotation (40 s^{-1} , Figure 2.7).

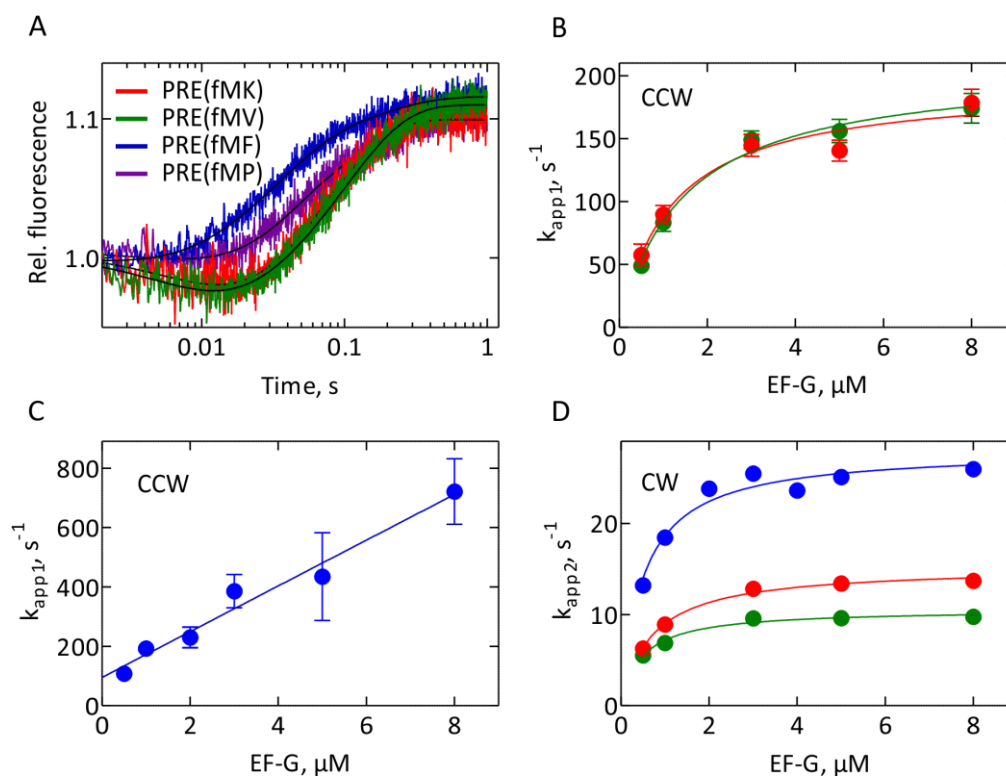


Figure 2.10 EF-G induced subunit rotation at 37°C.

(A) Time course of subunit rotation upon addition of EF-G-GTP (4 μM) to the PRE(fMX) complex (0.05 μM) in a stopped-flow apparatus. (B) and (C) EF-G concentration dependence of CCW rotation, k_{app1} , for (B) PRE(fMK) and PRE(fMV) and for (C) PRE(fMF). Colour codes are the same as in (A). (D) EF-G concentration dependence of CW rotation, k_{app2} for PRE(fMK), PRE(fMV) and PRE(fMF). Colour codes are the same as in (A). Smooth lines in A are exponential fits.

We also performed time course of subunit rotation for PRE(fMF) at increasing concentration of EF-G and estimated the rate constants with three-exponential fitting (**Figure 2.10C**). The apparent rate constant k_{app1} , reflecting CCW subunit rotation and constituting only 2% signal change, increased linearly with the EF-G concentration with a Y-axis intercept of $95 \pm 23 s^{-1}$ and slope of $77 \pm 7 \mu M^{-1} s^{-1}$. The linear dependence of k_{app1} implied a bimolecular binding step of EF-G with a K_d of about 1.2 μM . Although the exponential fitting should be used with caution for traces with delays and high k_{app} values, the results for PRE(fMF) were in good agreement with the expected linear concentration dependence and the K_d value obtained from numerical integration analysis (Belardinelli et al., 2016). This shows that the exponential fitting of PRE(fMF) could not resolve the EF-G binding step from subsequent CCW rotation. The hyperbolic fit of the apparent rate constant of CW rotation, k_{app2} , constituting >80% of signal change, yielded the rate constant of CW rotation of $28 \pm 1 s^{-1}$ with K_M of $0.5 \pm 0.1 \mu M$. The third phase is a minor phase (<20% of amplitude change) with k_{app3} of about $6 \pm 1 s^{-1}$ and is independent of the EF-G concentration. The biphasic behavior of CW rotation is consistent with the multi-step mechanism of translocation (Belardinelli et al., 2016). Similar results were obtained for PRE(fMP) by three-exponential fitting

with the apparent rate constant of CW rotation of, k_{app2} and k_{app3} , $30 \pm 6 \text{ s}^{-1}$ (70% amplitude change) and $6 \pm 1 \text{ s}^{-1}$ (30% amplitude change), respectively.

Next, we measured the rate of translocation for different complexes using the time-resolved Pmn assay and compared it with that of subunit rotation. To measure the rate of authentic translocation (k_{TL}) we prepared PRE complexes and rapidly mixed them with EF-G-GTP and Pmn. Time course of Pmn reaction of PRE complex was then compared to that of POST complex (Methods). The time required for PRE complex to react with Pmn includes the time for both translocation and the Pmn reaction of the resulting POST complex, which allowed us to determine the intrinsic rate of translocation (Holtkamp et al., 2014a). Single-exponential fitting of the time course of the Pmn reaction for PRE and POST complexes determined the rate constants k_{PRE} and k_{POST} , respectively. The rates of tRNA translocation (k_{TL}) calculated from k_{PRE} and k_{POST} were $12 \pm 2 \text{ s}^{-1}$ (37°C) for PRE(fMV) and $28 \pm 6 \text{ s}^{-1}$ (37°C) for PRE(fMF) (**Figure 2.11C and D**), which were almost identical to the rates of CW subunit rotation for these complexes indicating that the two processes are coupled (**Figure 2.11A**). This result was corroborated with the estimation of mRNA translocation rates, monitored as a decrease in the fluorescence of Alexa 405-labeled mRNA upon rapid mixing of PRE complexes with EF-G-GTP (**Figure 2.11B**).

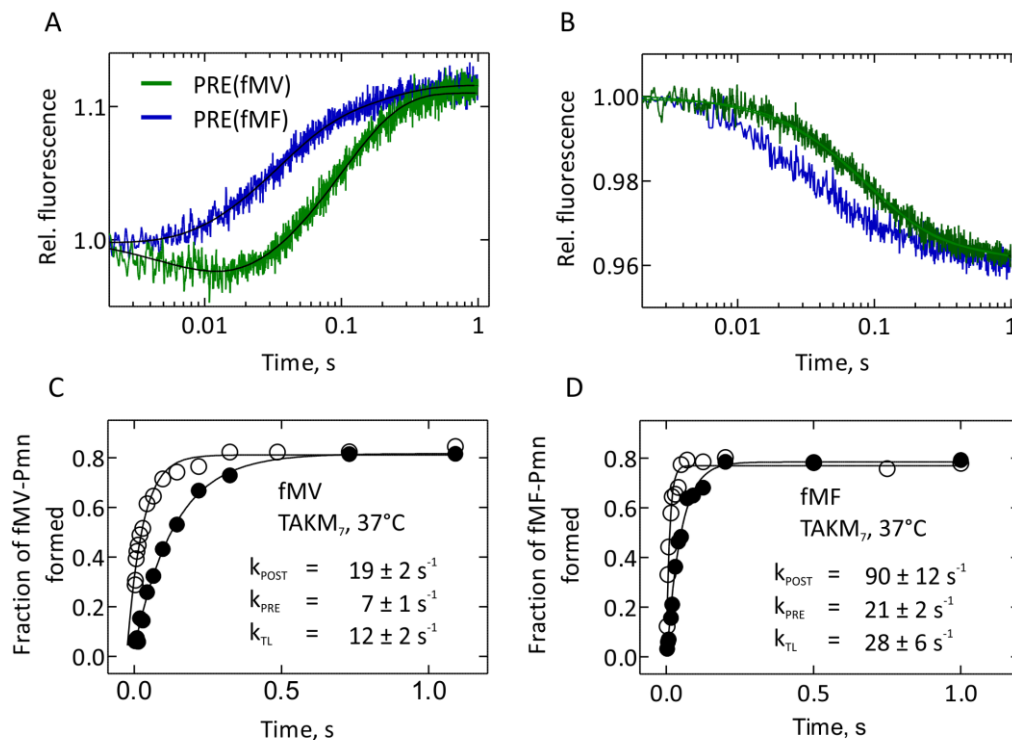


Figure 2.11 CW subunit rotation coupled to translocation.

(A) Time course of subunit rotation upon addition of EF-G-GTP (4 μM). The elemental rate constants of CW rotation, k_{CW} , obtained from data shown in Figure 2.10D are reported. (B) Time courses of mRNA translocation monitored as a decrease in the fluorescence of Alexa405-labeled mRNA. The apparent rate constants (k_{app1}) of the major phase (>80%) are reported. Colour codes are the same as in (A). (C) and (D) Time-resolved Pmn assay for (C) Val and (D) Lys in TAKM₇ at 37°C. Open circles represent the reaction of

Pmn (10 mM) with POST complex (0.1 μ M); closed circles represent the reaction of Pmn with PRE complex upon addition of EF-G (4 μ M). The rate of translocation (k_{TL}) was calculated from k_{POST} and k_{PRE} as described in Methods.

To further verify that the CW subunit rotation is coupled to the tRNA-mRNA translocation, we used EF-G(H583K), a slowly translocating mutant with single amino acid replacement in domain IV of EF-G or GTP γ S – a non-hydrolyzable GTP analogue. We monitored subunit rotation after rapidly mixing PRE(fMF) or PRE(fMV) with either EF-G(H583K)–GTP or EF-G–GTP γ S (**Figure 2.12**) and the time courses were analyzed with two-exponential and three-exponential fitting for PRE(fMV) and PRE(fMF), respectively, as described before for wild type EF-G–GTP. For PRE(fMV), the apparent rate of CCW rotation (k_{app1}) was only slightly affected by the use of either EF-G(H583K) or EF-G–GTP γ S (only ~2-3 times slower) however, the apparent rate constant (k_{app2}) for the CW subunit rotation were drastically impaired (70-fold slower). The large effect of EF-G(H583K) or EF-G–GTP γ S in case of PRE(fMF) allowed us to resolve the first step of CCW rotation, which was visually absent in the reaction with wild type EF-G. The amplitude change was only 2%, which is identical to the value determined by numerical integration analysis for EF-G–GTP (Belardinelli et al., 2016). The apparent rate of CCW rotation (k_{app1}) were $300 \pm 90 \text{ s}^{-1}$ or $140 \pm 30 \text{ s}^{-1}$ for EF-G(H583K) or EF-G–GTP γ S, respectively. For CW rotation, the values of k_{app2} were $2.3 \pm 0.2 \text{ s}^{-1}$ (36% of the amplitude change) or $13 \pm 4 \text{ s}^{-1}$ (64% of the amplitude change) and the values of k_{app3} were $0.40 \pm 0.02 \text{ s}^{-1}$ (90% of the amplitude change) or $0.50 \pm 0.1 \text{ s}^{-1}$ (90% of the amplitude change) for EF-G(H583K) or EF-G–GTP γ S, respectively. This is line with a multi-step mechanism of translocation that is altered in the absence of GTP hydrolysis or by the use of slow translocating EF-G mutants (Belardinelli et al., 2016). Translocation with the EF-G(H583K) was slow but complete, as the end level of fluorescence signal was the same as with the wild type EF-G. In contrast, GTP γ S blocks the CW subunit rotation and stabilizes EF-G on the ribosome resulting in a drastic reduction of the amplitudes. As there was no difference in the kinetics of CCW subunit rotation in the presence of GTP γ S, we concluded that the CCW subunit rotation is a step that follows EF-G binding but occurs before hydrolysis of GTP by EF-G. In depth kinetic analysis of EF-G-dependent translocation in the presence of GTP γ S is described in detail in section 2.6.

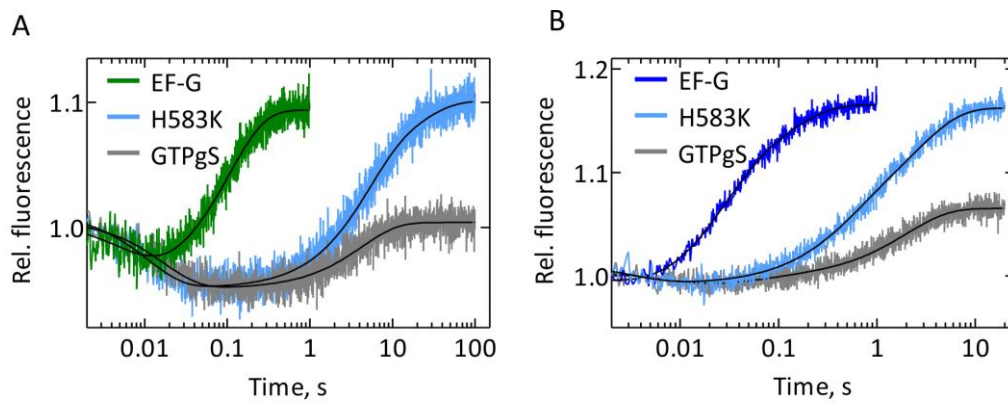


Figure 2.12 Inhibition of translocation and CW subunit rotation.

Time course of subunit rotation upon rapid mixing of (A) PRE(fMV) or (B) PRE(fMF) ($0.05 \mu\text{M}$) with EF-G–GTP, EF-G(H583K)–GTP or EF-G–GTP γ S ($4 \mu\text{M}$) in a stopped-flow apparatus. Smooth lines represent exponential fits.

In order to compare our results with smFRET observations (typically performed at 22°C) we performed time courses of subunit rotation for PRE(fMK) at increasing concentration of EF-G at 25°C and determined the rates of CCW ($k_{\text{app}1}$) and CW ($k_{\text{app}2}$) rotation by two-exponential fitting (**Figure 2.13**). The hyperbolic fit of EF-G concentration dependence of $k_{\text{app}1}$ and $k_{\text{app}2}$ yielded the rate constants, k_{CCW} of $50 \pm 3 \text{ s}^{-1}$ ($K_{\text{M}} = 0.7 \pm 0.2 \mu\text{M}$), which is 5-times faster than the spontaneous CCW rotation at 25°C (10 s^{-1} , compared to Figure 2.6) and k_{CW} of $4 \pm 0.1 \text{ s}^{-1}$ ($K_{\text{M}} = 0.8 \pm 0.1 \mu\text{M}$), similar to the rate of tRNA translocation at this temperature (2 s^{-1}) (**Figure 2.15**). The translocation rate (k_{TL}) for PRE(fMK) at 37°C was $12 \pm 2 \text{ s}^{-1}$ which is again similar to the rate of CW subunit rotation (**Figure 2.10D**) measured at this temperature. All these results suggested that EF-G accelerates the CCW rotation by a factor of five, compared to the spontaneous rotation, and that the tRNA-mRNA movement is much slower (by about 20-fold) than EF-G-induced CCW rotation and it is coupled to CW subunit rotation.

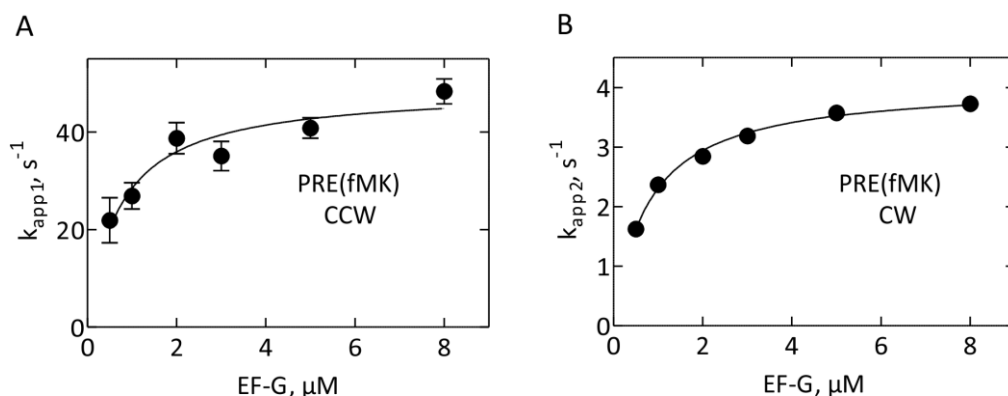


Figure 2.13 EF-G-induced subunit rotation at 25°C .

EF-G concentration dependence of (A) CCW and (B) CW subunit rotation monitored at 25°C for PRE(fMK) ($0.05 \mu\text{M}$).

In order to correlate the results from ensemble kinetics and smFRET, we performed the ensemble kinetic experiments under smFRET buffer and temperature conditions i.e in TAKM₁₅ with 1 mM spermidine and 8 mM putrescine at 22°C. Upon rapid mixing of PRE complex with EF-G–GTP, we observed a well resolved downward phase of CCW rotation followed by an upward phase of CW rotation for PRE(fMK) and PRE(fMV) (**Figure 2.14**). No downward phase was observed for PRE(fMF) even at these conditions.

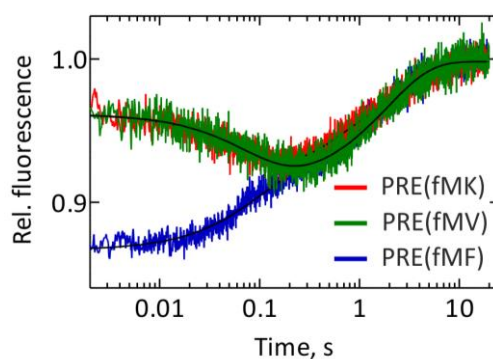


Figure 2.14 Rapid kinetics of subunit rotation monitored under smFRET conditions.

Time course of subunit rotation upon rapid mixing of PRE(fMX) (0.05 μ M) with EF-G–GTP (4 μ M) in stopped-flow. X is Lys, Val or Phe. Smooth lines represent exponential fits.

The ratios of the amplitudes change of CCW rotation (downward phase) to the overall transition from the R to N state (upward phase) estimated the fraction of ribosomes present in the N state prior to the addition of EF-G in PRE(fMK) and PRE(fMV). The fractions of the N state calculated were 60% for PRE(fMK) and 57% for PRE(fMV) complex, very close to the fractions obtained from state distributions in the smFRET experiments (**Figure 2.8**) indicating good agreement between two approaches. With the analogous calculation from the ratio of amplitude change of CCW and CW rotation, we estimated 41% and 35% of PRE complex in the N state in TAKM₇ at 37°C for PRE(fMK) and PRE(fMV), respectively and 44% of PRE(fMK) in the N state in TAKM₇ at 25°C (**Figures 2.10A and 2.13**). For PRE(fMF), the fraction of the N state calculated from the IFI values was 12% (Belardinelli et al., 2016). As the fractions of the N state in the PRE(fMK) and PRE(fMV) were higher than in PRE(fMF), the resulting amplitude of the CCW rotation (downward phase) upon reaction with EF-G was much larger for two complexes (**Figure 2.10**). From the kinetic analysis of ensemble experiments at smFRET conditions, we obtained the apparent rates of CCW and CW rotation by two exponential fitting. The apparent rates of CCW (k_{app1}) rotation were $14 \pm 1 \text{ s}^{-1}$ and $12 \pm 1 \text{ s}^{-1}$ for PRE(fMK) and PRE(fMV), respectively, which were again about five-times faster than spontaneous transitions (**Table 2.1**). The apparent rate of CW rotation (k_{app2}) were 1 s^{-1} and 0.6 s^{-1} which were identical to the rate of translocation (k_{TL}) for PRE(fMK) and PRE(fMV) (**Figure 2.15, Table 2.2**).

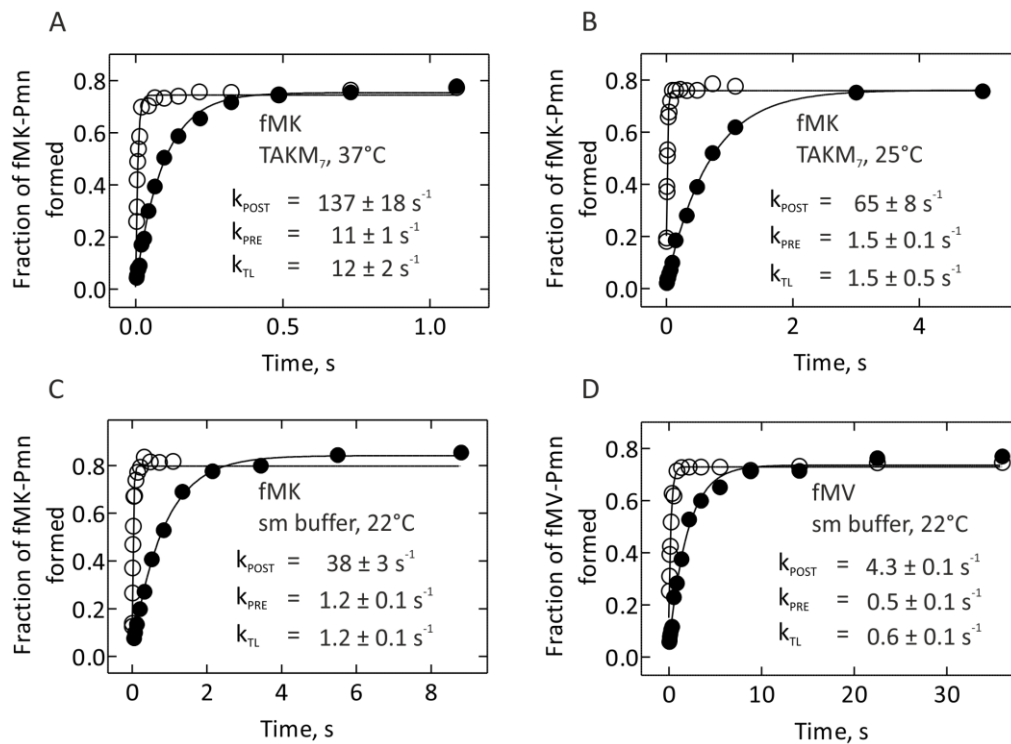


Figure 2.15 Time resolved Pmn assay to determine the rate of translocation.

Time course of Pmn reaction for fMK in TAKM₇ at (A) 37°C and (B) 25°C. Time course of Pmn reaction in sm buffer at 25°C for (C) fMK and (D) fMV. Open circles represent the reaction of Pmn with POST complex with apparent rate constant k_{POST} ; closed circles represent the reaction of Pmn with PRE complex upon addition of EF-G-GTP with apparent rate constant k_{PRE} . The rate of translocation (k_{TL}) was calculated from k_{POST} and k_{PRE} as described in methods.

Time courses of subunit rotation with PRE(fMF) did not show CCW rotation (downward phase) even though 47% of PRE(fMF) were in the N state (**Figure 2.14**). In-depth kinetic analysis of these complexes suggested that CCW rotation coincides with the initial binding step of EF-G and it is likely that at the high concentration of EF-G used in these experiments, the rate of CCW rotation became too high to be monitored with the stopped-flow apparatus (**Figure 2.10**). The CW rotation (upward phase) for PRE(fMF) showed a biphasic behavior with the apparent rate constants of $11 \pm 0.3 \text{ s}^{-1}$ and $0.50 \pm 0.01 \text{ s}^{-1}$. Thus, under all the conditions studied, EF-G accelerates the CCW subunit rotation on the fraction of PRE complex that remained in the N state after peptide bond formation and the CW subunit rotation is coupled to the tRNA-mRNA translocation.

Table 2.2 Summary of rates for EF-G-induced rotation and translocation.

PRE	k_{CCW}, s^{-1}	k_{CW}, s^{-1}	k_{TL}, s^{-1}
TAKM ₇ , 37°C			
fMK	200 ± 20	15 ± 1	12 ± 2
fMV	210 ± 10	11 ± 1	12 ± 2
fMV (EF-G-GTPγS)	60 ± 4	0.23 ± 0.01	-
fMV (EF-G(H853K))	100 ± 8	0.200 ± 0.002	-
smFRET buffer, 22°C			
fMK	14 ± 1	1.2 ± 0.1	1.2 ± 0.1
fMV	12 ± 1	0.5 ± 0.1	0.5 ± 0.1
TAKM ₇ , 25°C			
fMK	50 ± 3	4 ± 1	2 ± 1

2.6 Global-fitting of translocation kinetics

The finding that EF-G can bind to ribosome complexes in both the N and R state and that EF-G-induced CCW rotation is much faster than the tRNA-mRNA translocation has important consequences for understanding the thermodynamic landscape of translocation. In addition, we observed that CW rotation of the SSU is kinetically correlated with the tRNA-mRNA translocation. However, the exact sequence of events on the time axis of the translocation pathway is not clear. For these reasons, we reconstructed the choreography of collective motions of the ribosome during translocation by using nine different fluorescence reporters placed at strategic positions on the SSU, the LSU, tRNA, mRNA and on EF-G and monitored their motion in real time using ensemble kinetics (**Table 2.3**) (Belardinelli et al., 2016). We combined time courses obtained for PRE(FMF) complex with different FRET pairs at up to six different concentration of EF-G and performed a global analysis by numerical integration (**Figure 2.16**).

Table 2.3 Positions of fluorescence reporters used for kinetic studies of translocation*.

Positions and labels	Reaction monitored
L12Alx488–EF-G(QSY9)	EF-G association and dissociation
S13Alx488	EF-G association, conformational changes of the SSU
S6Alx488–L9Alx568 (S6–L9)	SSU body rotation
S13Atto540Q–L33Alx488 (S13–L33)	SSU head swiveling
tRNA ^{fMet} (Flu)	P-site tRNA movement
tRNA ^{fMet} (Flu)–S13Atto540Q	
tRNA ^{fMet} (Flu)–L33Atto540Q	
mRNA (3'end), Alx405 or Alx488	mRNA translocation

*Dr. Riccardo Belardinelli carried out all experiments with S13Alx488, S13Atto540Q–L33Alx488 and tRNA^{fMet} (Flu). Dr. Carlos E. Cunha performed experiments with L12Alx488–EF-G(QSY9) and mRNAAlx488. The data for mRNAAlx405 are from (Holtkamp et al., 2014a). Dr. Riccardo Belardinelli performed the numerical integration analysis of data for the kinetic model of translocation (Belardinelli et al., 2016).

We used a linear 5-step kinetic model with an initial reversible step accounting for EF-G binding and dissociation followed by four irreversible steps, which were the minimum number of steps required to fit all data satisfactorily (**Figure 2.16A**). We assumed that steps 2-5 were quasi-irreversible because translocation in the presence of EF-G and GTP is highly committed to forward movement. Global fitting of the data not only provided the elemental rate constant of

each step but also allowed us to calculate the characteristic fluorescence of the kinetic intermediates for each reporter at each step, called intrinsic fluorescence intensity (IFIs), which is analogous to the FRET values obtained in smFRET studies. The change in the IFI from one step to another provides characteristic fluorescence signature for a given FRET pair (**Figure 2.16B and C**). The IFIs were calculated in an unbiased manner without any prior assumption of how a given reporter might change the fluorescence at each step. Therefore, the values indicate the direction of motions of each component and decipher the sequence of rearrangements monitored with each FRET pair.

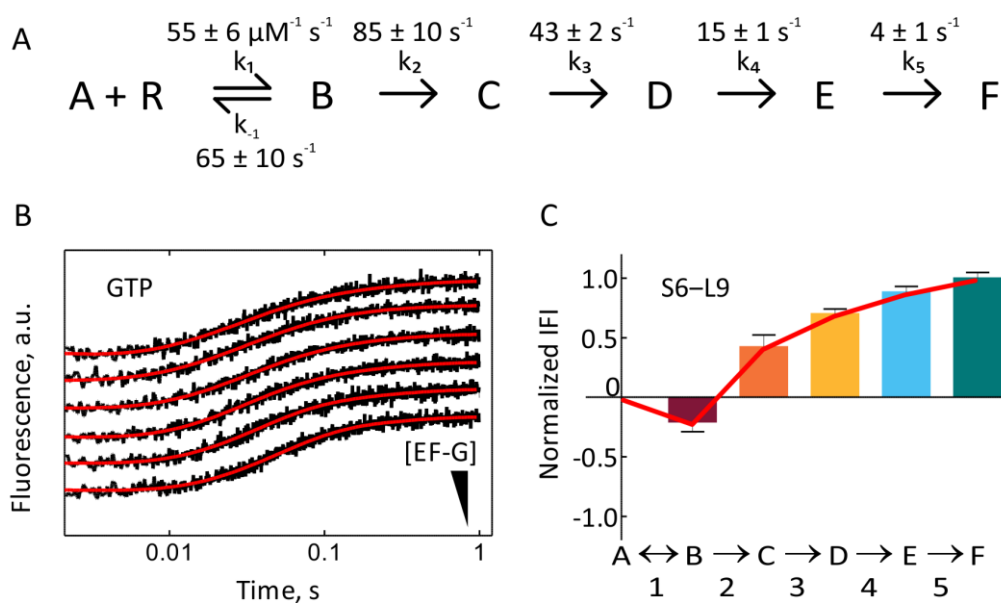


Figure 2.16 Global fitting of translocation kinetics with EF-G and GTP (traces for the S6–L9 FRET pair are shown).

(A) Linear 5-step model used for numerical integration analysis. Elemental rate constants indicated in the scheme are results of the global fit; values are mean \pm s.e.m. (B) Time courses of SSU body rotation for PRE(fMF) (0.05 μ M) (S6–L9 FRET pair) with increasing concentration of EF-G in the presence of GTP are shown in black and the respective global fits are shown in red (shifted relative to each other for visual clarity) (for each time course, $N_t = 8$, technical replicates). The direction of the increase of the concentration of EF-G is indicated. (C) Normalized intrinsic fluorescence intensities (IFI) of intermediates for S6–L9 FRET pair in each translocation step as indicated below the graph (normalized IFI values were used to compare fluorescence signatures of different observables for the same reaction (Belardinelli et al., 2016). Red lines represent fluorescence signatures for S6–L9 FRET pair; values are mean \pm s.d.

In step 1, EF-G binds to the ribosome, monitored as the FRET between the L12–EF-G pair or as a change in the fluorescence of S13Alx488. The reaction is rapid and reversible, consistent with previous reports (Chen et al., 2013a; Katunin et al., 2002; Peske et al., 2004; Rodnina et al., 1997). Inspection of the IFI values suggested that EF-G binding also led to a change in fluorescence of S6–L9 FRET pair (**Figure 2.16C**) (Belardinelli et al., 2016). This observation may be explained by EF-G-induced CCW rotation of the SSU upon EF-G binding. Analogous to the calculation of the ratio of N and R state in section 2.5, the ratio of change of the IFI value in step 1

(N-to-R transition) to the overall change in the IFI value from step 2 to step 5 (R-to-N transition) gave the proportion of PRE(fMF) complex in the N state prior to the addition of EF-G. Under our conditions, a large proportion of the PRE complex assumed the R state (88%) while the complexes that remained in the N state were converted to the R state upon EF-G binding thus resulting in the observed CCW rotation of the SSU body. In addition, the change in fluorescence of the S13–L33 FRET pair due to CCW swiveling of head of the SSU was also observed upon EF-G binding (Belardinelli et al., 2016).

In step 2, the largest change in the IFI value for the S6–L9 FRET pair was observed as the SSU body starts to rotate in CW direction while the SSU head continues its motion in CCW direction. This is evident from the trend of the fluorescence signatures for the S6–L9 and the S13–L33 FRET pairs that go in opposite directions, reflecting movements of body and head of the SSU in opposite direction (**Figure 2.17**). This indicates that the CW movement of the SSU body is an early step in the translocation pathway as opposed to previous report, in which the CW body rotation was proposed to be a late discrete step of translocation or occur simultaneously with the CW swiveling of the head (Ermolenko and Noller, 2011). Step 3 and step 4 represent synchronous movements of A-to-P and P-to-E displacement of the two tRNAs and the mRNA. At this point the head starts to swivel in CW direction, while the SSU body continues its gradual motion in CW direction followed by dissociation of EF-G from L12. Finally, at step 5 the SSU body and head reach their final POST positions and the deacylated tRNA dissociates from the ribosome through the E site.

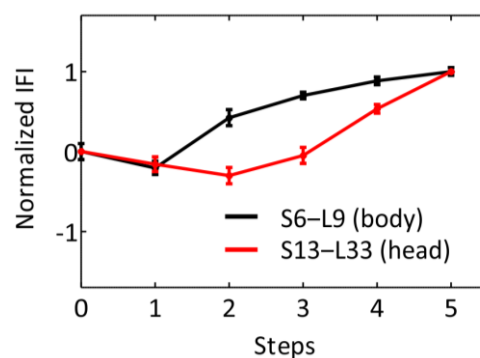


Figure 2.17 Fluorescence signatures composed of IFI values for 5-step kinetic model.

Comparison of the IFI signatures for the S6–L9 (black) and S13–L33 (red) FRET pairs during EF-G–GTP dependant translocation.

To uncouple the pre-hydrolysis steps from those accelerated by GTP hydrolysis, we performed the numerical integration analysis with a 5-step linear kinetic model of time courses obtained with different FRET pairs in the presence of GTP γ S (**Figure 2.18A and B**). We observed that replacing GTP with GTP γ S had little effect on the rate of step 1 confirming that GTP hydrolysis is not required for the CCW rotation of the SSU. Similarly, step 2 and 4 were slowed down by a

factor of 3 or 5, respectively. In contrast, the rate of step 3 and 5 were reduced dramatically by a factor of 40 and 20, respectively, consistent with results of previous reports showing the effect of GTP hydrolysis on the rate of translocation of the tRNA-mRNA complex (Cunha et al., 2013; Holtkamp et al., 2014a; Rodnina et al., 1997).

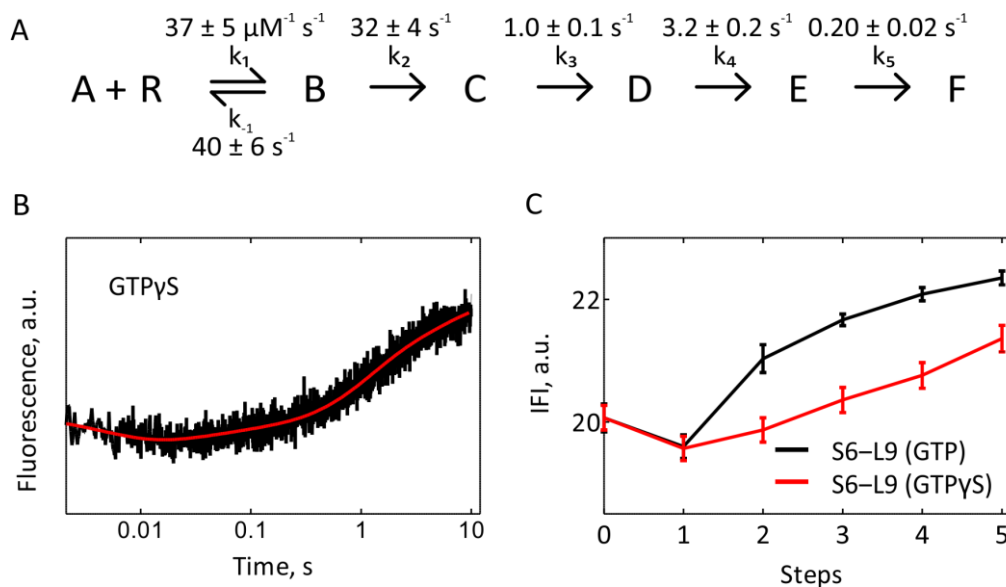


Figure 2.18 Effect of GTP hydrolysis on translocation.

(A) Linear 5-step kinetic model used for numerical integration with elemental rate constants resulting from the global fit; values are mean \pm s.e.m. (B) Time course of SSU body rotation obtained by rapid mixing of PRE(FMF) (0.05 μM) with EF-G (4 μM) in the presence GTP γ S (black) and the respective global fit (red) from numerical integration (Nt = 8, technical replicates). (C) Comparison of IFI signatures of EF-G-dependent translocation with GTP (black) and GTP γ S (red); values are mean \pm s.d.

In addition to the effect of GTP γ S on the rate constants, the fluorescence signature of some FRET pairs were altered. In the presence of GTP γ S, the largest change in the IFI for CW movement of the SSU body was observed in step 5 rather than in step 2 demonstrating that the SSU body started rotating in the CW direction after rather than before tRNA movement (**Figure 2.18C**). Similarly, the fluorescence signatures for S13Alx488, the S13-L33 and the L12-EF-G FRET pair were also changed indicating that when GTP hydrolysis is prevented, translocation proceed through a different pathway resulting in the formation of different intermediates than when GTP is hydrolyzed (Belardinelli et al., 2016).

2.7 Effect of variants of EF-G on subunit rotation

We established that binding of EF-G–GTP to the N state of the ribosome induces the CCW subunit rotation while GTP hydrolysis by EF-G promotes CW subunit rotation accompanied by tRNA–mRNA translocation. To further understand the role of EF-G in subunit rotation we used variants of EF-G which are either defective in GTP hydrolysis (EF-G(H91A)) or incapable of undergoing conformational rearrangements important for translocation (EF-G(Δ 4/5) or EF-G(XL)) (Cunha et al., 2013; Peske et al., 2000; Savelsbergh et al., 2003). EF-G(H91A) is a GTPase deficient mutant in which His 91 is replaced with Ala resulting in 30-fold decrease in the rate of translocation. EF-G(Δ 4/5) lacks domain IV and V while in EF-G(XL), the mobility of domain I and V is restricted by a reversible disulfide cross-link between the two domains. These mutants do not interfere with GTP hydrolysis but inhibit subsequent step of translocation. To monitor the effect of these variants on subunit rotation, we prepared PRE(fMF) complexes and rapidly mixed them with either EF-G–GTP, EF-G(H91A)–GTP or EF-G(Δ 4/5)–GTP in a stopped-flow apparatus (**Figure 2.19A**).

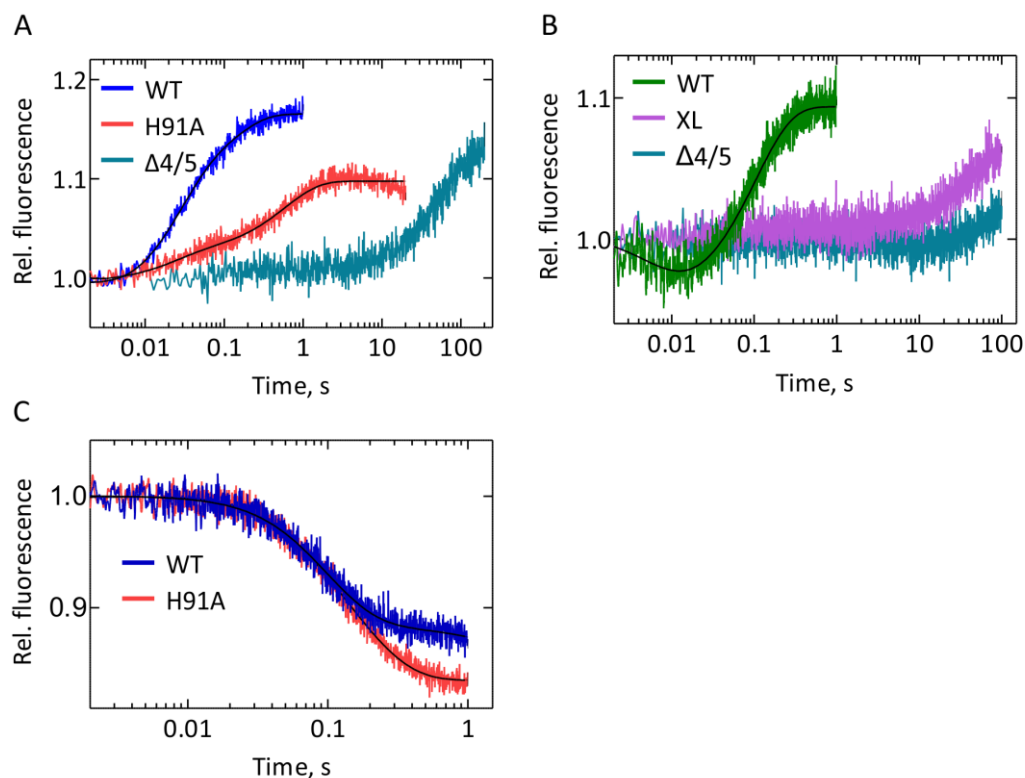


Figure 2.19 Subunit rotation monitored with variants of EF-G.

(A) Time course of subunit rotation upon rapid mixing of PRE(fMF) (0.05 μ M) with EF-G–GTP, EF-G(H91A)–GTP or EF-G(Δ 4/5)–GTP (4 μ M). (B) Time course of subunit rotation upon rapid mixing of PRE(fMV) (0.05 μ M) with EF-G–GTP, EF-G(XL)–GTP or EF-G(Δ 4/5)–GTP (4 μ M). (C) Time course of CCW subunit rotation upon rapid mixing of POST(fMV) (0.1 μ M) with Pmn (10 mM) in the absence or presence of EF-G(H91A) (4 μ M). Smooth lines represent exponential fits.

Time course of subunit rotation for PRE(fMF) with EF-G(H91A) showed a complex behavior and was fitted with three-exponential terms with a slope. The apparent rate of the

major phase of CW rotation, constituting 75% of the total signal change, was about $2.0 \pm 0.1 \text{ s}^{-1}$. This value is about 15 times smaller than the value obtained for wild type EF-G–GTP but in the same range as the apparent rate of subunit rotation observed with EF-G–GTPyS (0.5 s^{-1}). The subunit rotation with EF-G($\Delta 4/5$) showed an extremely slow upward phase with a long preceding delay. Since the signal did not reach the end level during the time window of measurement and because of long initial delay, the apparent rate constant of CW rotation could not be determined by exponential fitting. Domain IV of EF-G along with domain V is crucial for translocation and couples the conformational changes in EF-G to forward movement of the tRNAs. Therefore, the absence of these domains impairs the CW subunit rotation along with translocation.

The small amplitude ($\sim 2\%$) of CCW subunit rotation with the PRE(fMF) complex gave no information about the effect of the EF-G variants on this step. To monitor the effect of mutations in EF-G on CCW subunit rotation, we used PRE(fMV) complex in which 35% of the ribosome complexes were in the N state prior to addition of EF-G. We rapidly mixed PRE(fMV) complexes with either EF-G–GTP, EF-G($\Delta 4/5$)–GTP or EF-G(XL)–GTP in a stopped-flow apparatus (**Figure 2.19B**). With both mutants, no CW rotation was observed similar to PRE(fMF) complex. Unexpectedly, CCW subunit rotation was not observed, either. The absence of the fluorescence signal for the CCW subunit rotation with these mutants indicates that the binding of EF-G alone is not enough to induce CCW rotation. Instead, a specific conformational rearrangement in EF-G particularly involving domain IV, after binding but before GTP hydrolysis, is responsible for driving CCW subunit rotation. This is in agreement with the hyperbolic dependence of CCW subunit rotation with increasing concentrations of EF-G (**Figure 2.10B**).

EF-G stabilizes the R state of the ribosome upon binding. However, the life-time of the R state is very short, because EF-G binds very rapidly and drives the ribosome to the POST state and dissociate. To stabilize EF-G binding to the ribosome, EF-G is often trapped on the ribosome using either analogues of GTP or antibiotics. We used EF-G(H91A), which can stably remain bound to the ribosome and monitor the CCW subunit rotation (Cunha et al., 2013). We prepared POST(fMV) complex and rapidly mixed them with Pmn in the absence or presence of EF-G(H91A)–GTP (**Figure 2.19C**). We observed that the kinetics of the CCW subunit rotation was similar in both cases with the apparent rate constant of $10 \pm 1 \text{ s}^{-1}$ and $7 \pm 1 \text{ s}^{-1}$ in the absence and presence of EF-G(H91A), respectively. However, the change of the amplitude was greater when EF-G(H91A) was bound to the complex as compared to in its absence. This is consistent with the previously published smFRET report which showed that the binding of EF-G–GDPNP to the POST complex with deacylated tRNA^{fMet} in the P site increased the percentage of the ribosome in the R state (Cornish et al., 2008).

2.8 Effect of magnesium ion (Mg^{2+}) concentration on subunit rotation

In solution, the ribosome fluctuates between the N-C and R-H states and the distribution between the two states reflect the equilibrium. Formation of the H state depends on ionic conditions and in particular on Mg^{2+} ions concentration (Agirrezabala et al., 2008; Kim et al., 2007). SmFRET experiments have suggested that by increasing the concentration of Mg^{2+} ions, the lifetime of the C state increases but the lifetime of the H state is not affected (Kim et al., 2007). This means that at high Mg^{2+} ion concentrations (>15 mM) the majority of ribosomes should be in the C state. Because formation of the H state of the tRNAs is loosely coupled to the ribosome rearrangement into the R state, we wanted to measure the effect of the Mg^{2+} ions on the kinetics of subunit rotation and population distribution between the N and R state.

We prepared PRE(fMF) in TAKM_{3.5}, assuming that most of the PRE(fMF) complex would be in the R state because of the low Mg^{2+} ion concentration, and rapidly mixed it with TAKM₃₆ in a stopped-flow apparatus (**Figure 2.20A**). At the final Mg^{2+} ion concentration after the mixing (20 mM) the tRNAs in the PRE complex are expected to move to the C state and the ribosomal subunit should spontaneously rotate in the CW direction from R to N state. However, no change in the fluorescence signal was observed, indicating no change in the rotational state of the ribosome. Next, we measured the subunit rotation at 21 mM Mg^{2+} to monitor EF-G-dependent rotation at high Mg^{2+} concentration. If higher concentration of Mg^{2+} ion effects the population distribution between the N and R state, we would expect to observe downward phase for CCW rotation (which was absent in TAKM₇), followed by an upward phase for CW rotation upon translocation. Again, no CCW rotation was observed and the kinetics of CW rotation was similar to that in TAKM₇ with the apparent rate of the major phase of around $40 \pm 4 \text{ s}^{-1}$ (**Figure 2.20A**).

One potential explanations for the observed lack of the equilibrium upon changing Mg^{2+} concentration is that the kinetics of CCW subunit rotation for PRE(fMF) is very fast and cannot not be resolved even at high Mg^{2+} ion concentrations. Thus, PRE(fMF) may not be best substrate for studying concentration dependence of Mg^{2+} ions on spontaneous CCW subunit rotation. Therefore, we prepared PRE(fMV) in a high Mg^{2+} buffer and rapidly mixed with EF-G-GTP. At these conditions, the CCW rotation can be reliably monitored (**Figure 2.14**); if at high Mg^{2+} ion concentrations the N state of the PRE complex was stabilized, we would expected a greater change in the amplitude of CCW rotation. However, no difference in the amplitude change was observed for both the CCW and CW subunit rotation and the kinetics of subunit rotation were identical to that of TAKM₇ (**Figure 2.20B**). We concluded that the Mg^{2+} ions concentration has no effect on the stabilization of either N or R state. These results are in line with the smFRET study that demonstrated that the Mg^{2+} ion concentrations had no effect on the kinetics of subunit rotation (Marshall et al., 2008).

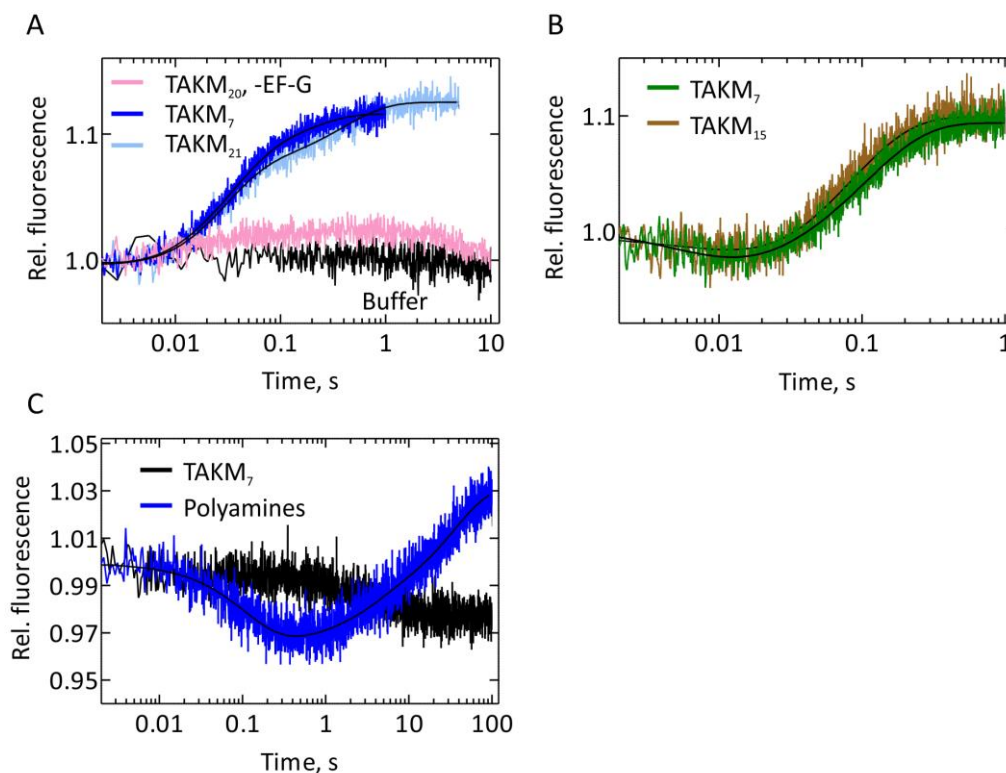


Figure 2.20 Effect of Mg²⁺ ion and polyamine concentrations on the kinetics of subunit rotation.

(A) Time course of subunit rotation upon rapid mixing of PRE(fMF) (0.05 mM) in TAKM_{3.5} with TAKM₃₆ such that the final concentration of Mg²⁺ in reaction buffer is 20 mM (pink). Time courses of subunit rotation upon rapid mixing of PRE(fMF) (0.05 μM) with EF-G-GTP (4 μM) in either TAKM₇ (blue) or TAKM₂₁ (light blue). Black trace represents the buffer control by rapid mixing of PRE(fMF) (0.05 μM) with TAKM₇. (B) Time course of subunit rotation upon rapid mixing of PRE(fMV) (0.05 μM) with EF-G-GTP (4 μM) in either TAKM₇ (green) or TAKM₁₅ (brown). (C) Complexes with deacylated tRNA^{Phe} in P site were rapidly mixed with TAKM₇ (black) or TAKM₇ containing polyamines (blue). Smooth lines represent exponential fits.

In smFRET studies, higher Mg²⁺ ion concentrations (~15 mM) are often used to maintain the integrity of ribosome complexes which are used in extremely low concentration (pico molar). However, the use of high Mg²⁺ ion concentrations reduces the fidelity² of the translation process and is in general not preferred (Blanchard et al., 2004a; Guo et al., 2011). In order to compensate for lower Mg²⁺ ion concentrations (5 mM-7 mM), polyamines are often used in translation buffers, for smFRET experiments, as they stabilize ribosome complexes and prevent them from dissociation. To check the effect of polyamines on spontaneous subunit rotation, we prepared POST(fMF) with deacylated tRNA^{Phe} in the P site and rapidly mixed them with TAKM₇ containing spermidine, putrescine and spermine in a stopped-flow apparatus (**Figure 2.20C**). We observed a biphasic change in the acceptor fluorescence with an initial downward phase followed by a very slow upward phase but there was no change in the fluorescence signal when POST(fMF) was rapidly mixed with TAKM₇ without polyamines. The apparent rate constants of the downward phase (k_{app1}) and the upward phase (k_{app2}) were $10 \pm 1 \text{ s}^{-1}$ and $0.32 \pm 0.05 \text{ s}^{-1}$, respectively. POST complex with deacylated tRNA in the P site were mostly in the R state. Spontaneous R to N transition upon reaction of POST complex with buffer containing polyamines indicated that

polyamines stabilize the N state of the ribosome. However, it is difficult to explain the appearance of initial downward phase of CCW rotation and more experiments are required to investigate the effect of specific polyamines on subunit rotation and translocation kinetics.

2.9 Effect of antibiotics on subunit rotation

Several antibiotics inhibit different stages of translocation and among them many antibiotics directly affect subunit rotation. To understand how different antibiotics affect the kinetics of SSU body rotation and head swiveling, we monitored body rotation using the S6-L9 FRET pair, as previously described, and head swiveling using S13–L33 FRET pair. The SSU protein S13 was labeled with Atto540Q, a non-fluorescent acceptor or quencher, and the LSU protein L33 was labeled with Alexa 488, serving as a FRET donor (Belardinelli et al., 2016).

We prepared PRE(fMF) with double-labeled ribosome either with the S6-L9 FRET pair to monitor body rotation or the S13-L33 FRET pair to monitor head swiveling, and rapidly mixed them with EF-G–GTP in the presence of different antibiotics. Both PRE complex and EF-G–GTP were pre-incubated with antibiotics before mixing. In general, we observed that body rotation was faster than head swiveling in agreement with the kinetic model of translocation (Belardinelli et al., 2016). Broadly, the effect of antibiotics can be classified into three different categories as described below.

2.9.1 Coupled inhibition of body rotation and head swiveling

Hygromycin B and spectinomycin are the drugs that inhibit translocation strongly while viomycin abolishes translocation completely (Peske et al., 2004). These antibiotics bind to the SSU; additionally viomycin binds also to the LSU (Borovinskaya et al., 2008; Borovinskaya et al., 2007b; Johansen et al., 2006). We measured the effect of these antibiotics on body rotation and head swiveling (SSU movements) during EF-G-promoted translocation (**Figure 2.21**). The rotation of the SSU body and the swiveling of the head were strongly inhibited in the presence of hygromycin B and spectinomycin. The time course of the body rotation and the head swiveling showed a small initial downward phase reporting on CCW movement of the SSU (both body and head) – a consequence of EF-G binding – and the upward phase reflecting on the CW movement of the SSU upon EF-G-promoted translocation. The CCW body rotation was not visible in the absence of hygromycin B with PRE(fMF) owing to its fast kinetics as explained before in section 2.5. The presence of the antibiotic slowed down the overall reaction and made it possible to resolve the two subsequent rotational steps of CCW and CW body rotation of the SSU (**Figure 2.21A**).

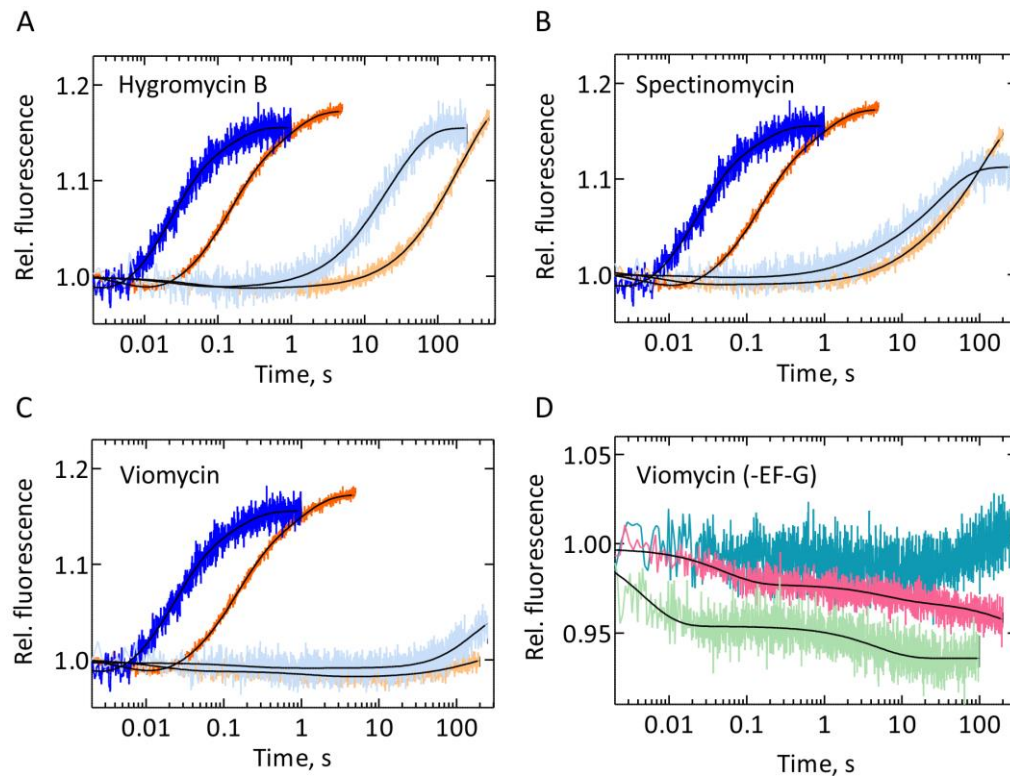


Figure 2.21 Coupled inhibition of body and head movements of the SSU.

Time courses of body rotation and head swiveling upon addition of EF-G-GTP ($4 \mu\text{M}$) to the PRE(fMF) complex ($0.05 \mu\text{M}$) in the absence or presence of antibiotics: (A) hygromycin B ($20 \mu\text{M}$), (B) spectinomycin (1 mM) and (C) viomycin ($200 \mu\text{M}$). Body rotation and head swiveling without antibiotic are depicted in blue and orange, respectively; the corresponding experiment in the presence of antibiotics is depicted in light blue and light orange, respectively. (D) PRE(fMF) ($0.05 \mu\text{M}$) was rapidly mixed with viomycin ($200 \mu\text{M}$) in the absence of EF-G to monitor body rotation (cyan) or head swiveling (pink). PRE(fMV) ($0.05 \mu\text{M}$) was rapidly mixed with viomycin ($200 \mu\text{M}$) in the absence of EF-G to monitor body rotation (green). Smooth lines are exponential fits.

Detailed analysis of time courses with three-exponential fitting showed that the apparent rate of the major phase for CW movements became extremely slow (75% of the amplitude) in the presence of hygromycin B for both body and head but the two motions (body rotation and head swiveling) remained synchronized (**Table 2.4**). Spectinomycin binding to the ribosome had a similar effect on translocation and SSU dynamics. However, unlike hygromycin B, body rotation in the presence of spectinomycin showed a delay preceding the CW body rotation (**Figure 2.21B**). The delay might occur due to extremely slow translocation in the presence of the antibiotic. Spectinomycin destabilizes the binding of peptidyl-tRNA in the A site leading to dissociation of PRE complex, which might explain the lower end levels of FRET signals observed in the presence of the antibiotic as compared to its absence. Hygromycin B binds to h44 of the 16S rRNA that forms the bridge B2a whereas spectinomycin binds to h34, near the neck of the SSU (Borovinskaya et al., 2008; Borovinskaya et al., 2007b; Schuwirth et al., 2005). Presumably, by binding to crucial regions of the SSU that are involved in subunit dynamics, these antibiotics slow down rotation and inhibit translocation.

In contrast to hygromycin B and spectinomycin, viomycin completely blocked the CW body rotation and head swiveling in line with its inhibitory effect on translocation (Peske et al., 2004) (**Figure 2.21C**). Essentially no fluorescence signal change was observed for the CW movement of the SSU except for a slight increase in the signal towards the end of each trace. Viomycin binds in a cleft formed between H69 of the LSU and h44 of the SSU at the subunit interface where the two helices form bridge B2a (Stanley et al., 2010). The antibiotic increases the affinity of tRNAs to the A site by 1000-fold which completely blocks translocation (Peske et al., 2004). In addition, by binding to both subunits, viomycin stabilizes the R state of the ribosome and imposes a strong inhibitory effect on subunit dynamics (Ermolenko et al., 2007b). To investigate the effect of the antibiotic alone (in the absence of EF-G) on subunit dynamics, we prepared PRE(fMF) and rapidly mixed them with viomycin (**Figure 2.21D**). The time course of body rotation for PRE(fMF) did not show any significant fluorescence change. Conversely, head swiveling was observed as a rapid decrease in the fluorescence signal followed by a much slower and continuous decrease. The apparent rate constant of CCW swiveling of the head was about 28 s^{-1} which is about 5-times slower than the rate of the reaction in the presence of EF-G–GTP without the antibiotic (**Table 2.4**).

Because the fraction of ribosome in the N state in the PRE(fMF) complex is as low as 12%, it is not surprising that we did not observe CCW body rotation upon reaction of PRE(fMF) with viomycin. Indeed, when we used PRE(fMV), in which 35% of the ribosomes remained in the N state, we observed a rapid decrease in the fluorescence signal reflecting the CCW body rotation followed by a slower continuous decrease in the fluorescence signal (**Figure 2.21D**). The apparent rate constant of the fastest step of CCW body rotation was as rapid as 230 s^{-1} , as determined by three-exponential fitting. Remarkably, a small molecule like viomycin can accelerate the CCW rotation of the SSU to the same extent as translational factor EF-G.

Thus, we concluded that the kinetics of body rotation and of head swiveling of the SSU got impaired to similar extent by antibiotics hygromycin B, spectinomycin and viomycin. The two motions of the SSU remained synchronized in the presence of these antibiotics during EF-G-facilitated translocation.

2.9.2 Uncoupling of body rotation and head swiveling

Streptomycin, neomycin and fusidic acid are the antibiotics that bind to the ribosome complex and stabilize transient intermediate states of translocation (Bodley et al., 1969; Carter et al., 2000; Feldman et al., 2010). We examined the subunit dynamics in the presence of these antibiotics to further investigate their mode of action (**Figure 2.22**). Streptomycin had only a small effect on the body rotation but significantly slowed down head swiveling (**Figure 2.22A, Table 2.4**). The

apparent rate constant of CCW head swiveling was similar to the reaction in the absence of streptomycin but the CW motion of the head showed a multiphasic behavior with three upward phases. The appearance of the third phase in the presence of streptomycin indicates stabilization of an additional intermediate of the ribosome complex due to binding of the antibiotic. The presence of streptomycin does not affect CCW but CW head swiveling indicates that the antibiotic stabilizes head in the swiveled position.

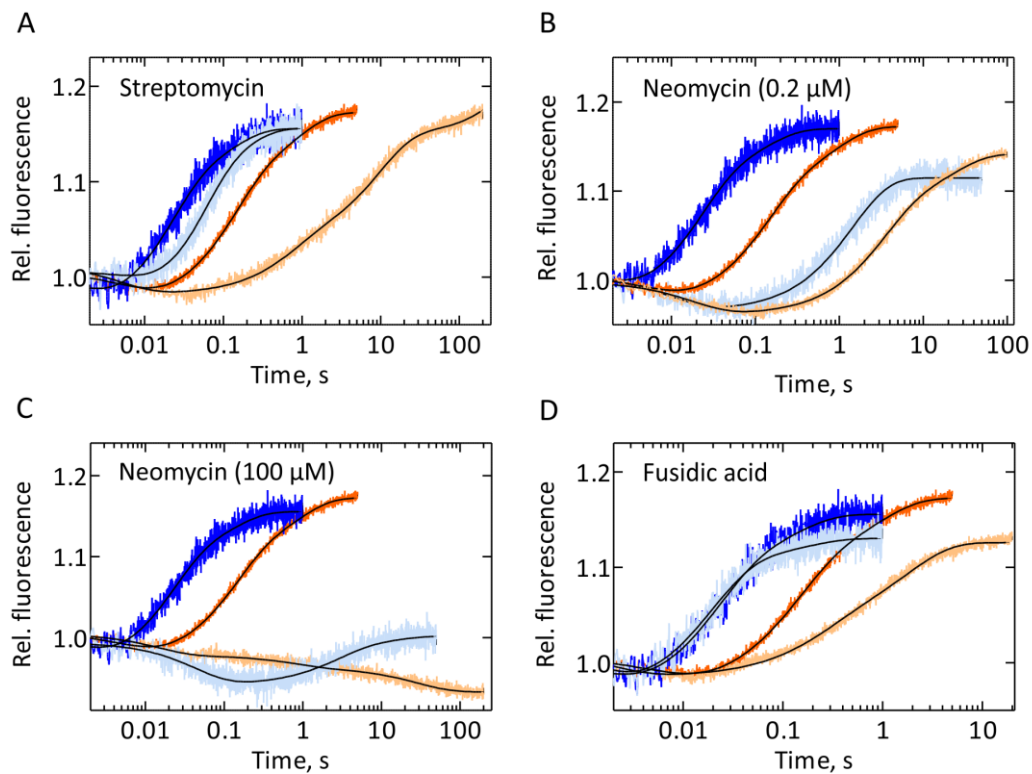


Figure 2.22 Decoupling of body rotation and head swiveling of the SSU.

Time course of body rotation and head swiveling upon addition of EF-G-GTP (4 μM) to the PRE(fMF) complex (0.05 μM) either in the presence or absence of antibiotics: (A) streptomycin (20 μM), (B) neomycin (0.2 μM), (C) neomycin (100 μM) and (D) fusidic acid (200 μM). Body rotation and head swiveling without antibiotic are depicted in blue and orange, respectively, and the corresponding experiments in the presence of antibiotics are depicted in light blue and light orange. Smooth lines are exponential fits.

Like viomycin, neomycin binds to both SSU and LSU at the subunit interface (Borovinskaya et al., 2007a). Neomycin exerts opposite effects on the dynamics of body rotation and head swiveling at different concentration. At a concentration of 0.2 μM , a biphasic change in the fluorescence signal was observed with an initial rapid downward phase followed by an upward phase reflecting CCW and CW movements of the SSU (head and body), respectively (**Figure 2.22B**, **Table 2.4**). This indicates that neomycin stabilized the rotated, swiveled state of the complex and slowed down translocation and CW movement of both head and body of the SSU. At higher concentrations of neomycin (i.e. 100 μM), the motion of body and head were uncoupled. The amplitude of CW body rotation was reduced drastically, indicative of an almost complete

inhibition of translocation (**Figure 2.22C**). Concerning the swiveling motion of the head, we noticed a continuous decrease in the fluorescence signal which could be fitted by three-exponentials (**Table 2.4**). These results are in line with the observation that at higher concentration (i.e. 100 μM) neomycin completely blocks translocation (Wang et al., 2012). The appearance of a slow CCW head swiveling indicates that at high concentrations, neomycin might stabilize a conformation of the ribosome with the head in swiveled state.

The appearance of the downward phase – i.e. CCW rotation – in the time course of body rotation might indicate that a large fraction of PRE complexes were in the N state prior to the reaction with EF-G. However, the expected fraction of the PRE(fMF) complexes in the N state is 12%, consistent with the observation that in the absence of the antibiotic this phase was not visible. This might indicate that pre-incubation of PRE complex with antibiotic might have influenced the equilibrium between the N and R states. To test this hypothesis, we rapidly mixed PRE(fMF) with neomycin (without EF-G) and observed changes in fluorescence signals (**Figure 2.23**). A rapid upward phase of CW body rotation was observed with an apparent rate constant of 80 s^{-1} , determined by single-exponential fitting. The time course of head swiveling showed a biphasic behavior with the initial upward phase of CW head swiveling with the apparent rate constant of 30 s^{-1} and a very slow downward phase of CCW head swiveling with the apparent rate constant of 0.03 s^{-1} . Therefore, like viomycin, neomycin can also induce SSU movements but in the opposite direction, towards the N state. Neomycin accelerated the rate of CW body rotation by 10-fold as compared to the spontaneous rotation of the SSU (**Table 2.1**) and stabilizes the N state of the ribosome (Feldman et al., 2010).

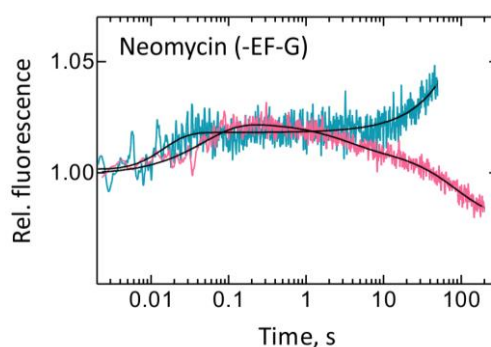


Figure 2.23 Effect of neomycin on subunit rotation in the absence of EF-G.

PRE(fMF) ($0.05\text{ }\mu\text{M}$) was rapidly mixed with neomycin ($100\text{ }\mu\text{M}$) to monitor the effect of the antibiotic alone (in the absence of EF-G) on the body rotation (cyan) and head swiveling (pink). Smooth lines are exponential fits.

Interestingly, the CW body rotation in the presence of fusidic acid was not affected and followed similar kinetics as without antibiotic with a slight decrease in the final amplitude (**Figure 2.22D**, **Table 2.4**). In contrast, fusidic acid had a noticeable effect and slowed down CW head

swiveling (**Table 2.4**). Fusidic acid binds to EF-G on the ribosome and inhibits the late EF-G remodeling steps, which in turn blocks EF-G dissociation (Adio et al., 2015; Cox et al., 2012; Ramrath et al., 2013). Presumably, inhibition of the rearrangement in EF-G caused by fusidic acid leads to an incomplete CW swiveling of the head into its final POST state. This is evident by the decrease in the amplitude change observed for the CW body rotation and head swiveling.

In conclusion, among the antibiotics tested, streptomycin, neomycin (at high concentration) and fusidic acid are the antibiotics that inhibit translocation by desynchronizing the movements of body and head of the SSU.

2.9.3 Antibiotics effecting rotational states of the ribosome

Kanamycin and paromomycin are antibiotics that stabilize the N state of the ribosome but how they affect the kinetics of subunit rotation is not clear (Feldman et al., 2010; Tsai et al., 2013; Wang et al., 2012). To investigate the nature of their inhibitory effect on subunit dynamics, we followed movements of body and head in the presence of kanamycin or paromomycin. Like neomycin, we observed a biphasic behavior with an initial rapid downward phase followed by an upward phase for CCW and CW movement of the SSU (head and body), respectively (**Figure 2.24A and B**).

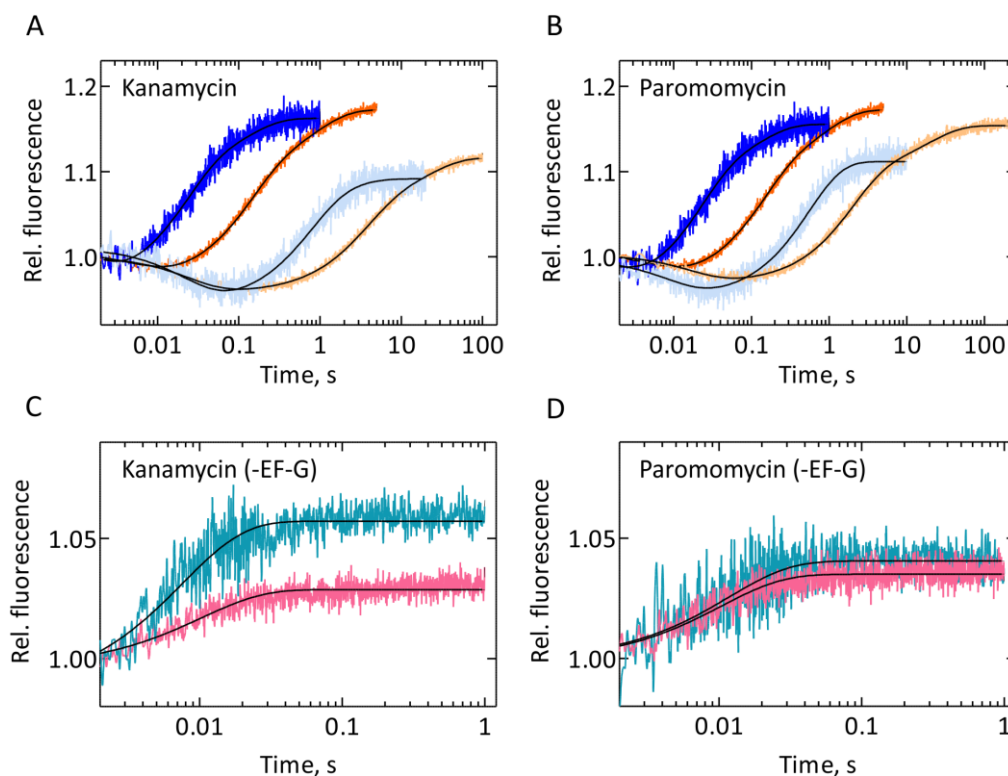


Figure 2.24 Effect of antibiotics on the rotational states of the ribosome.

Time courses of body rotation and head swiveling upon addition of EF-G-GTP (4 μ M) to the PRE(fMF) complex (0.05 μ M) in the absence or presence of antibiotics: (A) kanamycin (100 μ M) and (B) paromomycin (5 μ M). Body rotation and head swiveling without antibiotic are depicted in blue and orange, respectively, and the corresponding experiments in the presence of antibiotics are depicted in light blue and light orange. PRE(fMF) (0.05 μ M) was rapidly mixed with (C) kanamycin (100 μ M) or (D) paromomycin (5 μ M) to

monitor the effect of antibiotic alone on body rotation (cyan) and head swiveling (pink) in the absence of EF-G. Smooth lines are exponential fits.

The increase in the amplitude of downward phase indicates the stabilization of the N state prior to the reaction with EF-G. To monitor this effect directly, we rapidly mixed the PRE(fMF) with kanamycin or paromomycin (without EF-G) in a stopped-flow apparatus and recorded the rapid increase in the fluorescence signal indicating the CW movement of body and head, which in fact showed that antibiotic binding induced formation of the N state (**Figure 2.24C and D**). To test whether the CW motions are dependent on the concentration of the aminoglycoside, we measured time courses of body rotation and head swiveling at increasing concentration of kanamycin and calculated the apparent rate constants by single-exponential fitting (**Figure 2.25**). The concentration dependencies were not linear and were evaluated by hyperbolic fitting. The kanamycin concentration dependence of k_{app} saturated at $200 \pm 12 \text{ s}^{-1}$ with K_M of $50 \pm 85 \text{ }\mu\text{M}$ and $24 \pm 3 \text{ }\mu\text{M}$ for CW body rotation and head swiveling, respectively (**Figure 2.25**).

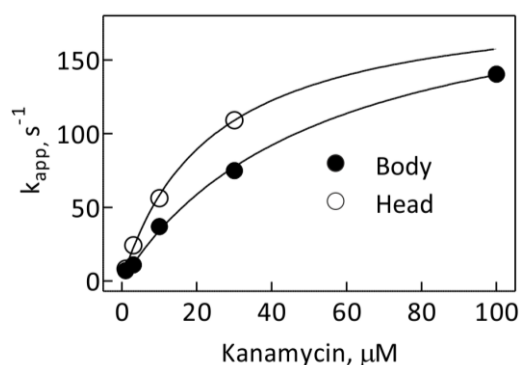


Figure 2.25 Kinetics of kanamycin-induced body rotation and head swiveling.

Kanamycin concentration dependence on the apparent rate constants, k_{app} , of CW body rotation (closed circles) and head swiveling (open circles). The k_{app} were measured upon rapid mixing of PRE(fMF) ($0.05 \text{ }\mu\text{M}$) with increasing concentration of kanamycin.

The rate of CW body rotation is about 20-fold faster than the rate of spontaneous CW rotation of the ribosome (**Table 2.1**). Therefore, upon binding to the R state of the ribosome, kanamycin and paromomycin not only induces but accelerate the rate of CW rotation resulting in stabilization of the N state of the ribosome. In principle, viomycin and neomycin also fall into this category as these antibiotics alone (in the absence of EF-G) induce CCW and CW movement of the SSU, respectively and thereby, alter the proportions of the N and R state of the ribosome.

Table 2.4 Apparent rate constants of SSU body rotation and head swiveling in the presence of EF-G and different antibiotics.

Antibiotics	Body rotation			Head swiveling		
	$k_{app1}, s^{-1} \blacktriangledown$	$k_{app2}, s^{-1} \blacktriangle$	$k_{app3}, s^{-1} \blacktriangle$	$k_{app1}, s^{-1} \blacktriangledown$	$k_{app2}, s^{-1} \blacktriangle$	$k_{app3}, s^{-1} \blacktriangle$
No antibiotic	523 ± 84	48 ± 3	8 ± 1	159 ± 7	8.0 ± 0.1	1.1 ± 0.1
Coupled inhibition of body rotation and head swiveling						
Hygromycin B	36 ± 14	0.12 ± 0.02	0.034 ± 0.002	20 ± 4	0.015 ± 0.002	0.004 ± 0.001
Spectinomycin	-	0.35 ± 0.05	0.033 ± 0.001	125 ± 28	0.09 ± 0.01	0.009 ± 0.001
Viomycin	5 ± 3	0.03 ± 0.03	0.006 ± 0.004	68 ± 17	0.73 ± 0.13 \blacktriangledown	0.006 ± 0.001
Viomycin (no EF-G)	213 ± 28	0.2 ± 0.02 \blacktriangledown	-	28 ± 4	1.0 ± 0.2 \blacktriangledown	0.03 ± 0.01 \blacktriangledown
Decoupling of body rotation and head swiveling						
Streptomycin	87 ± 14	22 ± 4	6 ± 1	171 ± 26	1.8 ± 0.1	0.15 ± 0.01
Neomycin (0.2 μM)	95 ± 8	0.70 ± 0.01	-	53 ± 2	0.3140 ± 0.004	0.046 ± 0.002
Neomycin (100 μM)	24 ± 1	0.3 ± 0.1	-	68 ± 7	1.2 ± 0.1 \blacktriangledown	0.034 ± 0.002 \blacktriangledown
Neomycin (no EF-G)	80 ± 12 \blacktriangle	-	-	30 ± 4 \blacktriangle	0.029 ± 0.001 \blacktriangledown	-
Fusidic Acid	750 ± 92	53 ± 2	7 ± 1	556 ± 84	4.4 ± 0.1	0.56 ± 0.01
Antibiotics affecting rotational states of the ribosome						
Kanamycin	45 ± 2	1.12 ± 0.02	-	40 ± 1	0.30 ± 0.01	0.05 ± 0.01
Kanamycin (no EF-G)	143 ± 3 \blacktriangle	-	-	105 ± 2 \blacktriangle	-	-
Paromomycin	113 ± 7	1.80 ± 0.02	-	56 ± 3	0.53 ± 0.01	0.054 ± 0.001
Paromomycin (no EF-G)	85 ± 3 \blacktriangle	-	-	97 ± 2 \blacktriangle	-	-

\blacktriangledown CCW body rotation and head swiveling.

\blacktriangle CW body rotation and head swiveling.

3. DISCUSSION

3.1 Spontaneous rotation of ribosomal subunits

In the present study we determined the rates of spontaneous and EF-G-induced subunit rotation using ensemble kinetics and compared them with the rates of preceding step of peptide bond formation and the following step of translocation. In principle, the formation of deacylated tRNA in the P site upon the peptidyl transfer reaction can drive the CCW rotation of the SSU relative to the LSU (Agirrezabala et al., 2008; Cornish et al., 2009; Julian et al., 2008). We estimated the rate of CCW subunit rotation, k_{CCW} , to about 40 s^{-1} independent of the identity of the tRNAs in the P or A site tested in this study and of the rate of peptide bond formation (**Figure 3.1**). On the contrary, the kinetics of peptidyl transfer reaction depends on the nature of tRNA in the P site, consistent with the previous reports (Wohlgemuth et al., 2008). The measured rate (k_{CCW}) is about 10 times faster than rates reported previously using smFRET setups (Cornish et al., 2009; Wasserman et al., 2016).

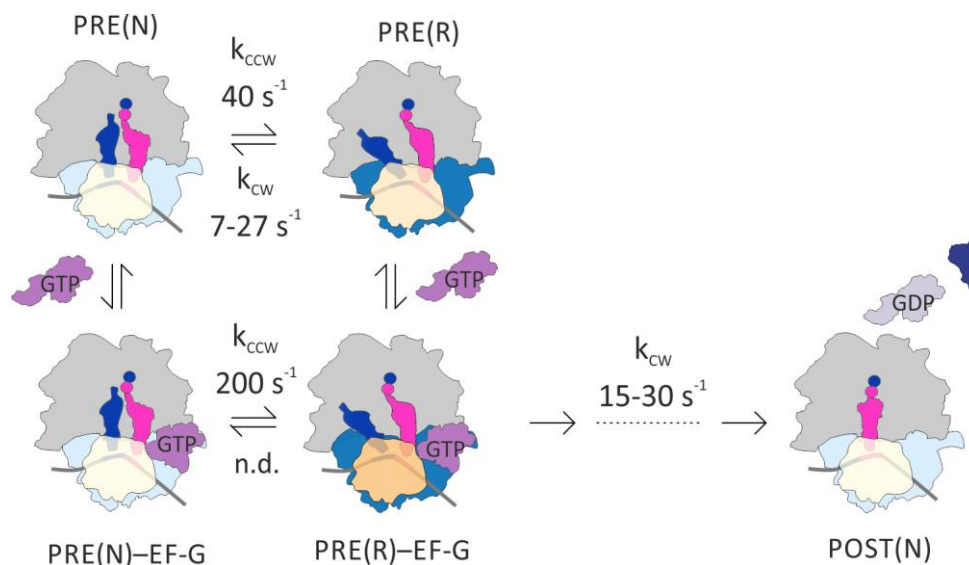


Figure 3.1 Model for subunit rotation coupled to the translocation pathway.

The rotation states of the SSU relative to the LSU (gray) are indicated by color intensity of the SSU body (light blue for N, dark blue for R). The swiveling motions of the SSU head (relative to the SSU body) are shown by color gradient from light yellow (classical non-swiveled) to orange (swiveled). Peptidyl-tRNA and deacylated tRNA in the PRE complex are shown in magenta and blue, respectively. EF-G (purple) is depicted in a compact as well as elongated conformation (Lin et al., 2015). After EF-G recruitment, translocation proceeds through a number of intermediates and reach the final POST state accompanied by CW rotation of the SSU to the N state. N is the non-rotated state and R is the rotated state of the ribosome. n.d. is not defined.

Spontaneous rotation implies that subunit rotation is an inherent property of the ribosome and that the peptide chain on the P-site tRNA acts as a barrier for SSU rotation. The deacylation of the P-site tRNA due to peptide bond formation releases the intrinsic reorganization

capability of the ribosome which allows for a different environment for the tRNAs to get established (Agirrezabala et al., 2008; Valle et al., 2003). As the ribosome attains the R state, the increased affinity of the 3' CCA end of deacylated tRNA makes it more prone to form the H state (Dorner et al., 2006; Moazed and Noller, 1989; Semenov et al., 2000). Alternatively, it has been suggested that the energy of peptide bond formation is directly utilized to drive the CCW rotation of the subunit, whereas the energy of GTP hydrolysis by EF-G is utilized to drive CW rotation during translocation (Marshall et al., 2008). The k_{CCW} measured at smFRET setups with the PRE complex resulting from either peptide bond formation or by direct binding of tRNA^{fMet} in the P site and a peptidyl analogue, N-Ac-Phe-tRNA^{Phe}, in the A site did not differ significantly (Cornish et al., 2008; Qin et al., 2014). This shows that the energy of peptide bond formation is not directly involved in driving subunit rotation. Moreover, we noted that the spontaneous transitions are reversible. The rate of spontaneous N-to-R transition is independent of the identity of tRNAs but the rates of R-to-N transition varied with different tRNAs present in the ribosome. Under our conditions of rapid translation the rate of CW rotation, k_{CW} , varied from 7 s⁻¹ to 27 s⁻¹ and the fraction of PRE complex remained in the N state varied from 0.1 to 0.4, respectively depending on the A-site tRNA (**Figure 3.1**). Therefore, different rates of CW rotation are responsible for setting different equilibrium between the N and R state in the presence of various tRNAs. The fraction of ribosomes in the N state increases in general at the conditions of smFRET experiments and their values along with rates of spontaneous transitions between the two rotational states of the ribosome determined by us were comparable to other smFRET studies (Cornish et al., 2008; Wasserman et al., 2016).

Overall, these findings are consistent with other smFRET and structural studies, as well as molecular dynamic simulations that report the existence of large population of iso-energetic fluctuating ribosome corresponding to different subunit rotational states, tRNA and L1 positions (Bock et al., 2013; Fischer et al., 2010; Fu et al., 2011; Munro et al., 2010a; Zhang et al., 2009). Thus, we conclude that peptide bond formation has a structural, rather than an energetic, effect on subunit rotation; the thermal energy is sufficient to power the spontaneous fluctuations of the PRE complex between the rotational states.

The ribosome is highly sensitive to Mg²⁺ ion concentrations. At low Mg²⁺ ion concentrations (<1 mM), the two subunits are loosely bound or even separated while at high concentrations (>10 mM) fidelity of translation is compromised. Therefore, an optimal Mg²⁺ ion concentration (1-10 mM) is essential for subunit association, for tRNA binding at the decoding center and in general to maintain the integrity of the ribosome. smFRET studies have suggested that increasing the Mg²⁺ ion concentration increases the population of the C state of the tRNAs by increasing its lifetime, whereas the lifetime of the H state was not affected (Kim et al., 2007).

Because, the N and R state of the ribosome are considered to be coupled to the C and H state of the tRNAs, respectively one would expect that the Mg^{2+} ions concentration also influences the proportion of two rotational states of the ribosome. Surprisingly, the proportion of the N and R state was independent of the Mg^{2+} ions concentration. Our observation is in line with another smFRET study which monitored subunit rotation at different Mg^{2+} ions concentrations (Marshall et al., 2008). We hypothesize that the transition between C and H state might entail an additional intermediate (INT), formation of which is independent of Mg^{2+} ion concentration. The N-to-R transition might be coupled to the C-to-INT transition, which is rapid, while transition between INT-to-H can be influenced by varying the concentration of Mg^{2+} ions. Such an INT state might be related to the H2 state (P/E, A/A) of the tRNA but the dependence of the H2 state on the Mg^{2+} ion concentration is not known (Munro et al., 2007). Alternatively, Mg^{2+} ion might act as a tool to uncouple the movement of the tRNAs from the subunit rotation. Detailed kinetic studies monitoring subunit rotation (body and head) along with tRNA movements at different conditions (buffer, Mg^{2+} ion or temperature) are essential to understand sequence of rearrangements and coupling between tRNAs and the ribosome motion during early steps of translocation.

3.2 EF-G-induced ribosomal subunit rotation

Upon initial binding to PRE complex EF-G stabilizes the R-H-L1_{closed} state by halting the spontaneous fluctuation towards N-C-L1_{open} state (Fei et al., 2008; Munro et al., 2010b; Wasserman et al., 2016). A question that remained controversial is whether EF-G can also bind to the ribosome in the N state or whether spontaneous N-to-R transition is prerequisite for EF-G binding. Ensemble kinetics have shown that changing the ratio of C to H state, by varying the Mg^{2+} ion concentration, does not affect either the rate of GTP hydrolysis or translocation (Holtkamp et al., 2014a; Rodnina et al., 1997; Walker et al., 2008). This indicates that either the spontaneous N-to-R transition is extremely rapid or that EF-G can bind to the ribosome in the N state and induces fast rotation of the SSU from N to R state. Additionally, smFRET experiments using an L11-tRNA or a tRNA-tRNA FRET pair have shown that EF-G can bind to the ribosome in both C and H state and when recruited to the C state the ribosome transiently visit the H state before moving to the POST state (Adio et al., 2015; Chen et al., 2011). Furthermore, two recent structures show EF-G bound to the ribosome in the N state (Li et al., 2015; Lin et al., 2015). These structures, together with the smFRET and ensemble kinetics provide strong evidence that EF-G can bind to both N-C and R-H state and engages in translocation via a transient N to R rotation with concomitant stabilization of the R-H state.

One major challenge in dissecting the mechanism of translocation is to estimate the effect of EF-G on the rate of N-to-R transition. This is because binding of EF-G induces rapid progression

of the PRE complex through translocation intermediates until the POST state is reached resulting in a very short lifetime of the R state. Experiments with ribosome complexes that do not translocate, i.e. with a vacant A site, suggest that EF-G accelerates the L1 closure by a factor of six to eight to a rate of up to 3 s^{-1} (Fei et al., 2009; Munro et al., 2010b). When subunit rotation is monitored using the S6-L9 reporter pair on the ribosome with a vacant A site, the effect is two-fold (to 1.2 s^{-1}) (Cornish et al., 2008). Here, we show that EF-G–GTP-induced CCW rotation on the fraction of PRE complexes that have remained in the N state after peptide bond formation is extremely fast (200 s^{-1}) (**Figure 3.1**). EF-G accelerates the CCW subunit rotation to a similar extent for different tRNAs or experimental conditions (different buffers and temperature), i.e., about five-fold compared to spontaneous rotation. This acceleration was not observed in previous smFRET experiments, either because the reaction is too fast for the time resolution of smFRET experiments or because CCW rotation is obscured by subsequent translocation events (Chen et al., 2013a; Cornish et al., 2008; Wasserman et al., 2016). On the other hand, our results are consistent with ensemble kinetic experiments (performed at 22°C) which noted a very rapid CCW rotation upon EF-G–GTP addition to a PRE complex with N-Ac-Phe-tRNA^{Phe} in the A site (Ermolenko and Noller, 2011). Likewise, our translocation experiments with the PRE(fMF) complex in the presence of either hygromycin B or EF-G–GTP γ S revealed a very rapid CCW subunit rotation upon EF-G binding preceding tRNA translocation and CW subunit rotation which become very slow.

X-ray crystallography and cryo-EM studies utilize antibiotics or GTP analogues to trap EF-G on the ribosome. Most of these antibiotics have no effect on N-to-R transition and influence later steps in translocation (Frank and Agrawal, 2000; Pulk and Cate, 2013; Ramrath et al., 2013; Valle et al., 2003; Zhou et al., 2014). Our ensemble kinetic experiment has shown that EF-G–GTP γ S has no influence on the rate of CCW rotation but slows down CW rotation by 70 fold. Moreover, EF-G–GDPNP dissociates 7.5 times faster from the N state than from the R state (Chen et al., 2013a). These observations explain why EF-G bound ribosome complex in structural studies were always observed in the R state. When we used EF-G(Δ 4/5) or EF-G(XL) in our translocation experiments, no CCW body rotation was observed. These mutants bind to the ribosome as rapid as the wild type EF-G but are incapable of undergoing necessary rearrangements involving domain IV that couples the conformation changes in EF-G to the forward movement of the tRNAs (Peske et al., 2000; Savelsbergh et al., 2003). In addition, EF-G binds to the N state of the ribosome in the compact form transiently while the extended form favors the R state (Lin et al., 2015). We propose that binding of EF-G is not sufficient to induce the CCW rotation of SSU rather a conformational rearrangement in EF-G towards the extended state, presumably involving the movement of domain IV, is necessary to drive the rotation of the SSU. Since, these mutants are

incapable of attaining the extended conformation of EF-G, the necessary rearrangements required to drive CCW rotation was inhibited.

In comparison to the CCW subunit rotation, the CW rotation and tRNA translocation are largely concomitant, but much slower steps (Belardinelli et al., 2016; Ermolenko and Noller, 2011). CW rotation and translocation appear to be coupled kinetically and structurally, as inhibiting tRNA translocation with either antibiotics or GTP analogues results in impaired CW rotation (Belardinelli et al., 2016; Wasserman et al., 2016).

3.3 Kinetic model of translocation

Our kinetic analysis provides a comprehensive description of the choreography of motions during EF-G-promoted tRNA translocation (**Figure 3.2**). As soon as an aa-tRNA has accommodated in the A site and peptide bond formation has taken place, the subunits start to rotate in CCW direction at the rate of 40 s^{-1} driven by thermal energy. The spontaneous fluctuations results in an equilibrium between the N and R state of the ribosome. Antibiotics kanamycin, paromomycin and neomycin (the latter at concentrations $<0.1 \mu\text{M}$) can disturb this equilibrium by stabilizing the N-C state of the ribosome (Tsai et al., 2013; Wang et al., 2012; Wasserman et al., 2015). Thus, these antibiotics increase the energy barrier for subunit rotation that inhibits translocation. At the high cellular EF-G concentrations, the factor is recruited to the ribosome with a rate $>500 \text{ s}^{-1}$ ($10 \mu\text{M}$ [EF-G] \times $55\text{-}150 \mu\text{M}^{-1}\text{s}^{-1}$; (Belardinelli et al., 2016; Katunin et al., 2002), almost instantaneously after EF-Tu has been released. EF-G – presumably in a compact form (Lin et al., 2015) – rapidly binds to either the N or the R state of the ribosome and accelerates the CCW subunit rotation of the ribosome that have remained in the N state to 200 s^{-1} . EF-G-induced N-to-R transition is one of the fastest events on the reaction coordinate of translocation and does not limit the global rate of the tRNA-mRNA translocation. The predicted lifetime of the PRE complex in the EF-G-bound N state is negligibly small and therefore has escaped detection.

After EF-G engagement and GTP hydrolysis the PRE complex enters the CHI1 state with a rate of 85 s^{-1} . In this state the PRE complex is stabilized in the R-H state and fluctuations between PRE(R-H) \leftrightarrow PRE(N-C) states are blocked (Adio et al., 2015). The CCW movement of the head continues until step 2 but body of the SSU starts rotating in CW direction towards the N state. For SSU body, this is the major rearrangement towards the POST state and which was characterized by X-ray and cryo-EM structures (Ramrath et al., 2013; Ratje et al., 2010; Zhou et al., 2014). The two opposite motions within the SSU might be crucial for overcoming the physical hurdles for tRNA-mRNA movement resulting in ribosome unlocking. CHI1 state may resemble ap/ap-pe/E state captured by X-ray crystallography (Zhou et al., 2014) and may also be structurally related to the ribosome-Viomycin/Neomycin-EF-G-complex, because viomycin or neomycin do not block

step 1 or step 2 but stabilize the ribosome in the R-H state or in an intermediate state of subunit rotation (Savelsbergh et al., 2003; Zhou et al., 2013, 2014). Structural studies also suggest that step 2 may entail an additional early intermediate where the body reaches a large scale rotation (6° - 12°) while head swiveling is still in the initial stage (3° - 7°) with tRNAs in the H state. In this state, EF-G occupies the inter-subunit space between L12 stalk and A-site tRNA (Brilot et al., 2013).

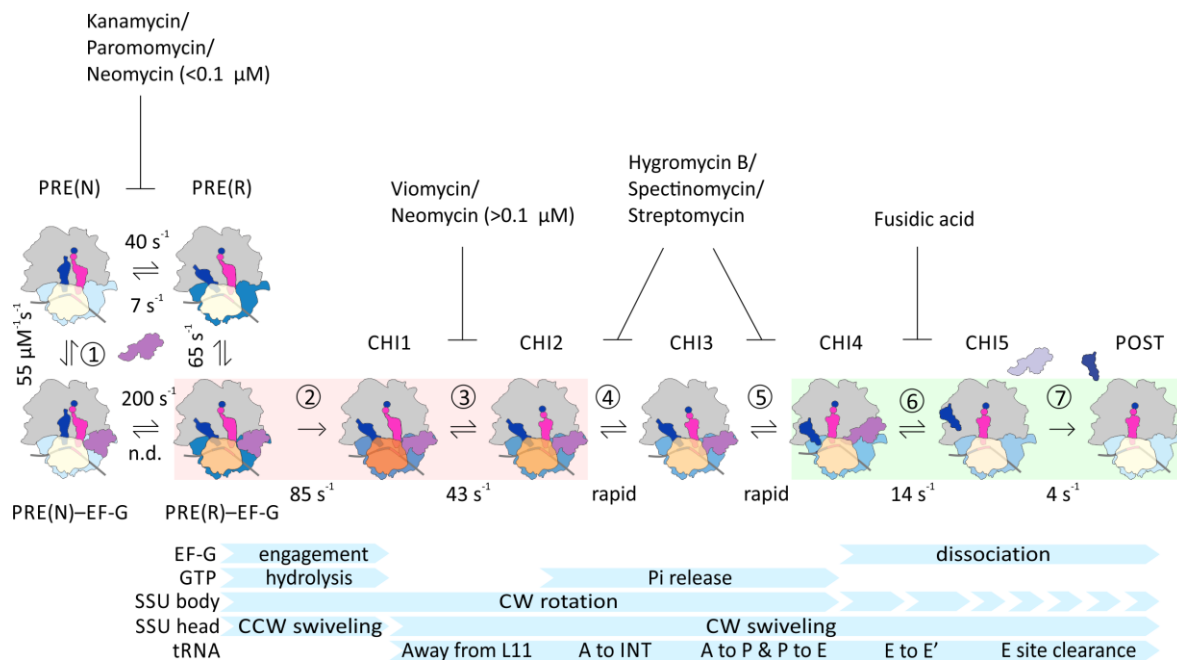


Figure 3.2 Kinetic model of translocation pathway.

The rotational states of the SSU relative to the LSU (gray) are indicated by color intensity of the SSU body (light blue for N, dark blue for R). The swiveling motions of the SSU head relative to the SSU body are shown by color gradient from light yellow (classical non-swiveled SSU head position) to orange (maximum degree of swiveling). tRNAs in the A and P sites of the PRE complex are shown in magenta and blue, respectively. EF-G (purple) is depicted in two conformations, a compact (Lin et al., 2015) and an extended one after engagement with the ribosome (Ramrath et al., 2013; Zhou et al., 2014). The light red background indicates complexes undergoing unlocking; the light green background shows complexes that move towards relocking. All rate constants, except the ones reported in Figure 3.1, are from ensemble kinetics studies with the PRE(fMF) complexes at 37°C (Belardinelli et al., 2016). Translocation intermediates (CHI1 to CHI4) are adopted from a smFRET study (Adio et al., 2015) and are consistent with other smFRET (Wasserman et al., 2016), ensemble kinetics (Belardinelli et al., 2016; Savelsbergh et al., 2003) and structural studies (CHI1 (Zhou et al., 2014); CHI4 (Ramrath et al., 2013)). An additional intermediate CHI5 was identified by ensemble kinetics (Belardinelli et al., 2016) and smFRET (Wasserman et al., 2016). The POST state may entail further conformational sub-states (Wasserman et al., 2016). Steps shown as ‘rapid’ are deduced from structures or smFRET experiments that utilized EF-G mutants or antibiotics to stall the intermediates (Adio et al., 2015; Wang et al., 2012; Wasserman et al., 2016), but are not resolved by kinetic measurements of unperturbed translocation. EF-G binding and dissociation is from (Belardinelli et al., 2016); GTP hydrolysis and Pi release from (Rodnina et al., 1997; Savelsbergh et al., 2003); movements of the SSU body and head from (Belardinelli et al., 2016). tRNA movement away from L11 was demonstrated by smFRET (Adio et al., 2015); A to INT is a movement of the 3’ end of the A/P-site tRNA further towards the P site.

CHI1 converts into CHI2 state with a rate of 43 s^{-1} , a rate-limiting step for unlocking. The unlocking step kinetically dominates the tRNA movement and the release of Pi from EF-G (Savelsbergh et al., 2003). In the CHI2 state, the A-site tRNA moves towards the P site as suggested by smFRET experiments where a decrease in the FRET between tRNA and ribosomal protein L11 was observed. The CHI2 state may resemble partial movement of the P-site tRNA towards the E site (Belardinelli et al., 2016; Pan et al., 2007). The precise mechanism leading to the unlocking of the ribosome is unknown. It is likely to involve concerted actions of the ribosome, tRNAs and EF-G that have to undergo rearrangements in order to circumvent the steric blocks for the tRNA-mRNA movement.

As the SSU head starts to swivel backwards (CW) while the body continues its gradual rotation in the CW direction, the process of relocking begins. Concurrent release of Pi from EF-G and tRNAs movement are rapid reactions (step 4 and step 5) (Savelsbergh et al., 2003), but may entail additional intermediates as the tRNAs move stepwise from the A to P and from the P to E site (Holtkamp et al., 2014a). In CHI3, the 3' CCA end of the peptidyl-tRNA moves towards the P site on the LSU and is not Pmn reactive yet, but the translocation of its ASL on the SSU is lagging behind. In principle, the CHI3 state is a short-lived intermediate, because translocation of tRNAs on both subunits is rapid and synchronized, but can be isolated by blocking translocation with antibiotics, hygromycin B, spectinomycin or streptomycin, mutations in EF-G or a lack of GTP hydrolysis (Holtkamp et al., 2014a; Pan et al., 2007; Peske et al., 2004).

The intermediate formed at step 5 represent CHI4 state and may corresponds to an intermediate stalled by fusidic acid whose structure has been solved by cryo-EM (Gao et al., 2009). The 3' CCA end of the peptidyl-tRNA completes its translocation and reaches the P site on the LSU which then becomes Pmn reactive. Finally, in step 6 and step 7 the E-site tRNA moves away from the E site at the rate of 14 s^{-1} through an intermediate E-site binding state (E') (CHI5) and then dissociates from the ribosome into solution (Belardinelli et al., 2016; Wasserman et al., 2016). The existence of the E' site has been noted before on the basis of biochemical assays and cryo-EM data (Fischer et al., 2010; Robertson et al., 1986). The head and the body of the SSU continue to move backwards until EF-G dissociates from the ribosome in a relatively slow reaction of about 4 s^{-1} which also completes the re-locking of the ribosome (Belardinelli et al., 2016); this process may entail additional intermediates or conformational varieties of the POST state (Wasserman et al., 2016).

While structural studies provide snapshots of intermediate states of ribosomal motions as the tRNAs are translocated from the A to P site and from P to E site, our rapid kinetic approach places intermediate states along a time axis of translocation. Although the ribosome is a very large particle, movements of its parts are rapid, spontaneous and driven by thermal energy.

Translocation is gated by the ribosome ligands, tRNAs and EF-G, which control the conformational state of the ribosome, maintain the reading frame, and promote directional movement of the ribosome along the mRNA. The smooth continues motion of the ribosome can be perturbed by small molecules antibiotics making their study essential to combat infections.

3.4 Effect of antibiotics on subunit dynamics

Controlling translation is one of the central questions in understanding the regulation of gene expression in the cell. The rate of translation can be substantially compromised by even modest changes in dynamic conformational events within the ribosome. Here, we show that binding of antibiotics allosterically affects ribosome dynamics and the mechanism of translation by interfering with the process of subunit rotation. Based on the effect of the antibiotic tested, we broadly classified them into three different categories, (i) antibiotics resulting in coupled inhibition of body rotation and head swiveling (hygromycin B, spectinomycin and viomycin), (ii) antibiotics that uncouple body rotation and head swiveling (streptomycin, neomycin and fusidic acid) and (iii) antibiotics affecting the equilibrium between the two rotational states of the ribosome (kanamycin, paromomycin, viomycin and neomycin).

Hygromycin B, spectinomycin and viomycin inhibit translocation but maintain the synchronized movements of body and head. In addition to stabilizing peptidyl-tRNA in the A site (Peske et al., 2004), hygromycin B blocks the rearrangement required for SSU rotation by binding to the major groove of h44 of the 16S rRNA in the decoding site, where h44 forms a well conserved intersubunit bridge B2a with H69 of the 23S rRNA (Borovinskaya et al., 2008; Yusupov et al., 2001). On the contrary, spectinomycin destabilizes the A-site tRNA by binding to h34 (i.e. near the neck of the SSU) of the 16S rRNA (Borovinskaya et al., 2007b; Peske et al., 2004). The antibiotic prevents the conformation change in the head domain of the SSU that potentially involves h34 and stabilizes the head in a less swiveled state which in turn inhibits translocation (Borovinskaya et al., 2007b). Overall, by inhibiting the motion of body and head of the SSU, hygromycin B and spectinomycin impose a strong inhibitory effect on translocation. Viomycin, on the other hand, impairs subunit dynamics by locking the ribosome in the R state and stabilizing A-site tRNA that abolish translocation completely (Ermolenko et al., 2007b; Modolell and Vazquez, 1977). Surprisingly, the antibiotic alone (in the absence of EF-G) induces CCW body rotation and head swiveling. Although the magnitude of the rotation is small, the rate measured for CCW body rotation induced by viomycin was 200 s^{-1} , identical to the EF-G-accelerated body rotation. However, the rate of viomycin-induced CCW head swiveling was about 5-times slower than that induced by EF-G. The 5-fold acceleration of CCW body rotation compared to

spontaneous SSU rotation suggests that binding of viomycin promotes an essential rearrangement at the subunit interface that drives subunit rotation.

Streptomycin, neomycin (at high concentration) and fusidic acid influences body rotation and head swiveling to a different extent and therefore uncouple their motion. Streptomycin binds between helices 1, 18, 27, 28 and 44 of 16S rRNA and protein S12 of the SSU (Carter et al., 2000). The antibiotic did not affect body rotation substantially but markedly attenuated the rate of CW head swiveling. Biochemical and structural data showed that despite 45-fold tRNA stabilization in the A site, streptomycin decreases the rate of translocation only by 2-fold (Peske et al., 2004). This suggests that binding of streptomycin might trap the head in an intermediate state that is inherently more prone to rapid translocation, which in turn would compensate for the increased energy barrier for translocation due to stabilization of the A-site tRNA. We observed that CCW swiveling of the head was not affected by streptomycin but CW movement was hampered suggesting that the antibiotic traps the head domain of the ribosome in a swiveled conformation that favors translocation mainly by distorting h44 of the 16S rRNA (Demirci et al., 2013).

Our kinetic data showed that during EF-G-promoted translocation, neomycin (100 μM) substantially slowed down body rotation and uncoupled it from the movement of the head which probably attained a high degree swiveled state. This is in line with structural data that demonstrate the attenuation of the overall extent of subunit rotation and the uncoupling of body rotation from SSU head and platform motions in the presence of neomycin (Wang et al., 2012). Additionally, we observed that the antibiotic (in the absence of EF-G) induces CW movement of body and head of the SSU. The rates measured for the CW rotation of the body was 80 s^{-1} , 10-fold faster than the spontaneous CW body rotation. These observations are consistent with the bimodal effect of neomycin action caused by the two binding sites, the high-affinity binding site on the SSU (i.e. h44) and the low-affinity binding site on the LSU (i.e. H69). Lower concentrations of neomycin saturate the canonical h44 binding site whereas a higher concentration is required to additionally saturate the H69 binding site (Feldman et al., 2010; Wasserman et al., 2015). As for most aminoglycosides, the latter binding site overlaps with inter-subunit bridge B2a. Binding of neomycin to the high affinity binding position in h44 stabilizes the complexes in the N state, which was observed as an initial increase in the fluorescence signal reflecting CW rotation, whereas its binding to the lower affinity position in H69 uncouples body and head movements, perhaps stabilizing an intermediate state of rotation with a high degree of head swiveling, which is recorded as a decrease in the fluorescence signal for CCW head swiveling (Wasserman et al., 2015).

Kinetically, fusidic acid had no influence on body rotation but reduced the rate of head swiveling. Fusidic acid binds to EF-G on the ribosome and inhibits the late EF-G remodeling steps

after tRNA-mRNA translocation, which in turn blocks EF-G dissociation (Bodley et al., 1969; Cox et al., 2012; Tanaka et al., 1968). Because CW swiveling of the head is one of the late events of translocation which reaches completion with EF-G dissociation (Belardinelli et al., 2016), we can conclude that inhibition of the rearrangement in EF-G caused by fusidic acid leads to a slower CW swiveling of the head into its final POST state.

Kanamycin and paromomycin act early on the translocation pathway by altering the equilibrium between the two rotational states of the ribosome (Tsai et al., 2013; Wasserman et al., 2015). Kanamycin binds to the h44 of the SSU while paromomycin interacts with both h44 and H69 of the SSU and the LSU, respectively (Carter et al., 2000; Wasserman et al., 2015). Both antibiotics induce the CW movement of body and head and substantially accelerate CW rotation of the body to the rate of 150 s^{-1} , 20-fold faster compared to the spontaneous transition from R-to-N state of the ribosome (7 s^{-1} for PRE(fMF) complex). Similar to neomycin, these antibiotics stabilize the N state of the ribosome, probably by preventing remodeling events of the bridge B2a that accompany SSU rotation, thereby increasing the energy barrier for subunit rotation and inhibiting translocation. smFRET and structural studies have shown that, like neomycin, paromomycin can also employ a bimodal mechanism by interacting with the apical tip of H69 of the LSU at higher concentrations and stabilizing an intermediate state of subunit rotation (Wasserman et al., 2015).

Most antibiotics tested here interact with either h44 or both h44 and H69 of the SSU and the LSU, respectively. These are structurally different but functionally linked site and have an impact on the nature and the kinetics of subunit rotation. Subtle differences in the functional groups of some of these antibiotics and their interaction sites on the ribosome lead to significant differences in their way of mechanism of inhibition of translocation. The observation that small molecules like antibiotics bind to a supra-molecular machine, the ribosome, and can induce movement of the SSU in a specific direction is surprising. Until now, there is a strong debate whether EF-G, a motor protein and ligand of the ribosome, can induce the N-to-R transition of the SSU. Here we show that not only EF-G, but also antibiotics have a capability to reshape the energy landscape of the ribosome, although unlike EF-G that promotes translocation, they stabilize a specific conformation of the ribosome and increase the energy barrier for conformational transitions, thus inhibiting translocation.

3.5 Ribosome as a Brownian machine

The ribosome, a macromolecular machine, ubiquitously performs the work of synthesizing proteins in all cells. Like for any other biological machine, understanding the working of the ribosome is a fascinating but challenging task. Brownian motions are underlie the movements of

its parts and ligands (Rodnina and Wintermeyer, 2011). Large scale conformational changes are divided into small discrete steps with low energy barriers that can be overcome with thermal fluctuations. Large numbers of different conformations of tRNAs coupled to spontaneous rearrangements in the ribosome during translocation lead to a metastable energy landscape. The landscape entails energy wells that represent distinct intermediate states available to the ribosome during translocation and the activation energy governing the rates of transition between them (Munro et al., 2009). In the absence of EF-G, the tRNAs in the PRE complex make rapid and spontaneous movements in both the forward and backward direction and the preferential directionality of the movement of a tRNA is determined by its affinities towards different binding sites (Semenkov et al., 2000). This makes the ribosome essentially a thermal machine that can drive spontaneous translocation according to the thermodynamic gradient of tRNA binding, albeit very slowly. Translocation in the absence of EF-G and GTP hydrolysis shows that it is the inherent property of the ribosome and that energy of thermal fluctuations is sufficient to drive translocation (Fredrick and Noller, 2003; Shoji et al., 2006).

The ribosome being a supramolecular assembly, one would imagine that thermally-driven spontaneous conformational changes, such as subunit rotation, within the ribosome would also be very slow as they require concerted action of different components of the ribosome and multiple rearrangement steps resulting in high kinetic barrier. To our surprise, we observed that the spontaneous rotation of the ribosomal subunit is rapid and takes place with the rate of 40 s^{-1} . This makes ribosome a highly dynamic machine despite of its large size. Our results are consistent with the computational studies showing that movements of ribosomal elements, such as subunit rotation or L1 dynamics, are extremely rapid and take place on micro-second time scales (Bock et al., 2013). The presence of low energy barriers for movements of different components seems to be general feature of the ribosome that makes it a highly efficient machine. On the contrary, of all the movements, the highest energy barriers are associated with the tRNA movements, which take place on millisecond time scales (Bock et al., 2013). Thus, understanding the coupling between the collective motions of the tRNAs and the ribosome is highly important to understand the mechanism of translocation.

EF-G contributes to the kinetics rather than to the thermodynamics of the translocation pathway, consistent with the notion that it is a catalyst of the translocation reaction. EF-G decreases the activation energy for translocation by binding to the tRNA-ribosome complex and facilitates rapid tRNA-mRNA movement on the ribosome at the cost of GTP hydrolysis. An unresolved question is whether EF-G acts as a motor protein that utilizes the energy of GTP hydrolysis and actively pushes the A-site tRNA by generating a power stroke or whether it acts as a Brownian ratchet that biases the thermal fluctuation towards the forward movement of the

tRNA-mRNA complex. Three possibilities by which EF-G can promote the tRNA-mRNA translocation are: (i) we showed that the energy contribution by non-covalent binding of EF-G to the ribosome is sufficient to accelerate the N-to-R transition by 5-fold compared to spontaneous transition, thereby promoting translocation on the LSU – a step that does not require GTP hydrolysis. (ii) The energy of GTP hydrolysis might be utilized for accelerating the conformation rearrangements within the ribosome (displacing ribosomal elements that act as hurdles for tRNA movement) coupled to structural changes of the factor (movement of domain IV) that are essential for unlocking the ribosome for translocation on the SSU (Holtkamp et al., 2014b; Rodnina and Wintermeyer, 2011). This idea is supported by the observation that prevention of GTP hydrolysis by using non-hydrolysable analogues decreased the rate of translocation by 50-fold (Cunha et al., 2013; Holtkamp et al., 2014a; Katunin et al., 2002; Rodnina et al., 1997). (iii) Upon GTP hydrolysis, EF-G undergoes conformational change that places domain IV of the factor, which act as a pawl, in the A-site and therefore biases the thermal motion in the forward direction by suppressing the backward movement of the tRNAs (Chen et al., 2013b; Peske et al., 2000; Pulk and Cate, 2013; Savelsbergh et al., 2009). In principle, all these possibilities are not mutually exclusive. The ribosome and EF-G might use both a power-stroke and a Brownian ratchet mechanism to ensure efficient translocation (Chen et al., 2016). Understanding the way EF-G remodels the energy landscape of the ribosome to drive rapid tRNA-mRNA translocation will also help us to understand the workings of other molecular machines coupled to their ligands.

4. MATERIALS AND METHODS

4.1 Buffers

Reaction buffers

TAKM ₇	50 mM Tris-HCl , pH 7.5 at 37°C 70 mM NH ₄ Cl 30 mM KCl 7 mM MgCl ₂
-------------------	--

smFRET buffer	50 mM Tris-HCl, pH 7.5 at RT 70 mM NH ₄ Cl 30 mM KCl 15 mM MgCl ₂ 8 mM Putrescine 1 mM Spermidine
---------------	--

Protein expression and purification buffers

Lysis Buffer	20 mM Tris-HCl, pH 7.5 at RT 300 mM NaCl
--------------	---

Buffer A for purification of S6 protein (anion-exchange chromatography)	20 mM NaOAc, pH 5.6 at RT 20 mM KCl 6 M Urea 6 mM 2-mercaptoethanol
--	--

Buffer B for purification of S6 protein (anion-exchange chromatography)	20 mM NaOAc, pH 5.6 at RT 1000 mM KCl 6 M Urea, 6 mM 2-mercaptoethanol
--	---

Buffer C for purification of L9 protein (ion- exchange chromatography)	20 mM Tris-HCl, pH 8.0 at RT 20 mM KCl 6 M Urea 6 mM 2-mercaptoethanol
---	---

MATERIALS AND METHODS

Buffer D for purification of L9 protein (ion- exchange chromatography)	20 mM Tris-HCl, pH 8.0 at RT 1000 mM KCl 6 M Urea 6 mM 2-mercaptoethanol
---	---

Labeling and reconstitution buffers

Labeling buffer	50 mM HEPES, pH 7.25 at RT 400 mM KCl 6 M Urea
Buffer E (gel filtration chromatography)	50 mM HEPES, pH 7.25 at RT 400 mM KCl 6 M Urea 6 mM 2-mercaptoethanol
Reconstitution buffer for Δ S6 ribosomes	50 mM HEPES, pH 7.5 at RT 400 mM KCl 4 mM MgCl ₂ 6 mM 2-mercaptoethanol 5% Glycerol
Reconstitution buffer for Δ L9 ribosomes	50 mM HEPES, pH 7.5 at RT 400 mM NH ₄ Cl 4 mM MgCl ₂ 6 mM 2-mercaptoethanol 5% Glycerol

HPLC buffers

Buffer F for HPLC	0.1% Trifluoroacetic acid
Buffer G for HPLC	0.1% Trifluoroacetic acid 65% Acetonitrile

DNA gel buffer

TAE	40 mM Tris-acetate, pH 8.0 at RT 1 mM EDTA
DNA loading sample dye (STEB, 4x)	150 mM Tris-HCl, pH 8.0 at RT 0.1 mM EDTA, pH 8.0 at RT 1.1 M Sucrose 0.6 mM Bromophenol blue 0.6 mM Xylene cyanol

SDS-PAGE buffers

SDS-PAGE running buffer (1x)	25 mM Tris base 200 mM Glycine 0.1% SDS
Sample loading buffer for SDS-PAGE (4x)	200 mM Tris-HCl, pH 6.8 at RT 8% SDS 40% Glycerol 0.4% Bromophenol blue 400 mM 2-mercaptoethanol
Destaining solution for SDS-PAGE	10% Ethanol 5% Acetic acid
Staining solution for SDS-PAGE gels	10% Ethanol 5% Acetic acid 1 ml Coomassie blue solution
Coomassie Blue solution for SDS-PAGE	1% Coomassie blue in ethanol

Western blot buffers

PBST	8 mM Na ₂ HPO ₄ , pH 7.4 at RT 2 mM KH ₂ PO ₄ 150 mM NaCl 3 mM KCl 0.1% Tween 20
------	--

Transfer buffer	25 mM Tris-base 192 mM Glycine 20% Methanol
Wash buffer	150 mM NaCl 0.5% Triton-X 0.2% SDS
Blocking buffer	20% Skimmed milk in PBST

4.2 Cell culture media

LB broth	10 g/l NaCl 10 g/l Tryptone 5 g/l Yeast extract
LB agar	10 g/l NaCl 10 g/l Tryptone 5 g/l Yeast extract 15 g/l Agar

4.3 Chemicals

2-Mercaptoethanol	Sigma-Aldrich, Steinheim, Germany
4-(2-hydroxyethyl)-1-piperazineethane sulfonic acid (HEPES)	Sigma-Aldrich, Steinheim, Germany
Acetic acid	Merck KGaA, Darmstadt, Germany
Acetonitrile	Merck KGaA - Darmstadt, Germany
Acrylamide (29:1) 40%	Serva, Heidelberg, Germany
Agar	BD, Le Pont de Claix, France
Agarose SERVA for DNA electrophoresis	SERVA electrophoresis, Heidelberg, Germany
Ammonium chloride (NH ₄ Cl)	Merck KGaA, Darmstadt, Germany
Ammonium persulfate (APS)	Merck KGaA, Darmstadt, Germany
Bromphenol Blue sodium salt	Merck KGaA, Darmstadt, Germany
Casein from bovine milk	Sigma-Aldrich, Steinheim, Germany
Complete EDTA free protease inhibitor	Roche, Indianapolis, USA

Coomassie Blue G250	Merck KGaA, Darmstadt, Germany
Dimethyl sulfoxide (DMSO)	Merck KGaA, Darmstadt, Germany
Disodium hydrogen phosphate dihydrate (Na_2HPO_4)	Merck KGaA, Darmstadt, Germany
Dodecylsulphate-Na-salt pellets (SDS)	SERVA electrophoresis, Heidelberg, Germany
DTT Biochemica	AppliChem, Darmstadt, Germany
Ethanol	Merck KGaA, Darmstadt, Germany
Ethylenediamine tetraacetic acid (EDTA)	Merck KGaA, Darmstadt, Germany
Formic acid	Merck KGaA, Darmstadt, Germany
Glacial acetic acid	Merck KGaA, Darmstadt, Germany
Glycerol	Merck KGaA, Darmstadt, Germany
Glycine	Merck KGaA, Darmstadt, Germany
Hydrochloric acid (HCl)	J.T Baker, Daventer, Netherlands
Isopropyl β -D-1-thiogalactopyranoside (IPTG)	Carl Roth, Karlsruhe, Germany
Magnesium chloride hexahydrate ($\text{MgCl}_2 \cdot 6\text{H}_2\text{O}$)	Merck KGaA, Darmstadt, Germany
Methanol	Merck KGaA, Darmstadt, Germany
N,N,N',N'-tetramethylethylenediamine (TEMED)	Sigma-Aldrich, Steinheim, Germany
Perfect protein marker 15-150 kDa	Novagen, San Diego, USA
Phosphoenolpyruvate (PEP)	Sigma-Aldrich, Steinheim, Germany
Potassium chloride (KCl)	Merck KGaA, Darmstadt, Germany
Potassium dihydrogen phosphate (KH_2PO_4)	Merck KGaA, Darmstadt, Germany
Potassium hydroxide (KOH)	Merck KGaA, Darmstadt, Germany
Putrescine dihydrochloride	Sigma-Aldrich, Steinheim, Germany
Scintillation cocktail Lumasafe plus	PerkinElmer, Massachusetts, USA
Scintillation cocktail Quickszint 361	Zinsser analytic, Frankfurt, Germany
SERVA DNA Stain G	SERVA electrophoresis, Heidelberg, Germany
SmartLadder	Eurogentec Deutschland, Köln, Germany
Sodium acetate (NaOAc)	Merck KGaA, Darmstadt, Germany
Sodium chloride (NaCl)	Merck KGaA, Darmstadt, Germany
Spermidine trihydrochloride	Sigma-Aldrich, Steinheim, Germany
Spermine trihydrochloride	Sigma-Aldrich, Steinheim, Germany
Sucrose	Merck KGaA, Darmstadt, Germany
TCEP (<i>tris</i> (2-carboxyethyl)phosphine)	Sigma-Aldrich, Steinheim, Germany
Trichloro acetic acid (TCA)	Merck KGaA, Darmstadt, Germany
Trifluoro acetic acid (TFA)	Merck KGaA, Darmstadt, Germany

Tris(hydroxymethyl)-aminomethane (Tris)	Merck KGaA, Darmstadt, Germany
Triton-X	Merck KGaA, Darmstadt, Germany
Tryptone	Carl Roth, Karlsruhe, Germany
Urea	Merck KGaA, Darmstadt, Germany
Xylene cyanol FF	Merck KGaA, Darmstadt, Germany
Yeast Extract	Carl Roth, Karlsruhe, Germany

4.4 Antibiotics

Ampicillin sodium salt	Sigma-Aldrich, Steinheim, Germany
Fusidic acid sodium salt	Sigma-Aldrich, Steinheim, Germany
Hygromycin B	Sigma-Aldrich, Steinheim, Germany
Kanamycin sulfate	SERVA electrophoresis, Heidelberg, Germany
Neomycin sulfate	Sigma-Aldrich, Steinheim, Germany
Paromomycin sulfate	Sigma-Aldrich, Steinheim, Germany
Puromycin dihydrochloride	Sigma-Aldrich, Steinheim, Germany
Spectinomycin dihydrochloride pentahydrate	Sigma-Aldrich, Steinheim, Germany
Streptomycin sulfate	Sigma-Aldrich, Steinheim, Germany
Viomycin sulfate	Fitzgerald, Massachusetts, USA

4.5 Fluorophores and Radioactive compounds

Alexa 488 maleimide (Alx488)	Life Technologies, Darmstadt, Germany
Alexa 568 maleimide (Alx568)	Life Technologies, Darmstadt, Germany
Atto 540Q maleimide (Atto540Q)	Life Technologies, Darmstadt, Germany
Cy3 maleimide monoreactive dye	GE Healthcare Life Sciences, Freiburg, Germany
Cy5 maleimide monoreactive dye	GE Healthcare Life Sciences, Freiburg, Germany
³ [H]Methionine	Perkin Elmar, Massachusetts, USA
¹⁴ [C]Lysine	Perkin Elmar, Massachusetts, USA
¹⁴ [C]Valine	Perkin Elmar, Massachusetts, USA
¹⁴ [C]Phenylalanine	Perkin Elmar, Massachusetts, USA
¹⁴ [C]Proline	Perkin Elmar, Massachusetts, USA

4.6 Nucleotides

Deoxy-nucleotide triphosphate (dNTP)	New England BioLabs (NEB), Frankfurt, Germany
Guanosine-5'-triphosphate (GTP)	Jena Biosciences, Jena, Germany
Guanosine 5'-O-[γ -thio]triphosphate (GTP γ S)	Jena Biosciences, Jena, Germany

4.7 Kits

BCA Protein Assay kit	Thermo Scientific, Rockford, USA
Quick and Easy <i>E. coli</i> Gene Deletion kit	Gene Bridges, Heidelberg, Germany
In-fusion Cloning kit	Clontech – Saint-Germain-en-Laye, France
Macharey-Nagel Plasmid Preparation Kit	MACHEREY-NAGEL GmbH & Co. KG, Düren, Germany
NucleoSpin Gel and PCR clean up	Macherey Nagel, Düren, Germany

4.8 Plasmids

pET28a (+)	Novagen, San Diego, USA
------------	-------------------------

4.9 Enzymes

DNase	Sigma-Aldrich, Steinheim, Germany
<i>Dpn1</i>	NEB, Frankfurt, Germany
Lysozyme	Sigma-Aldrich, Steinheim, Germany
Pyruvate kinase (PK)	Roche Diagnostics, Mannheim, Germany
Phusion High Fidelity DNA Polymerase provided with 5x HF buffer	NEB, Frankfurt, Germany

4.10 Cell strains

<i>E. coli</i> BL21(DE3)	Novagen San Diego, USA
<i>E. coli</i> Bw25113	DMSZ, Braunschweig, Germany
<i>E. coli</i> K12 Δ L33	Prof. Janine Maddock
<i>E. coli</i> K12 Δ S13	Prof. Rachel Green
<i>E. coli</i> MRE600	UAB, Alabama, USA

4.11 Chromatographic columns

Chromolith®RP-8e	Merck KGaA, Darmstadt, Germany
HiTrap™ Capto™ Q	GE Healthcare, Uppsala, Sweden

HiTrap™ Capto™ S

GE Healthcare, Uppsala, Sweden

superdex™ 10/300 GL

GE Healthcare, Uppsala, Sweden

4.12 Other consumables

Amicon centrifugal filters

Merck KGaA, Darmstadt, Germany

Beckman Coulter centrifuge tubes

Beckman Coulter, Krefeld, Germany

Cellulose acetate syringe filter

Sartorius Biolab, Göttingen, Germany

Cellulose nitrate filter

Sartorius Biolab, Göttingen, Germany

Cellulose nitrate filter

Sartorius Biolab, Göttingen, Germany

D-Tube Dialyzers

Merck KGaA, Darmstadt, Germany

Ministrant syringe filters

Sartorius Biolab, Göttingen, Germany

Stopped-flow cut-off filters KV418,

Schott AG, Mainz, Germany

KV500, OG590

4.13 Instruments

Äkta Purifier Plus

GE Healthcare, Braunschweig, Germany

Avanti® J-26S XP centrifuge

Beckman Coulter, Krefeld, Germany

Avanti™ J-30I centrifuge

Beckman Coulter, Krefeld, Germany

Branson Digital Sonifier

Emerson, St. Louis, USA

Cell density meter- Ultrospec 10

GE Healthcare, Uppsala, Sweden

Cell power supply (Mini PROTEAN Tetra)

BIORAD, California, USA

Centrifuge 5810R (F3Y-6-30 rotor)

Eppendorf AG, Hamburg, Germany

Electrophoresis chamber

BIORAD, California, USA

Emulsiflex –C3

Avestin, Ottawa, Canada

Eppendorf centrifuge 5415R

Eppendorf AG, Hamburg, Germany

HPLC

Waters, Massachusetts, USA

Innova 44 shaker

Eppendorf AG, Hamburg, Germany

IX 81 inverted microscope using a PLAPON 60 ×

Olympus, Tokyo, Japan

1.45 numerical aperture objective

Lab pH meter inoLab® pH 720

WTW, Weilheim, Germany

Liquid scintillation counter

PerkinElmer, Massachusetts, USA

Milli-Q water purification system

Merck KGaA, Darmstadt, Germany

NanoDrop 2000c UV-Vis Spectrophotometer

Thermo Fisher Scientific, Karlsruhe, Germany

Optima™ L-100 XP ultracentrifuge

Beckman Coulter, Krefeld, Germany

Optima™ MAX-XP ultracentrifuge

Beckman Coulter, Krefeld, Germany

PeqLab UV transilluminator	VWR International, Darmstadt, Germany
Phosphorimager Fuji Film Fla 7000/9000	GE Healthcare, Germany
Quench Flow	KIN-TEK Laboratories, Texas, USA
Rotors : 50.2 Ti	Beckmann Coulter, California, USA
JLA 8.1000	Beckmann Coulter, California, USA
MLA 130	Beckmann Coulter, California, USA
TLS-55	Beckmann Coulter, California, USA
Spectrophotometer	PerkinElmer, Massachusetts, USA
SX-20MV stopped-flow apparatus	Applied Photophysics, Leatherhead, UK
Thermo-cycler PeqStar	VWR International, Darmstadt, Germany
Thermomixer comfort	Eppendorf AG, Hamburg, Germany
Vortex Genie 2	Scientific Industries, Inc., Bohemia, NY, USA

4.14 Softwares

Prism	GraphPad Software, California, USA
KinTek Explorer	KinTek, Texas, USA
Multigauge	Fujifilm, Tokyo, Japan
Prodata viewer	Applied Photophysics

4.15 DNA primers

Insertion of kanamycin cassette into the *E. coli* genome for deletion of S6 gene (*rpsF*) (refer to Quick & Easy *E. coli* Gene Deletion Kit).

Upper oligonucleotide 5'GATTCGGCTGACCCAGACAGGAGGCTGAATAATCCGTAAGG
AGCAATTCGAATTAACCCTCACTAAAGGGCG3'

Lower oligonucleotide 5'GGAGCCCTGCACACGGTGCCGGACAACACCAGACGGTTGGT
CATCAGAAATAATACGACTCACTATAGGGCTC3'

Insertion of kanamycin cassette into the *E. coli* genome for deletion of L9 gene (*rplI*) (refer to Quick & Easy *E. coli* Gene Deletion Kit).

Upper oligonucleotide 5'CATCAGTAATCGGTCACGGTCCATTAATACGACTTTGAGAGG
ATAAGGTAAATTAACCCTCACTAAAGGGC3'

Lower oligonucleotide 5'GCAAACGCCGACCAATGGTCGGCGTTTTTACGTCTCGTTGA
ATAACGAATAATACGACTCACTATAGGGCTC3'

Linearization of pET28a (+) vector and removal of MCS and C- terminal His tag for in-fusion reaction.

Forward Primer 5'GTGATGATGATGATGATGGCTGCTGCC3'

Reverse Primer 5'TAACAAAGCCCGAAAGGAAGCTGAGTTG3'

Amplification of the S6 gene from the *E. coli* genome

Forward Prime 5'TTTCGGGCTTTGTTACTTCTTCAGAATCCCCAGCTTCAGC3'

Reverse Primer 5'CATCATCATCATCACATGCGTCATTACGAAATCGTTTTTATG3'

Removal of N-terminal His tag from pET28a (+) – S6 vector

Forward Primer: 5'GGTATATCTCCTTCTTAAAGTTAAAC3'

Reverse Primer: 5'ATGCGTCATTACGAAATCGTTTTTATG3'

Amplification of the L9 gene from the *E. coli* genome

Forward Primer 5'TTTCGGGCTTTGTTATTCAGCTACTACGTTTACGATCAC3'

Reverse Primer 5'GTGCCGCGCGGCAGCATGCAAGTTATTCTGCTTGATAAAG3'

Removal of N-terminal His tag from pET28a (+) – L9 vector

Forward Primer	5'ATGCAAGTTATTCTGCTTGATAAAGTAG3'
Reverse Primer	5'CATGGTATATCTCCTTCTTAAAGTTAAAC3'

Site-directed mutagenesis in S6 (D41C)

Forward Primer	5'CACCGTCTGGAATGCTGGGGCCGCGTC3'
Reverse Primer	5'GACGGCGGCCCCAGCATTCCAGACGGTG3'

Site-directed mutagenesis in L9 (N11C)

Forward Primer	5'CTTGATAAAGTAGCATGCCTGGGTAGCC3'
Reverse Primer	5'GGCTACCCAGGCATGCTACTTTATCAAG3'

*All primers were from Eurofins Genomics, Ebersberg, Germany

4.16 mRNAs**Rapid kinetic approach**

mMK	5'GUU AACAGGU AUACA UACU <u>AUGAAA</u> UUC AUUAC3'
mMV	5'GUU AACAGGU AUACA UACU <u>AUGGUGU</u> UUC AUUAC3'
mMF	5'GUU AACAGGU AUACA UACU <u>AUGUUU</u> GUU AUUAC3'
mMP	5'GGCAAGGAGGU AAAUAA <u>UGCCG</u> UUC AUU3'

smFRET experiments (mRNAs with 5'- Biotin)

mMK	5'CAACCUAAAACU UACACACCCGGCAAGGAGGU AAAUAA <u>AUG</u> <u>AAGU</u> AAACGAUU3'
mMV	5'CAACCUAAAACU UACACACCCGGCAAGGAGGU AAAUAA <u>AUG</u> <u>GUU</u> AAACGAUU3'
mMF	5'CAACCUAAAACU UACACACCCGGCAAGGAGGU AAAUAA <u>AUG</u> <u>UUC</u> AAACGAUU3'

*All mRNAs were ordered from IBA, Göttingen, Germany

4.17 Preparation of fluorescence-labeled ribosomes

4.17.1 Development and verification of S6 and L9 knockout strains

The chromosomal genes for protein S6 (*rpsF*) and L9 (*rplI*) were deleted in *E. coli* strain BW25113 using the Quick & Easy *E. coli* Gene Deletion kit which utilizes homologous recombination to replace a gene of interest with the kanamycin resistant gene for generation of knockout strains. The deletion of genes was confirmed on both genetic level using gene specific primers in a PCR reaction (as mentioned in the protocol, **Figure 4.1**) and on protein level by western blotting (**Figure 4.2**).

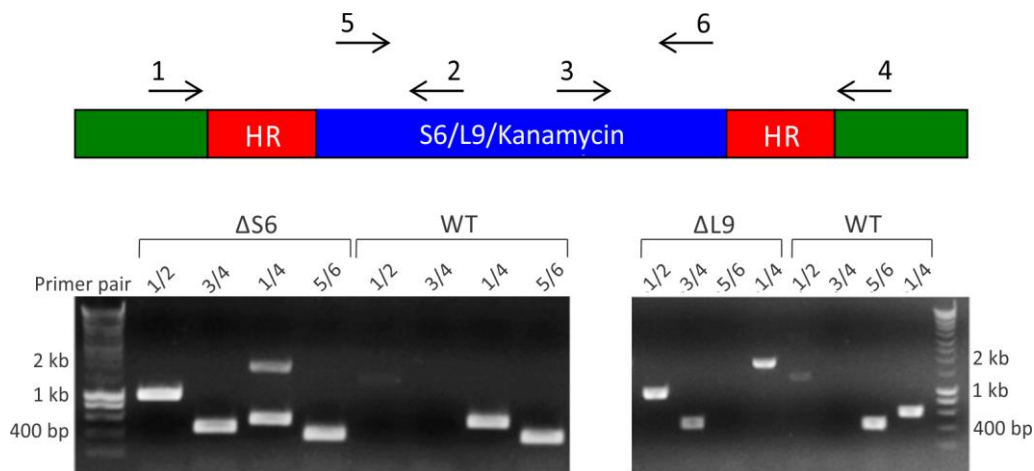


Figure 4.1 Verification of the S6 and L9 knockouts by PCR.

The top panel represents the segment of the *E. coli* chromosomal genome with either the gene coding for protein S6 or L9 or the kanamycin resistance gene (blue). The region of the genome flanking the gene (red) was used to amplify the kanamycin resistance gene from a separate plasmid for the homologous recombination. The homologous recombination replaces the gene for protein S6 or L9 with the gene for kanamycin resistance. The adjacent immediate regions of the chromosome are shown in green. The numbers indicate primers and the arrows indicate the region of amplification in the PCR reaction for the verification of knockouts. In PCR reactions, combination of primers 1/2 or 3/4 should show amplification of product if the gene for proteins is replaced by the kanamycin resistance gene. Primers 5/6 are specific for genes of proteins S6 or L9 while primers 1/4 should show products of different sizes depending on whether the gene for protein S6 or L9 is present or whether it is replaced by the kanamycin resistance gene. The lower panel shows PCR amplification products obtained by combinations of different primers. Size of genes for protein S6 and L9 are 396 bp (base pair) and 450 bp, respectively.

In the $\Delta L9$ strain no amplification of the L9 gene was observed confirming successful knockout of the gene. Additionally, the use of different combination of primers gave amplified products that corresponded to the insertion of the kanamycin gene in place of the L9 gene. On the contrary, an unexpected result was observed with the $\Delta S6$ strain. The amplified products observed with different combination of primers corresponded to the presence of genes for both S6 and the kanamycin resistance. The non-specific insertion of the kanamycin cassette to other regions of the chromosome was ruled out as the PCR reaction with the primers complimentary to the flanking region of the gene gave amplified products corresponding to the presence of both S6

and kanamycin resistance gene (primers 1/4). Possibility that the gene of kanamycin resistance was inserted adjacent to the gene of protein was also ruled out based on the size of the amplified products in PCR reaction. These observations can be explained by the fact that some regions of the chromosomes are prone to undergo partial gene duplication during DNA replication. A duplicated gene might be inactive as the duplication is only partial and the gene loses its accessory segments (promoter or other regulatory elements of the DNA) necessary for transcription (Yamamoto et al., 2009). In order to confirm the absence of protein S6 in the Δ S6 strain we used western blotting and mass spectrometry (**Figure 4.2**).

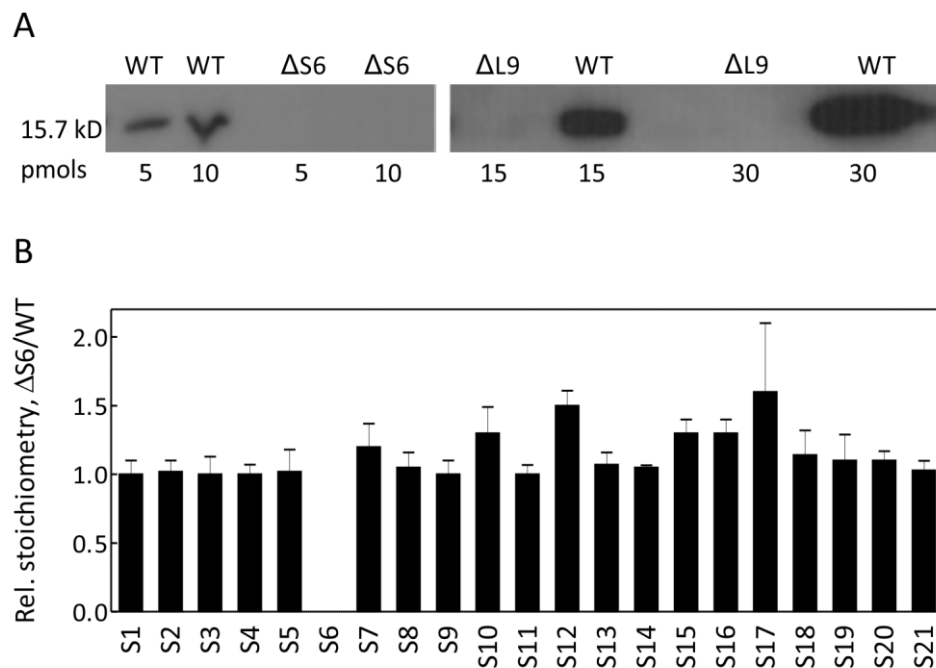


Figure 4.2 Verification of S6 and L9 knockouts by western blot analysis and mass spectrometry.

(A) Crude ribosomes were prepared from wild type (WT), Δ S6 and Δ L9 *E. coli* strains and were subjected to western blot analysis using specific anti-S6 or anti-L9 antibodies. No band was visible for protein S6 or L9 in the Δ S6 or Δ L9 strain, respectively confirming the absence of these proteins in the ribosomes. (B) Quantification of ribosomal proteins by mass spectrometry confirming the absence of protein S6 in Δ S6 strain (Values are mean \pm s.d. (Nt = 3 technical replicates). The ratio of the average protein concentrations Δ S6/WT was plotted. The mass spectrometry experiment was performed by Dr. Ingo Wohlgenuth.

The colonies that showed insertion of the kanamycin resistance gene were inoculated in 3 ml LB broth containing 30 μ g/ml kanamycin and the culture was grown overnight at 37°C. On the next day, 200 μ l of pre-culture was used to inoculate 200 ml of fresh LB medium containing 30 μ g/ml kanamycin and the culture was grown until an OD of 0.8 was reached and the cells were harvested by centrifugation at 6,000 rpm for 30 min in an Avantis™ J-30I centrifuge using rotor JA-30.5 Ti. The pellets (~1 g) were dissolved in 5 ml TAKM₇ containing 10% glycerol, 6 mM 2-mercaptoethanol, Complete Protease Inhibitor and trace amounts of DNase I. Samples were sonicated, using sonifier, for 10 min (30 s pause time, 15 s pulse time and 30% of amplitude) and

centrifuged at 12,000 rpm, in an Avantis™ J-30I centrifuge using rotor JA-30.5 Ti, for 30 min. The supernatant was separated from the pellet and 1 ml of the supernatant was loaded on a 400 µl of a 40% sucrose cushion (in TAKM₇) followed by centrifugation at 259,000 x g in a rotor TLS 55 and Optima™ MAX-XP ultracentrifuge for 2.5 h at 4°C. The pellets were re-suspended in 30 µl TAKM₇ and the ribosome concentrations were determined by absorption measurements at 260 nm (23 pmols of 70S ribosomes equal to one OD at 260 nm in one ml and one cm path length) and the samples were used for western blot analysis. For mass spectrometry the one hundred picomoles of purified wild type and ΔS6 ribosomes were proteolyzed with trypsin and analyzed by LC-ESI MS/MS as described in (Maracci et al., 2015).

4.17.2 Cloning and expression

E. coli genes for proteins S6 and L9 were PCR-amplified from strain BW25113 and were cloned into the plasmid pET28a (+) (without any tag) using the in-fusion cloning kit. Both proteins lack native cysteine. The cysteine residues were introduced at position 41 in protein S6 replacing aspartic acid and at position 11 in protein L9 replacing asparagine, by a two-step polymerase chain reaction for site-directed mutagenesis (Wang and Malcolm, 2002). Plasmids coding for recombinant proteins were transformed into BL21(DE3) cells and cultures were grown in LB medium supplemented with kanamycin (30 µg/ml) at 37°C overnight. On the next day, 3 L of LB medium was inoculated with pre-culture to a starting OD of ~0.1. At 0.5 OD₆₀₀, the protein expression was induced by addition of 1 mM IPTG and cultures were grown for another 4 h. Cells were harvested by centrifugation at 5,000 rpm for 30 min, in an Avantis® J-26 XP centrifuge with a rotor JLA 8.1 and pellets were dissolved in lysis buffer with the addition of Complete Protease Inhibitor and trace amounts of DNase I (5 ml of lysis buffer for 1 gm of cells). Cells were opened using an Emulsiflex apparatus and the extract was centrifuged for 30 min at 50,000 x g using a rotor 50.2 Ti and an Optima™ L-100 XP ultracentrifuge. Proteins in inclusion bodies were pelleted along with the cell debris and each protein was purified as described below.

4.17.3 Purification of protein S6

The purification of protein S6 was performed as described in (Hickerson et al., 2005). The pellet containing inclusion bodies was dissolved in 20 ml of buffer B. Insoluble matter was pelleted at 7,000 rpm at 4°C in an Eppendorf 5810R centrifuge for 30 min and the supernatant containing solubilized protein was dialyzed three times against buffer A for 2 h at 4°C. The solution was cleared by centrifugation in an Eppendorf 5810R centrifuge and rotor F34-6-3 followed by filtration of the supernatant through a 0.45 µm cellulose acetate syringe filter. The purification was carried out by FPLC using two 5 ml HiTrap™ Capto™ Q columns in series with a 200 ml 0-40 % linear gradient of buffer B in buffer A. Fractions containing protein S6 were pooled, aliquoted, fast

froze and stored in -80°C . The purity of the protein was checked by SDS PAGE (polyacrylamide gel electrophoresis).

4.17.4 Purification of protein L9

The pellet containing inclusion bodies was dissolved in 20 ml of buffer D. Insoluble matter was pelleted at 7,000 rpm at 4°C in an Eppendorf 5810R centrifuge for 30 min and the supernatant containing solubilized protein was dialyzed three times against buffer C for 2 h at 4°C . The solution was cleared by centrifugation in an Eppendorf 5810R centrifuge using a rotor F34-6-30 and the supernatant was filtered through a $0.45\ \mu\text{m}$ cellulose acetate syringe filter. The purification was carried out by FPLC using two 5 ml HiTrap[™] Capto[™] Q columns in series in buffer C. Flow through and wash were collected (in buffer C) which contained the protein. Columns were washed with buffer D to elute all unwanted proteins so that columns can be reused. Flow through and wash were then loaded to two 5 ml HiTrap[™] Capto[™] S column in series and washed with buffer C. Again, flow-through and wash were collected as they contained the protein. The standard procedure of ion exchange chromatography could not be applied to the purification of protein L9 as under no condition the protein bound to any of the column tested. Therefore, we used the two-step purification with two different ion-exchange columns to remove unwanted proteins and collected flow-through and wash which also yielded pure protein. Flow-through and wash were pooled, aliquoted, fast-frozen and stored in -80°C . The purity of the protein was checked by SDS PAGE.

4.17.5 Labeling of proteins

Both proteins S6 and L9 were first dialyzed 2 times for 6 h against labeling buffer at 4°C to remove 2-mercaptoethanol using D-tubes with a 3K cut-off. The concentration of proteins was determined by densitometry using SDS PAGE and the bicinchoninic acid (BCA) assay with lysozyme as a standard protein. The dyes used for labels, Alexa 488, Alexa 568, Cy3 and Cy5 were dissolved in 100% DMSO to get a final concentration not more than 10 mM. To reduce possibly formed disulfide bonds, proteins were incubated with a 10-fold molar excess of TCEP for 30 min at room temperature before labeling.

Labeling of protein S6 with Alexa 488 or Cy5 and protein L9 with Alexa 568 or Cy3 was performed under denaturing conditions with a 8-fold molar excess of the dye over protein overnight at 4°C in labeling buffer. The volume of the labeling reaction was adjusted such that in the final mixture the percentage of DMSO is not more than 10%. After overnight incubation, labeling of protein was checked by SDS PAGE followed by a fluorescence scan and coomassie staining. The reaction was then quenched with 2-mercaptoethanol (6 mM). Excess dye was removed by gel filtration column Superdex[™] 10/300 GL in buffer E. Fractions containing labeled

proteins were pooled together, concentrated by amicon ultra centrifugal filters with 3 KDa cut-off and refolded by stepwise dialysis to remove urea (6 M, 4 M, 2 M, 1 M, 0 M) in reconstitution buffers for 6 h in each buffer at 4°C. The concentration of the labeled protein was determined spectroscopically by absorption measurement and extinction coefficients as described in **Table 4.1**. Labeled proteins were aliquoted, fast frozen and stored in -80°C.

Table 4.1 Fluorescence dyes and their properties.

Dyes	Absorption maxima (λ_{max}), nm	Emission maxima nm	Extinction coefficient (ϵ), $\text{cm}^{-1}\text{M}^{-1}$
Alexa 488	495	519	73,000
Alexa 568	578	603	88,000
Cy3	550	570	150,000
Cy5	650	670	250,000

4.17.6 Reconstitution

Δ S6 and Δ L9 mutant ribosomal SSU and LSU were prepared by zonal centrifugation according to the protocol described in (Peske et al., 2005; Rodnina and Wintermeyer, 1995). Purified Δ S6 SSUs were reconstituted with a 2-fold excess of labeled protein S6 in reconstitution buffer for 30 min at 42°C. After 30 min the concentration of Mg^{2+} ions was raised to 20 mM and the reaction was further incubated for 30 min at 42°C. Purified Δ L9 LSUs were reconstituted with a 2-fold excess of labeled protein L9 in reconstitution buffer for 1 h at 37°C. After one 1 h of reconstitution, the reaction mixture was incubated for 15 min on ice and then centrifuged at 13,000 rpm for 15 min using an Eppendorf centrifuge 5415R (Ermolenko et al., 2007a).

The excess of labeled protein was separated from the reconstituted subunits by passing through a 30% sucrose cushion for 3 h at 259,000 x g using a rotor MLA130 and an Optima™ MAX-XP ultracentrifuge. The extent of subunit labeling determined spectroscopically was close to 100% (**Table 4.1**). Subunit concentrations were determined by absorption measurements at 260 nm (67 pmols of SSUs or 37 pmols of LSUs equal to one OD at 260 nm in one ml and one cm path length (Richter, 1976)). The recovery of the subunits was 85-95%.

4.18 Preparation of ribosome complexes

Preparation and purification of initiation complex, PRE and POST complexes were carried out as described previously (Belardinelli et al., 2016; Rodnina et al., 1997). Labeled SSU were heat-activated in TAKM buffer with 21 mM MgCl_2 (TAKM₂₁) for 30 min at 37°C. Activated SSU were incubated with a 1.5-fold excess of labeled LSU, a 3-fold excess of mRNA, a 2-fold excess of IF1,

IF2, IF3 each and a 2.5-fold excess of f[³H]Met-tRNA^{fMet} in TAKM₇ containing 1 mM GTP for 30 min at 37°C to form initiation complex. Ternary complexes with EF-Tu-GTP-[¹⁴C]X-tRNA^X (X is Lys, Val, Phe or Pro) were prepared by incubating EF-Tu (2-fold excess over tRNA) with 1 mM GTP, 3 mM phosphophenolpyruvate and 0.1 mg ml⁻¹ pyruvate kinase for 15 min at 37°C followed by the addition of X-tRNA^X. PRE complex (PRE(fMX)) was formed by mixing initiation complex with a 2-fold excess of ternary complex and incubation for 1 min at 37°C. POST complexes (fMX) were prepared by adding EF-G (5 nM) to the PRE complexes with 1 mM GTP and incubation for 1 min at 37°C. The resulting initiation complex, PRE or POST complexes were purified through 1.1 M sucrose cushion in TAKM₂₁ by centrifugation at 259,000 x g using a rotor TLS 55 and an OptimaTM MAX-XP ultracentrifuge for 2 h. The pellets were re-suspended in TAKM₂₁ and tRNA binding was verified by nitrocellulose filtration. The concentration of the complexes was determined by radioactivity counting of the ribosome bound radioactive tRNAs.

4.19 Rapid kinetics experiments

We performed rapid kinetic experiments with the double-labeled ribosomes (S6Alx488–L9Alx568). Rates of peptide bond formation were measured using a quench-flow apparatus and subunit rotation was monitored using a stopped-flow apparatus in TAKM₇ at 37°C unless otherwise stated. To monitor subunit rotation, Alexa 488 was excited at 470 nm and the fluorescence of the acceptor and the donor was monitored after passing through an OG590 or a KV500 cut-off filter, respectively. All concentrations reported are the final concentration after mixing of the reactants in quench-flow or the stopped-flow apparatus.

4.19.1 Characterization of the double-labeled ribosomes

To test the translocation activity of the double-labeled ribosomes, we prepared PRE complex (described above) with tRNA^{fMet} in the P site and fMetPhe-tRNA^{Phe} (PRE(fMF)) in the A site using either wild type, S6Alx488–L9Alx568-labeled or S6Cy5–L9Cy3-labeled ribosomes. PRE(fMF) complexes (0.1 μM) were rapidly mixed with Pmn (10 mM) and EF-G (4 μM) in the presence of GTP (1 mM) in a quench-flow apparatus to perform a time-resolved Pmn assay (described below). To confirm that the presence of high concentrations of EF-G or DTT does not affect the Pmn reaction, POST complex with fMetPhe-tRNA^{Phe} (0.1 μM) in the P site was rapidly mixed with Pmn (10 mM) in the absence or presence of EF-G (4 μM) or DTT (1 mM) in a quench-flow apparatus.

To monitor the fluorescence change due to subunit rotation, initiation complex (0.05 mM) was rapidly mixed with ternary complex (10 μM), PRE(fMF) complex (0.05 μM) was rapidly mixed with EF-G (4 μM) or initiation complex was rapidly mixed with ternary complex (10 μM) and EF-G (4 μM). All experiments were performed in the presence of GTP (1 mM). As control experiments, we prepared single-labeled PRE(fMF) complex with either S6Alx488 or L9Alx568 and rapidly mixed

them with EF-G (4 μ M) in the presence of GTP (1 mM). The labeled ribosomes were excited at 470 nm and the fluorescence was recorded in both acceptor and donor channels after passing through an OG590 and a KV500 cut-off filter, respectively. Additionally, single-labeled-L9Aix568 PRE(fMF) was rapidly mixed with EF-G (4 μ M) in the presence of GTP (1 mM). Ribosomes were excited at 560 nm (excitation wavelength for Alexa 568) and the fluorescence signal was recorded in both acceptor and donor channels as before.

4.19.2 Kinetics of spontaneous subunit rotation with different tRNAs in the P site

Rates of peptide bond formation were measured using a quench-flow apparatus and CCW subunit rotation was monitored using a stopped-flow apparatus in TAKM₇ at 37°C unless otherwise mentioned. Time course of peptide bond formation was measured by rapidly mixing POST complexes (fMX, 0.1 μ M) with Pmn (10 mM) in a quench-flow machine and the reaction was quenched with KOH (0.5 M). Peptides were released by incubation for 45 min at 37°C followed by the addition of 100% acetic acid (one-tenth of reaction volume) to neutralize the reaction making it compatible with HPLC buffers. Samples were analyzed by reversed phase HPLC (Chromolith®RP-8e) using gradient of acetonitrile (buffer G and H) and quantified by radioactivity counting. We monitored subunit rotation by rapidly mixing POST complex (fMX, 0.1 μ M) with Pmn (10 mM) in a stopped-flow apparatus.

The concentration dependence of peptide bond formation and spontaneous subunit rotation with fMK complex (0.1 μ M) were performed upon addition of increasing concentrations of Pmn (0.1–20 mM) in either stopped-flow or quench-flow experiments. The temperature dependence of spontaneous subunit rotation was measured by rapid mixing of PRE(fMK) complex (0.1 μ M) with Pmn (10 mM) at 15, 20, 25, 30 and 37°C using a stopped-flow apparatus.

4.19.3 Kinetics of spontaneous subunit rotation with different tRNAs in the A site

We prepared initiation complex (0.1 μ M) using different mRNAs with codons for Lys, Val, Phe or Pro in the second position and rapidly mixed them with ternary complex EF-Tu-GTP-[¹⁴C]X-tRNA^X (X is Lys, Val, Phe or Pro) (10 μ M) to measure the rate of peptide bond formation and CCW subunit rotation in the quench-flow and stopped-flow apparatus, respectively, similar to the reaction of POST complexes with Pmn (described above). In addition, we prepared POST complexes (0.1 μ M) with fMetPhe-tRNA^{Phe} or fMetVal-tRNA^{Val} in the P site and rapidly mixed them with EF-Tu-GTP-[¹⁴C]Val-tRNA^{Val} or EF-Tu-GTP-[¹⁴C]Phe-tRNA^{Phe}, respectively to monitor CCW subunit rotation.

4.19.4 Effect of EF-G on subunit rotation

We prepared PRE complexes with tRNA^{fMet} in the P site and fMetX-tRNA^X in the A site (where X is Lys, Val, Phe or Pro) as described above. Time courses for EF-G-induced subunit rotation were monitored after rapidly mixing PRE complexes (PRE(fMX)) (0.05 μ M) with EF-G (4 μ M) in a stopped-flow apparatus in TAKM₇ at 37°C or in smFRET buffer at 22°C. The concentration dependence of subunit rotation for PRE(fMK), PRE(fMV) and PRE(fMF) complex (0.05 μ M) was monitored with increasing concentration of EF-G (0.5 - 8 μ M) in TAKM₇ at 37°C and also at 25°C for PRE(fMK). Time courses of subunit rotation were also measured with PRE(fMV) or PRE(fMF) complex (0.05 μ M) in the presence of EF-G (4 μ M) and GTP (1 mM) or GTP γ S (1 mM); or EF-G(H583K) (4 μ M) and GTP (1 mM) in TAKM₇, 37°C. In addition, we also monitored subunit rotation upon rapid mixing of PRE(fMV) complex (0.05 μ M) with EF-G(XL) (cross-linked mutant) (4 μ M) or EF-G(Δ 4/5) (4 μ M) and of PRE(fMF) (0.05 μ M) with EF-G(H91A) (4 μ M) or EF-G(Δ 4/5) (4 μ M) in the presence of GTP (1 mM). In order to see the stabilization effect of EF-G on the R state of the ribosome, we prepared POST(fMV) complex (0.05 μ M) and rapidly mixed it with Pmn (10 mM) in the presence or absence of EF-G(H91A) (4 μ M) and monitored subunit rotation in a stopped-flow apparatus.

4.19.5 Effect of Mg²⁺ ion concentration on subunit rotation

To monitor the effect of the Mg²⁺ ion concentration on subunit rotation, we prepared PRE(fMF) complex (0.05 μ M) in TAK buffer containing 3.5 mM MgCl₂ (TAKM_{3.5}) and rapidly mixed it with TAK buffer with 36 mM MgCl₂ (TAKM₃₆) in a stopped-apparatus. As equal volumes of the two reactants are mixed in the apparatus, the final concentration of Mg²⁺ ions in the reaction mixture was 20 mM. Additionally, PRE(fMF) or PRE(fMV) complex (0.05 μ M) were rapidly mixed with EF-G (4 μ M) in the presence of GTP (1 mM) in either TAKM₇ or TAK buffer with 21 mM MgCl₂ (TAKM₂₁) to monitor EF-G-promoted subunit rotation at different Mg²⁺ ion concentrations.

Further, to study the effect of polyamines on subunit rotation, we prepared POST(fMF) complex (0.05 μ M) with fMetLys-tRNA^{Lys} in the P site (described above). The dipeptide was removed by the addition of 1 mM Pmn to the POST complex. The resulting POST complexes carrying deacylated tRNA in the P site were then rapidly mixed with either TAKM₇ as a control or with TAKM₇ containing 0.5 mM spermidine, 8 mM putrescine and 0.6 mM spermine in a stopped-flow apparatus.

4.19.6 Effect of antibiotics on subunit rotation

SSU body rotation was measured as described. Head swiveling was measured using double-labeled ribosomes (S13Atto540Q–L33Alx488) (Belardinelli et al., 2016). Alexa 488 was excited at

470 nm and the emission was recorded after passing through a KV500 cut-off filter. To measure the effect of antibiotics binding on the rotational state of the ribosome, double-labeled PRE complexes (0.05 μM) were rapidly mixed with antibiotics (Hygromycin B, 20 μM ; Streptomycin, 20 μM ; Spectinomycin, 1 mM; Kanamycin, 100 μM ; Paromomycin, 5 μM ; Neomycin, 0.2 and 100 μM , and Viomycin, 200 μM). Subunit rotation upon EF-G-induced translocation – in the presence of antibiotic – was monitored after mixing PRE complexes (0.05 μM) with saturating concentration of EF-G (4 μM) and GTP (1 mM), where both complexes and EF-G were pre-incubated with the respective antibiotic (see above). The concentration dependencies of SSU body rotation and head swiveling were assessed upon mixing PRE complex (0.05 μM) with increasing concentrations of kanamycin (1, 3, 10, 30 and 100 μM).

4.19.7 Time-resolved Pmn assay

The functional activity of ribosome complexes was tested by the time-resolved Pmn assay (Holtkamp et al., 2014a). Briefly, fluorescence-labeled or non-labeled PRE(fMF) complexes (0.2 μM) were rapidly mixed with Pmn (10 mM), EF-G (4 μM), and GTP (1 mM) in the quench-flow apparatus. The reaction was quenched with 50% formic acid and samples were treated with 1.5 M sodium acetate saturated with MgSO_4 . f[^3H]Met[^{14}C]Phe-Pmn was extracted into ethyl acetate and quantified by double-label radioactivity counting.

To determine the rate of translocation for PRE(fMK) and PRE(fMV) complexes, PRE or POST complexes (0.2 μM) were mixed with Pmn (10 mM) and EF-G (4 μM) or Pmn (10 mM), respectively in TAKM₇ at 37°C, in smFRET buffer at 22°C, or in TAKM₇ at 25°C. The reaction was quenched with KOH (0.5 M) and the peptides were released by incubation for 45 min at 37°C, analyzed by reversed-phase HPLC (Chromolith®RP-8e), and quantified by double-label radioactivity counting (Wohlgemuth et al., 2008). The time required for the PRE complex to react ($1/k_{\text{PRE}}$) includes the time needed for translocation ($1/k_{\text{TL}}$) and for the Pmn reaction of the resulting POST state ($1/k_{\text{POST}}$). Deconvolution of the translocation rate from the two values ($k_{\text{TL}} = k_{\text{PRE}} \times k_{\text{POST}} / (k_{\text{PRE}} - k_{\text{POST}})$) gives the rate of tRNA translocation (Holtkamp et al., 2014).

4.19.8 Data analysis

Exponential fittings as well as hyperbolic and linear fitting of concentration dependence of k_{app} values were performed using GraphPad Prism. Global fitting was required to dissect the multiple processes combined in a single model and was performed by numerical integration analysis using KinTek Explorer (Johnson et al., 2009). Global fitting gives information about the values of the amplitude change, absolute value of the intrinsic fluorescence intensities of each reporter (IFIs) and rate constants of each step. For calculation of the spontaneous rate of subunit rotation, time courses of peptide bond formation by quench-flow and time courses of subunit rotation by

stopped-flow were evaluated collectively by numerical integration analysis using a 2-or 3-step model. Standard deviations (s.d.) were calculated from the fitting of three individual experiments while standard errors (s.e.m.) were calculated from fitting of the average derived from 7-10 time courses.

4.19.9 smFRET experiments

smFRET experiments were carried out in smFRET buffer (Adio et al., 2015) using double-labeled ribosomes (S6Cy5–L9Cy3). Initiation complexes were formed by incubating ribosomes (0.1 μ M) with a 1.7-fold excess of IF1, IF2 and IF3, a 3-fold excess of mRNA biotinylated at the 5' end, a 4-fold excess of fMet-tRNA^{fMet}, and GTP (1 mM) in TAKM₇ at 37°C for 30 min. Ternary complexes were prepared as described above with EF-Tu (1 μ M) and X-tRNA^X (X is Lys, Val, Phe) (0.5 μ M). Initiation complexes was mixed with a 5-fold excess of ternary complex and incubated for 1 min at room temperature to form PRE complexes. POST complexes were formed by incubating PRE complexes with EF-G (0.1 μ M) and GTP (1 mM). Imaging was performed using a TIRF imaging setup and the data was analysed using custom-made Matlab software (MathWorks) according to published protocols (Adio et al., 2015).

5. REFERENCES

- Adio, S., Senyushkina, T., Peske, F., Fischer, N., Wintermeyer, W., and Rodnina, M.V. (2015). Fluctuations between multiple EF-G-induced chimeric tRNA states during translocation on the ribosome. *Nat. Commun.* **6**, 7442.
- Agirrezabala, X., and Frank, J. (2010). From DNA to proteins via the ribosome: structural insights into the workings of the translation machinery. *Hum. Genomics* **4**, 226-237.
- Agirrezabala, X., Lei, J., Brunelle, J.L., Ortiz-Meoz, R.F., Green, R., and Frank, J. (2008). Visualization of the hybrid state of tRNA binding promoted by spontaneous ratcheting of the ribosome. *Mol. Cell* **32**, 190-197.
- Agrawal, R.K., Linde, J., Sengupta, J., Nierhaus, K.H., and Frank, J. (2001). Localization of L11 protein on the ribosome and elucidation of its involvement in EF-G-dependent translocation. *J. Mol. Biol.* **311**, 777-787.
- Agrawal, R.K., Penczek, P., Grassucci, R.A., and Frank, J. (1998). Visualization of elongation factor G on the Escherichia coli 70S ribosome: the mechanism of translocation. *Proc. Natl. Acad. Sci. USA* **95**, 6134-6138.
- Aitken, C.E., Petrov, A., and Puglisi, J.D. (2010). Single ribosome dynamics and the mechanism of translation. *Ann. Rev. of Biophys.* **39**, 491-513.
- Allen, G.S., Zavialov, A., Gursky, R., Ehrenberg, M., and Frank, J. (2005). The cryo-EM structure of a translation initiation complex from Escherichia coli. *Cell* **121**, 703-712.
- Ban, N., Nissen, P., Hansen, J., Moore, P.B., and Steitz, T.A. (2000). The complete atomic structure of the large ribosomal subunit at 2.4 Å resolution. *Science* **289**, 905-920.
- Belardinelli, R., Sharma, H., Caliskan, N., Cunha, C.E., Peske, F., Wintermeyer, W., and Rodnina, M.V. (2016). Choreography of molecular movements during ribosome progression along mRNA. *Nat. Struct. Mol. Biol.* **23**, 342-348.
- Beringer, M., Adio, S., Wintermeyer, W., and Rodnina, M. (2003). The G2447A mutation does not affect ionization of a ribosomal group taking part in peptide bond formation. *RNA* **9**, 919-922.
- Beringer, M., Bruell, C., Xiong, L., Pfister, P., Bieling, P., Katunin, V.I., Mankin, A.S., Bottger, E.C., and Rodnina, M.V. (2005). Essential mechanisms in the catalysis of peptide bond formation on the ribosome. *J. Biol. Chem.* **280**, 36065-36072.
- Bieling, P., Beringer, M., Adio, S., and Rodnina, M.V. (2006). Peptide bond formation does not involve acid-base catalysis by ribosomal residues. *Nat. Struct. Mol. Biol.* **13**, 423-428.
- Blanchard, S.C., Gonzalez, R.L., Kim, H.D., Chu, S., and Puglisi, J.D. (2004a). tRNA selection and kinetic proofreading in translation. *Nat. Struct. Mol. Biol.* **11**, 1008-1014.
- Blanchard, S.C., Kim, H.D., Gonzalez, R.L., Jr., Puglisi, J.D., and Chu, S. (2004b). tRNA dynamics on the ribosome during translation. *Proc. Natl. Acad. Sci. USA* **101**, 12893-12898.
- Bock, L.V., Blau, C., Schroder, G.F., Davydov, I., Fischer, N., Stark, H., Rodnina, M.V., Vaiana, A.C., and Grubmüller, H. (2013). Energy barriers and driving forces in tRNA translocation through the ribosome. *Nat. Struct. Mol. Biol.* **20**, 1390-1396.

- Bock, L.V., Blau, C., Vaiana, A.C., and Grubmuller, H. (2015). Dynamic contact network between ribosomal subunits enables rapid large-scale rotation during spontaneous translocation. *Nucleic Acids Res.* *43*, 6747-6760.
- Bodley, J.W., Zieve, F.J., Lin, L., and Zieve, S.T. (1969). Formation of the ribosome-G factor-GDP complex in the presence of fusidic acid. *Biophys Res. Commun.* *37*, 437-443.
- Borovinskaya, M.A., Pai, R.D., Zhang, W., Schuwirth, B.S., Holton, J.M., Hirokawa, G., Kaji, H., Kaji, A., and Cate, J.H. (2007a). Structural basis for aminoglycoside inhibition of bacterial ribosome recycling. *Nat. Struct. Mol. Biol.* *14*, 727-732.
- Borovinskaya, M.A., Shoji, S., Fredrick, K., and Cate, J.H. (2008). Structural basis for hygromycin B inhibition of protein biosynthesis. *RNA* *14*, 1590-1599.
- Borovinskaya, M.A., Shoji, S., Holton, J.M., Fredrick, K., and Cate, J.H. (2007b). A steric block in translation caused by the antibiotic spectinomycin. *ACS Chem. Biol.* *2*, 545-552.
- Bretscher, M.S. (1968). Translocation in protein synthesis: a hybrid structure model. *Nature* *218*, 675-677.
- Brilot, A.F., Korostelev, A.A., Ermolenko, D.N., and Grigorieff, N. (2013). Structure of the ribosome with elongation factor G trapped in the pretranslocation state. *Proc. Natl. Acad. Sci. USA* *110*, 20994-20999.
- Carter, A.P., Clemons, W.M., Brodersen, D.E., Morgan-Warren, R.J., Wimberly, B.T., and Ramakrishnan, V. (2000). Functional insights from the structure of the 30S ribosomal subunit and its interactions with antibiotics. *Nature* *407*, 340-348.
- Chen, C., Cui, X., Beausang, J.F., Zhang, H., Farrell, I., Cooperman, B.S., and Goldman, Y.E. (2016). Elongation factor G initiates translocation through a power stroke. *Proc. Natl. Acad. Sci. USA* *113*, 7515-7520.
- Chen, C., Stevens, B., Kaur, J., Cabral, D., Liu, H., Wang, Y., Zhang, H., Rosenblum, G., Smilansky, Z., Goldman, Y.E., *et al.* (2011). Single-molecule fluorescence measurements of ribosomal translocation dynamics. *Mol. Cell* *42*, 367-377.
- Chen, J., Petrov, A., Tsai, A., O'Leary, S.E., and Puglisi, J.D. (2013a). Coordinated conformational and compositional dynamics drive ribosome translocation. *Nat. Struct. Mol. Biol.* *20*, 718-727.
- Chen, Y., Feng, S., Kumar, V., Ero, R., and Gao, Y.G. (2013b). Structure of EF-G-ribosome complex in a pretranslocation state. *Nat. Struct. Mol. Biol.* *20*, 1077-1084.
- Cornish, P.V., Ermolenko, D.N., Noller, H.F., and Ha, T. (2008). Spontaneous intersubunit rotation in single ribosomes. *Mol. Cell* *30*, 578-588.
- Cornish, P.V., Ermolenko, D.N., Staple, D.W., Hoang, L., Hickerson, R.P., Noller, H.F., and Ha, T. (2009). Following movement of the L1 stalk between three functional states in single ribosomes. *Proc. Natl. Acad. Sci. USA* *106*, 2571-2576.
- Cox, G., Thompson, G.S., Jenkins, H.T., Peske, F., Savelsbergh, A., Rodnina, M.V., Wintermeyer, W., Homans, S.W., Edwards, T.A., and O'Neill, A.J. (2012). Ribosome clearance by FusB-type proteins mediates resistance to the antibiotic fusidic acid. *Proc. Natl. Acad. Sci. USA* *109*, 2102-2107.
- Cunha, C.E., Belardinelli, R., Peske, F., Holtkamp, W., Wintermeyer, W., and Rodnina, M.V. (2013). Dual use of GTP hydrolysis by elongation factor G on the ribosome. *Translation (Austin, Tex)* *1*, e24315.

- Davydov, I.I., Wohlgemuth, I., Artamonova, I.I., Urlaub, H., Tonevitsky, A.G., and Rodnina, M.V. (2013). Evolution of the protein stoichiometry in the L12 stalk of bacterial and organellar ribosomes. *Nat. Commun.* *4*, 1387.
- Demirci, H., Murphy, F.T., Murphy, E., Gregory, S.T., Dahlberg, A.E., and Jøgl, G. (2013). A structural basis for streptomycin-induced misreading of the genetic code. *Nat. Commun.* *4*, 1355.
- Diaconu, M., Kothe, U., Schlunzen, F., Fischer, N., Harms, J.M., Tonevitsky, A.G., Stark, H., Rodnina, M.V., and Wahl, M.C. (2005). Structural basis for the function of the ribosomal L7/12 stalk in factor binding and GTPase activation. *Cell* *121*, 991-1004.
- Dorner, S., Brunelle, J.L., Sharma, D., and Green, R. (2006). The hybrid state of tRNA binding is an authentic translation elongation intermediate. *Nat. Struct. Mol. Biol.* *13*, 234-241.
- Dunkle, J.A., and Cate, J.H. (2010). Ribosome structure and dynamics during translocation and termination. *Annu. Rev. Biophys.* *39*, 227-244.
- Dunkle, J.A., Wang, L., Feldman, M.B., Pulk, A., Chen, V.B., Kapral, G.J., Noeske, J., Richardson, J.S., Blanchard, S.C., and Cate, J.H. (2011). Structures of the bacterial ribosome in classical and hybrid states of tRNA binding. *Science* *332*, 981-984.
- Ermolenko, D.N., Majumdar, Z.K., Hickerson, R.P., Spiegel, P.C., Clegg, R.M., and Noller, H.F. (2007a). Observation of intersubunit movement of the ribosome in solution using FRET. *J. Mol. Biol.* *370*, 530-540.
- Ermolenko, D.N., and Noller, H.F. (2011). mRNA translocation occurs during the second step of ribosomal intersubunit rotation. *Nat. Struct. Mol. Biol.* *18*, 457-462.
- Ermolenko, D.N., Spiegel, P.C., Majumdar, Z.K., Hickerson, R.P., Clegg, R.M., and Noller, H.F. (2007b). The antibiotic viomycin traps the ribosome in an intermediate state of translocation. *Nat. Struct. Mol. Biol.* *14*, 493-497.
- Fei, J., Bronson, J.E., Hofman, J.M., Srinivas, R.L., Wiggins, C.H., and Gonzalez, R.L., Jr. (2009). Allosteric collaboration between elongation factor G and the ribosomal L1 stalk directs tRNA movements during translation. *Proc. Natl. Acad. Sci. USA* *106*, 15702-15707.
- Fei, J., Kosuri, P., MacDougall, D.D., and Gonzalez, R.L., Jr. (2008). Coupling of ribosomal L1 stalk and tRNA dynamics during translation elongation. *Mol. Cell* *30*, 348-359.
- Fei, J., Richard, A.C., Bronson, J.E., and Gonzalez, R.L., Jr. (2011). Transfer RNA-mediated regulation of ribosome dynamics during protein synthesis. *Nat. Struct. Mol. Biol.* *18*, 1043-1051.
- Feldman, M.B., Terry, D.S., Altman, R.B., and Blanchard, S.C. (2010). Aminoglycoside activity observed on single pre-translocation ribosome complexes. *Nat. Chem. Biol.* *6*, 244.
- Fischer, N., Konevega, A.L., Wintermeyer, W., Rodnina, M.V., and Stark, H. (2010). Ribosome dynamics and tRNA movement by time-resolved electron cryomicroscopy. *Nature* *466*, 329-333.
- Frank, J., and Agrawal, R.K. (2000). A ratchet-like inter-subunit reorganization of the ribosome during translocation. *Nature* *406*, 318-322.
- Fredrick, K., and Noller, H.F. (2003). Catalysis of ribosomal translocation by sparsomycin. *Science* *300*, 1159-1162.

- Fu, J., Munro, J.B., Blanchard, S.C., and Frank, J. (2011). Cryoelectron microscopy structures of the ribosome complex in intermediate states during tRNA translocation. *Proc. Natl. Acad. Sci. USA* *108*, 4817-4821.
- Gao, Y.G., Selmer, M., Dunham, C.M., Weixlbaumer, A., Kelley, A.C., and Ramakrishnan, V. (2009). The structure of the ribosome with elongation factor G trapped in the posttranslocational state. *Science* *326*, 694-699.
- Gavrilova, L.P., Kostiyashkina, O.E., Koteliansky, V.E., Rutkevitch, N.M., and Spirin, A.S. (1976). Factor-free ("non-enzymic") and factor-dependent systems of translation of polyuridylic acid by *Escherichia coli* ribosomes. *J. Mol. Biol.* *101*, 537-552.
- Gromadski, K.B., and Rodnina, M.V. (2004). Streptomycin interferes with conformational coupling between codon recognition and GTPase activation on the ribosome. *Nat. Struct. Mol. Biol.* *11*, 316-322.
- Guo, Z., Gibson, M., Sitha, S., Chu, S., and Mohanty, U. (2011). Role of large thermal fluctuations and magnesium ions in t-RNA selectivity of the ribosome. *Proc. Natl. Acad. Sci. USA* *108*, 3947-3951.
- Guo, Z., and Noller, H.F. (2012). Rotation of the head of the 30S ribosomal subunit during mRNA translocation. *Proc. Natl. Acad. Sci. USA* *109*, 20391-20394.
- Hansen, J.L., Moore, P.B., and Steitz, T.A. (2003). Structures of five antibiotics bound at the peptidyl transferase center of the large ribosomal subunit. *J. Mol. Biol.* *330*, 1061-1075.
- Harms, J., Schluenzen, F., Zarivach, R., Bashan, A., Gat, S., Agmon, I., Bartels, H., Franceschi, F., and Yonath, A. (2001). High resolution structure of the large ribosomal subunit from a mesophilic eubacterium. *Cell* *107*, 679-688.
- Hickerson, R., Majumdar, Z.K., Baucom, A., Clegg, R.M., and Noller, H.F. (2005). Measurement of internal movements within the 30 S ribosomal subunit using Forster resonance energy transfer. *J. Mol. Biol.* *354*, 459-472.
- Hiller, D.A., Singh, V., Zhong, M., and Strobel, S.A. (2011). A two-step chemical mechanism for ribosome-catalysed peptide bond formation. *Nature* *476*, 236-239.
- Holtkamp, W., Cunha, C.E., Peske, F., Konevega, A.L., Wintermeyer, W., and Rodnina, M.V. (2014a). GTP hydrolysis by EF-G synchronizes tRNA movement on small and large ribosomal subunits. *EMBO J.* *33*, 1073-1085.
- Holtkamp, W., Wintermeyer, W., and Rodnina, M.V. (2014b). Synchronous tRNA movements during translocation on the ribosome are orchestrated by elongation factor G and GTP hydrolysis. *Bioessays* *36*, 908-918.
- Horan, L.H., and Noller, H.F. (2007). Intersubunit movement is required for ribosomal translocation. *Proc. Natl. Acad. Sci. USA* *104*, 4881-4885.
- Johansen, S.K., Maus, C.E., Plikaytis, B.B., and Douthwaite, S. (2006). Capreomycin binds across the ribosomal subunit interface using tlyA-encoded 2'-O-methylations in 16S and 23S rRNAs. *Mol. Cell* *23*, 173-182.
- Johnson, K.A., Simpson, Z.B., and Blom, T. (2009). Global kinetic explorer: a new computer program for dynamic simulation and fitting of kinetic data. *Anal. Biochem.* *387*, 20-29.

- Julian, P., Konevega, A.L., Scheres, S.H., Lazaro, M., Gil, D., Wintermeyer, W., Rodnina, M.V., and Valle, M. (2008). Structure of ratcheted ribosomes with tRNAs in hybrid states. *Proc. Natl. Acad. Sci. USA* *105*, 16924-16927.
- Julian, P., Milon, P., Agirrezabala, X., Lasso, G., Gil, D., Rodnina, M.V., and Valle, M. (2011). The Cryo-EM structure of a complete 30S translation initiation complex from *Escherichia coli*. *PLoS Biol.* *9*, e1001095.
- Katunin, V.I., Savelsbergh, A., Rodnina, M.V., and Wintermeyer, W. (2002). Coupling of GTP hydrolysis by elongation factor G to translocation and factor recycling on the ribosome. *Biochemistry* *41*, 12806-12812.
- Kavran, J.M., and Steitz, T.A. (2007). Structure of the base of the L7/L12 stalk of the *Haloarcula marismortui* large ribosomal subunit: analysis of L11 movements. *J. Mol. Biol.* *371*, 1047-1059.
- Kim, H.D., Puglisi, J.D., and Chu, S. (2007). Fluctuations of transfer RNAs between classical and hybrid states. *Biophys. J.* *93*, 3575-3582.
- Konevega, A.L., Fischer, N., Semenov, Y.P., Stark, H., Wintermeyer, W., and Rodnina, M.V. (2007). Spontaneous reverse movement of mRNA-bound tRNA through the ribosome. *Nat. Struct. Mol. Biol.* *14*, 318-324.
- Konevega, A.L., Soboleva, N.G., Makhno, V.I., Semenov, Y.P., Wintermeyer, W., Rodnina, M.V., and Katunin, V.I. (2004). Purine bases at position 37 of tRNA stabilize codon-anticodon interaction in the ribosomal A site by stacking and Mg²⁺-dependent interactions. *RNA* *10*, 90-101.
- Korobeinikova, A.V., Garber, M.B., and Gongadze, G.M. (2012). Ribosomal proteins: structure, function, and evolution. *Biochemistry* *77*, 562-574.
- Kothe, U., Wieden, H.J., Mohr, D., and Rodnina, M.V. (2004). Interaction of helix D of elongation factor Tu with helices 4 and 5 of protein L7/12 on the ribosome. *J. Mol. Biol.* *336*, 1011-1021.
- Kuhlenkoetter, S., Wintermeyer, W., and Rodnina, M.V. (2011). Different substrate-dependent transition states in the active site of the ribosome. *Nature* *476*, 351-354.
- Li, W., Liu, Z., Koripella, R.K., Langlois, R., Sanyal, S., and Frank, J. (2015). Activation of GTP hydrolysis in mRNA-tRNA translocation by elongation factor G. *Sci. Adv.* *1*.
- Lin, J., Gagnon, M.G., Bulkley, D., and Steitz, T.A. (2015). Conformational changes of elongation factor G on the ribosome during tRNA translocation. *Cell* *160*, 219-227.
- Llano-Sotelo, B., Azucena, E.F., Jr., Kotra, L.P., Mobashery, S., and Chow, C.S. (2002). Aminoglycosides modified by resistance enzymes display diminished binding to the bacterial ribosomal aminoacyl-tRNA site. *Chem. Biol.* *9*, 455-463.
- Majumdar, Z.K., Hickerson, R., Noller, H.F., and Clegg, R.M. (2005). Measurements of internal distance changes of the 30S ribosome using FRET with multiple donor-acceptor pairs: quantitative spectroscopic methods. *J. Mol. Biol.* *351*, 1123-1145.
- Maracci, C., Wohlgemuth, I., and Rodnina, M.V. (2015). Activities of the peptidyl transferase center of ribosomes lacking protein L27. *RNA* *21*, 2047-2052.
- Marshall, R.A., Aitken, C.E., and Puglisi, J.D. (2009). GTP hydrolysis by IF2 guides progression of the ribosome into elongation. *Mol. Cell* *35*, 37-47.

- Marshall, R.A., Dorywalska, M., and Puglisi, J.D. (2008). Irreversible chemical steps control intersubunit dynamics during translation. *Proc. Natl. Acad. Sci. USA* *105*, 15364-15369.
- Moazed, D., and Noller, H.F. (1989). Intermediate states in the movement of transfer RNA in the ribosome. *Nature* *342*, 142-148.
- Modolell, J., and Vazquez (1977). The inhibition of ribosomal translocation by viomycin. *Eur. J. Biochem.* *81*, 491-497.
- Mohr, D., Wintermeyer, W., and Rodnina, M.V. (2002). GTPase activation of elongation factors Tu and G on the ribosome. *Biochemistry* *41*, 12520-12528.
- Munro, J.B., Altman, R.B., O'Connor, N., and Blanchard, S.C. (2007). Identification of two distinct hybrid state intermediates on the ribosome. *Mol. Cell* *25*, 505-517.
- Munro, J.B., Altman, R.B., Tung, C.S., Cate, J.H., Sanbonmatsu, K.Y., and Blanchard, S.C. (2010a). Spontaneous formation of the unlocked state of the ribosome is a multistep process. *Proc. Natl. Acad. Sci. USA* *107*, 709-714.
- Munro, J.B., Altman, R.B., Tung, C.S., Sanbonmatsu, K.Y., and Blanchard, S.C. (2010b). A fast dynamic mode of the EF-G-bound ribosome. *EMBO J.* *29*, 770-781.
- Munro, J.B., Sanbonmatsu, K.Y., Spahn, C.M., and Blanchard, S.C. (2009). Navigating the ribosome's metastable energy landscape. *Trends Biochem. Sci.* *34*, 390-400.
- Naganuma, T., Nomura, N., Yao, M., Mochizuki, M., Uchiyama, T., and Tanaka, I. (2010). Structural basis for translation factor recruitment to the eukaryotic/archaeal ribosomes. *J. Biol. Chem.* *285*, 4747-4756.
- Nissen, P., Hansen, J., Ban, N., Moore, P.B., and Steitz, T.A. (2000). The structural basis for ribosome activity in peptide bond synthesis. *Science* *289*, 920-930.
- Nissen, P., Kjeldgaard, M., Thirup, S., Polekhina, G., Reshetnikova, L., Clark, B.F., and Nyborg, J. (1995). Crystal structure of the ternary complex of Phe-tRNA^{Phe}, EF-Tu, and a GTP analog. *Science* *270*, 1464-1472.
- Noller, H.F., Hoffarth, V., and Zimniak, L. (1992). Unusual resistance of peptidyl transferase to protein extraction procedures. *Science* *256*, 1416-1419.
- Ogle, J.M., Brodersen, D.E., Clemons, W.M., Jr., Tarry, M.J., Carter, A.P., and Ramakrishnan, V. (2001). Recognition of cognate transfer RNA by the 30S ribosomal subunit. *Science* *292*, 897-902.
- Ogle, J.M., Murphy, F.V., Tarry, M.J., and Ramakrishnan, V. (2002). Selection of tRNA by the ribosome requires a transition from an open to a closed form. *Cell* *111*, 721-732.
- Pan, D., Kirillov, S.V., and Cooperman, B.S. (2007). Kinetically competent intermediates in the translocation step of protein synthesis. *Mol. Cell* *25*, 519-529.
- Pape, T., Wintermeyer, W., and Rodnina, M. (1999). Induced fit in initial selection and proofreading of aminoacyl-tRNA on the ribosome. *EMBO J.* *18*, 3800-3807.
- Pape, T., Wintermeyer, W., and Rodnina, M.V. (2000). Conformational switch in the decoding region of 16S rRNA during aminoacyl-tRNA selection on the ribosome. *Nat. Struct. Biol.* *7*, 104-107.

- Peske, F., Matassova, N.B., Savelsbergh, A., Rodnina, M.V., and Wintermeyer, W. (2000). Conformationally restricted elongation factor G retains GTPase activity but is inactive in translocation on the ribosome. *Mol. Cell* *6*, 501-505.
- Peske, F., Rodnina, M.V., and Wintermeyer, W. (2005). Sequence of steps in ribosome recycling as defined by kinetic analysis. *Mol. Cell* *18*, 403-412.
- Peske, F., Savelsbergh, A., Katunin, V.I., Rodnina, M.V., and Wintermeyer, W. (2004). Conformational changes of the small ribosomal subunit during elongation factor G-dependent tRNA-mRNA translocation. *J. Mol. Biol.* *343*, 1183-1194.
- Pulk, A., and Cate, J.H. (2013). Control of ribosomal subunit rotation by elongation factor G. *Science* *340*, 1235970.
- Qin, P., Yu, D., Zuo, X., and Cornish, P.V. (2014). Structured mRNA induces the ribosome into a hyper-rotated state. *EMBO Rep.* *15*, 185-190.
- Ramakrishnan, V. (2014). The ribosome emerges from a black box. *Cell* *159*, 979-984.
- Ramrath, D.J., Lancaster, L., Sprink, T., Mielke, T., Loerke, J., Noller, H.F., and Spahn, C.M. (2013). Visualization of two transfer RNAs trapped in transit during elongation factor G-mediated translocation. *Proc. Natl. Acad. Sci. USA* *110*, 20964-20969.
- Ratje, A.H., Loerke, J., Mikolajka, A., Brunner, M., Hildebrand, P.W., Starosta, A.L., Donhofer, A., Connell, S.R., Fucini, P., Mielke, T., *et al.* (2010). Head swivel on the ribosome facilitates translocation by means of intra-subunit tRNA hybrid sites. *Nature* *468*, 713-716.
- Richter, D. (1976). Stringent factor from *Escherichia coli* directs ribosomal binding and release of uncharged tRNA. *Proc. Natl. Acad. Sci. USA* *73*, 707-711.
- Robertson, J.M., Paulsen, H., and Wintermeyer, W. (1986). Pre-steady-state kinetics of ribosomal translocation. *J. Mol. Biol.* *192*, 351-360.
- Rodnina, M.V., Savelsbergh, A., Katunin, V.I., and Wintermeyer, W. (1997). Hydrolysis of GTP by elongation factor G drives tRNA movement on the ribosome. *Nature* *385*, 37-41.
- Rodnina, M.V., and Wintermeyer, W. (1995). GTP consumption of elongation factor Tu during translation of heteropolymeric mRNAs. *Proc. Natl. Acad. Sci. USA* *92*, 1945-1949.
- Rodnina, M.V., and Wintermeyer, W. (1998). Form follows function: structure of an elongation factor G-ribosome complex. *Proc. Natl. Acad. Sci. USA* *95*, 7237-7239.
- Rodnina, M.V., and Wintermeyer, W. (2001). Fidelity of aminoacyl-tRNA selection on the ribosome: kinetic and structural mechanisms. *Annu. Rev. Biochem.* *70*, 415-435.
- Rodnina, M.V., and Wintermeyer, W. (2010). The ribosome goes Nobel. *Trends Biochem. Sci.* *35*, 1-5.
- Rodnina, M.V., and Wintermeyer, W. (2011). The ribosome as a molecular machine: the mechanism of tRNA-mRNA movement in translocation. *Biochem. Soc. Trans.* *39*, 658-662.
- Salsi, E., Farah, E., Netter, Z., Dann, J., and Ermolenko, D.N. (2015). Movement of elongation factor G between compact and extended conformations. *J. Mol. Biol.* *427*, 454-467.
- Satterthwait, A.C., and Jencks, W.P. (1974). The mechanism of the aminolysis of acetate esters. *J. Am. Chem. Soc.* *96*, 7018-7031.

- Savelsbergh, A., Katunin, V.I., Mohr, D., Peske, F., Rodnina, M.V., and Wintermeyer, W. (2003). An elongation factor G-induced ribosome rearrangement precedes tRNA-mRNA translocation. *Mol. Cell* *11*, 1517-1523.
- Savelsbergh, A., Rodnina, M.V., and Wintermeyer, W. (2009). Distinct functions of elongation factor G in ribosome recycling and translocation. *RNA* *15*, 772-780.
- Schlutzen, F., Tocilj, A., Zarivach, R., Harms, J., Gluehmann, M., Janell, D., Bashan, A., Bartels, H., Agmon, I., Franceschi, F., *et al.* (2000). Structure of functionally activated small ribosomal subunit at 3.3 angstroms resolution. *Cell* *102*, 615-623.
- Schmeing, T.M., and Ramakrishnan, V. (2009). What recent ribosome structures have revealed about the mechanism of translation. *Nature* *461*, 1234-1242.
- Schuetz, J.C., Murphy, F.V.t., Kelley, A.C., Weir, J.R., Giesebrecht, J., Connell, S.R., Loerke, J., Mielke, T., Zhang, W., Penczek, P.A., *et al.* (2009). GTPase activation of elongation factor EF-Tu by the ribosome during decoding. *EMBO J.* *28*, 755-765.
- Schuwirth, B.S., Borovinskaya, M.A., Hau, C.W., Zhang, W., Vila-Sanjurjo, A., Holton, J.M., and Cate, J.H. (2005). Structures of the bacterial ribosome at 3.5 Å resolution. *Science* *310*, 827-834.
- Semenkov, Y.P., Rodnina, M.V., and Wintermeyer, W. (2000). Energetic contribution of tRNA hybrid state formation to translocation catalysis on the ribosome. *Nat. Struct. Biol.* *7*, 1027-1031.
- Sharma, D., Southworth, D.R., and Green, R. (2004). EF-G-independent reactivity of a pre-translocation-state ribosome complex with the aminoacyl tRNA substrate puromycin supports an intermediate (hybrid) state of tRNA binding. *RNA* *10*, 102-113.
- Sharma, H., Adio, S., Senyushkina, T., Belardinelli, R., Peske, F., and Rodnina, M.V. (2016). Kinetics of Spontaneous and EF-G-Accelerated Rotation of Ribosomal Subunits. *Cell Rep.* *16*, 2187-2196.
- Shoji, S., Walker, S.E., and Fredrick, K. (2006). Reverse translocation of tRNA in the ribosome. *Mol. Cell* *24*, 931-942.
- Shoji, S., Walker, S.E., and Fredrick, K. (2009). Ribosomal translocation: one step closer to the molecular mechanism. *ACS Chem. Biol.* *4*, 93-107.
- Sievers, A., Beringer, M., Rodnina, M.V., and Wolfenden, R. (2004). The ribosome as an entropy trap. *Proc. Natl. Acad. Sci. USA* *101*, 7897-7901.
- Spiegel, P.C., Ermolenko, D.N., and Noller, H.F. (2007). Elongation factor G stabilizes the hybrid-state conformation of the 70S ribosome. *RNA* *13*, 1473-1482.
- Spirin, A.S. (1968). [On the mechanism of ribosome function. The hypothesis of locking-unlocking of subparticles]. *Dokl. Akad. Nauk SSSR* *179*, 1467-1470.
- Stanley, R.E., Blaha, G., Grodzicki, R.L., Strickler, M.D., and Steitz, T.A. (2010). The structures of the anti-tuberculosis antibiotics viomycin and capreomycin bound to the 70S ribosome. *Nat. Struct. Mol. Biol.* *17*, 289-293.
- Steitz, T.A. (2008). A structural understanding of the dynamic ribosome machine. *Nat. Rev. Mol. Cell Biol.* *9*, 242-253.
- Takyar, S., Hickerson, R.P., and Noller, H.F. (2005). mRNA helicase activity of the ribosome. *Cell* *120*, 49-58.

- Tanaka, N., Kinoshita, T., and Masukawa, H. (1968). Mechanism of protein synthesis inhibition by fusidic acid and related antibiotics. *Biochem. Biophys. Res. Commun.* *30*, 278-283.
- Tourigny, D.S., Fernandez, I.S., Kelley, A.C., and Ramakrishnan, V. (2013). Elongation factor G bound to the ribosome in an intermediate state of translocation. *Science* *340*, 1235-1240.
- Tsai, A., Uemura, S., Johansson, M., Puglisi, E.V., Marshall, R.A., Aitken, C.E., Korch, J., Ehrenberg, M., and Puglisi, J.D. (2013). The impact of aminoglycosides on the dynamics of translation elongation. *Cell Rep.* *3*, 497-508.
- Valle, M., Zavialov, A., Sengupta, J., Rawat, U., Ehrenberg, M., and Frank, J. (2003). Locking and unlocking of ribosomal motions. *Cell* *114*, 123-134.
- Villa, E., Sengupta, J., Trabuco, L.G., LeBarron, J., Baxter, W.T., Shaikh, T.R., Grassucci, R.A., Nissen, P., Ehrenberg, M., Schulten, K., *et al.* (2009). Ribosome-induced changes in elongation factor Tu conformation control GTP hydrolysis. *Proc. Natl. Acad. Sci. USA* *106*, 1063-1068.
- Voorhees, R.M., and Ramakrishnan, V. (2013). Structural basis of the translational elongation cycle. *Annu. Rev. Biochem.* *82*, 203-236.
- Walker, S.E., Shoji, S., Pan, D., Cooperman, B.S., and Fredrick, K. (2008). Role of hybrid tRNA-binding states in ribosomal translocation. *Proc. Natl. Acad. Sci. USA* *105*, 9192-9197.
- Wang, L., Pulk, A., Wasserman, M.R., Feldman, M.B., Altman, R.B., Cate, J.H., and Blanchard, S.C. (2012). Allosteric control of the ribosome by small-molecule antibiotics. *Nat. Struct. Mol. Biol.* *19*, 957-963.
- Wang, W., and Malcolm, B.A. (2002). Two-stage polymerase chain reaction protocol allowing introduction of multiple mutations, deletions, and insertions, using QuikChange site-directed mutagenesis. *Methods Mol. Biol.* *182*, 37-43.
- Wasserman, M.R., Alejo, J.L., Altman, R.B., and Blanchard, S.C. (2016). Multiperspective smFRET reveals rate-determining late intermediates of ribosomal translocation. *Nat. Struct. Mol. Biol.* *23*, 333-341.
- Wasserman, M.R., Pulk, A., Zhou, Z., Altman, R.B., Zinder, J.C., Green, K.D., Garneau-Tsodikova, S., Cate, J.H., and Blanchard, S.C. (2015). Chemically related 4,5-linked aminoglycoside antibiotics drive subunit rotation in opposite directions. *Nat. Commun.* *6*, 7896.
- Wimberly, B.T., Brodersen, D.E., Clemons, W.M., Jr., Morgan-Warren, R.J., Carter, A.P., Vornrhein, C., Hartsch, T., and Ramakrishnan, V. (2000). Structure of the 30S ribosomal subunit. *Nature* *407*, 327-339.
- Wimberly, B.T., Guymon, R., McCutcheon, J.P., White, S.W., and Ramakrishnan, V. (1999). A detailed view of a ribosomal active site: the structure of the L11-RNA complex. *Cell* *97*, 491-502.
- Wittinghofer, A., and Vetter, I.R. (2011). Structure-function relationships of the G domain, a canonical switch motif. *Annu. Rev. Biochem.* *80*, 943-971.
- Wohlgemuth, I., Brenner, S., Beringer, M., and Rodnina, M.V. (2008). Modulation of the rate of peptidyl transfer on the ribosome by the nature of substrates. *J. Biol. Chem.* *283*, 32229-32235.
- Wohlgemuth, I., Pohl, C., Mittelstaet, J., Konevega, A.L., and Rodnina, M.V. (2011). Evolutionary optimization of speed and accuracy of decoding on the ribosome. *Philos. Trans. R. Soc. Lond. B Biol. Sci.* *366*, 2979-2986.

REFERENCES

- Yamamoto, N., Nakahigashi, K., Nakamichi, T., Yoshino, M., Takai, Y., Touda, Y., Furubayashi, A., Kinjyo, S., Dose, H., Hasegawa, M., *et al.* (2009). Update on the Keio collection of *Escherichia coli* single-gene deletion mutants. *Mol. Syst. Biol.* *5*, 335.
- Youngman, E.M., Brunelle, J.L., Kochaniak, A.B., and Green, R. (2004). The active site of the ribosome is composed of two layers of conserved nucleotides with distinct roles in peptide bond formation and peptide release. *Cell* *117*, 589-599.
- Yusupov, M.M., Yusupova, G.Z., Baucom, A., Lieberman, K., Earnest, T.N., Cate, J.H., and Noller, H.F. (2001). Crystal structure of the ribosome at 5.5 Å resolution. *Science* *292*, 883-896.
- Zhang, W., Dunkle, J.A., and Cate, J.H. (2009). Structures of the ribosome in intermediate states of ratcheting. *Science* *325*, 1014-1017.
- Zhou, J., Lancaster, L., Donohue, J.P., and Noller, H.F. (2013). Crystal structures of EF-G-ribosome complexes trapped in intermediate states of translocation. *Science* *340*, 1236086.
- Zhou, J., Lancaster, L., Donohue, J.P., and Noller, H.F. (2014). How the ribosome hands the A-site tRNA to the P site during EF-G-catalyzed translocation. *Science* *345*, 1188-1191.
- Zhou, J., Lancaster, L., Trakhanov, S., and Noller, H.F. (2012). Crystal structure of release factor RF3 trapped in the GTP state on a rotated conformation of the ribosome. *RNA* *18*, 230-240.

6. APPENDIX

6.1 Abbreviations

μM	Micromolar
A_{260}	Absorbance at 260 nm
aa-tRNA	Aminoacyl-tRNA
Alx488	Alexa 488
Alx568	Alexa 568
ASL	Anticodon stem loop
bL9	Bacterial protein L9
bp	Base pair
bS6	Bacterial protein S6
C	Classical
CCW	Counterclockwise
Cryo-Em	Cryo-Electron microscopy
CW	Clockwise
DC	Decoding center
DNA	Deoxyribonucleic acid
EF	Elongation factors (EFs),
EF-G	Elongation factor G
EF-Tu	Elongation factor Tu
FRET	Förster resonance energy transfer
g	Relative centrifugal force
g/l	Grams per liter
gm	Gram
GTP	Guanosine triphosphate
H	Hybrid
h	Hour
h34	Helix 34 of the 16S rRNA
h44	Helix 44 of the 16S rRNA
H69	Helix 69 of the 23 rRNA
IF	Initiation factors
IF1	Intrinsic fluorescence intensities

k_{app}	Apparent rate constant
k_d	Dissociation constant
kDa	Kilodalton
k_{off}	Dissociation rate constant
k_{on}	Association rate constant
L	Liters
LSU	Large subunit
MDa	Megadalton
min	Minutes
ml	Milliliters
mM	Millimolar
mRNA	Messenger RNA
N	Non-rotated
n	Number of experiments
n.d.	Not defined
nm	Nanometer
Nt	Number of technical replicates
OD ₆₀₀	Absorbance at 600 nm
PDB	Protein Data Bank
Pmn	Puromycin
pmol	Picomol
POST	Posttranslocation complex
PRE	Pretranslocation complex
PTC	Peptidyl transferase center
R	Rotated
RF	Release factors
RNA	Ribonucleic acid
rpm	Rotation per minute
RRF	Ribosome recycling factor
rRNA	Ribosomal RNA
RT	Room temperature
S	Svedberg unit
s	Seconds
s.d	Standard deviation
s.e.m	Standard error mean

sm	Single molecule
SRL	Sarcin-ricin loop
SSU	Small subunit
TC	Ternary complex
tRNA	Transfer RNA
WT	Wild type

6.2 List of Figures

Figure 1.1 The prokaryotic ribosome.....	4
Figure 1.2 Overview of the elongation cycle.....	8
Figure 1.3 Movements of the SSU of the ribosome.....	11
Figure 1.4 Motions in the ribosome during translocation.	14
Figure 1.5 Different conformations of EF-G.	17
Figure 1.6 Schematic depicting subunit rotation during translocation.	19
Figure 2.1 Position of the fluorescence reporters on ribosomal subunits used for FRET measurements.....	26
Figure 2.2 Time-resolved Pmn assay for S6–L9 double-labeled ribosomes.....	27
Figure 2.3 Subunit rotation monitored with S6–L9 FRET pair.....	28
Figure 2.4 Controls for subunit rotation monitored with S6–L9 FRET pair.....	29
Figure 2.5 Peptide bond formation and spontaneous CCW subunit rotation with different P-site tRNAs.	32
Figure 2.6 Temperature dependence of spontaneous CCW subunit rotation.....	34
Figure 2.7 Spontaneous CCW subunit rotation with different tRNAs in the A site.	35
Figure 2.8 Population distribution of N and R state measured by smFRET.	37
Figure 2.9 Spontaneous transition of CCW and CW subunit rotation observed by smFRET.	38
Figure 2.10 EF-G induced subunit rotation at 37°C.	41
Figure 2.11 CW subunit rotation coupled to translocation.....	42
Figure 2.12 Inhibition of translocation and CW subunit rotation.....	44
Figure 2.13 EF-G-induced subunit rotation at 25°C.	44
Figure 2.14 Rapid kinetics of subunit rotation monitored under smFRET conditions.....	45
Figure 2.15 Time resolved Pmn assay to determine the rate of translocation.	46
Figure 2.16 Global fitting of translocation kinetics with EF-G and GTP (traces for the S6–L9 FRET pair are shown).....	49
Figure 2.17 Fluorescence signatures composed of IFI values for 5-step kinetic model.	50
Figure 2.18 Effect of GTP hydrolysis on translocation.	51
Figure 2.19 Subunit rotation monitored with variants of EF-G.....	52
Figure 2.20 Effect of Mg ²⁺ ion and polyamine concentrations on the kinetics of subunit rotation.	55
Figure 2.21 Coupled inhibition of body and head movements of the SSU.	58
Figure 2.22 Decoupling of body rotation and head swiveling of the SSU.....	60
Figure 2.23 Effect of neomycin on subunit rotation in the absence of EF-G.	61

Figure 2.24 Effect of antibiotics on the rotational states of the ribosome.	62
Figure 2.25 Kinetics of kanamycin-induced body rotation and head swiveling.	63
Figure 3.1 Model for subunit rotation coupled to the translocation pathway.	65
Figure 3.2 Kinetic model of translocation pathway.	70
Figure 4.1 Verification of the S6 and L9 knockouts by PCR.	88
Figure 4.2 Verification of S6 and L9 knockouts by western blot analysis and mass spectrometry. .	89

6.3 List of Tables

Table 2.1 Rates of spontaneous N-to-R and R-to-N transitions determined by smFRET and ensemble kinetics	38
Table 2.2 Summary of rates for EF-G-induced rotation and translocation.	47
Table 2.3 Positions of the fluorescence reporters used for kinetic studies of translocation.....	48
Table 2.4 Apparent rate constants of SSU body rotation and head swiveling in the presence of EF-G and different antibiotics.....	64
Table 4.1 Fluorescence dyes and their properties.....	92

ACKNOWLEDGMENTS

I would like to express my deep gratitude to my supervisor Prof. Dr. Marina V. Rodnina for giving me an opportunity to be a part of the fascinating field of translation. Thank you Marina, for your constant support, guidance and for keeping me focused. You are a role model for many of us. I also thank Prof. Dr. Wolfgang Wintermeyer for his timely advices and ideas.

I would like to thank my committee members Prof. Dr. Kai Tittmann and Prof. Dr. Holger Stark for their time and useful suggestions in the committee meetings and Prof. Dr. Wolfgang Wintermeyer, Prof. Dr. Patrick Cramer and Prof. Dr. Ralf Ficner for being a part of the extended thesis committee.

A special thanks goes to Frank for being a supercool supervisor who believed in me and supported me throughout my doctoral studies starting from my first lab rotation. I learnt a lot from him and our stimulating discussions helped in timely completion of the project. I am also grateful to Riccardo, who spent hours troubleshooting with me and not to mention, for hand grinding 100 grams of cells in cold room for my ribosome preparations. I thank Dr. Sarah Adio and Dr. Tamara Senyushkina for performing single-molecule FRET experiments and analysis, respectively that resulted in a fruitful collaboration and added to the impact of the project. I also thank Dr. Ingo Wohlgemuth for mass spectrometry experiments and his valuable advices. I am grateful to Boehringer Ingelheim Fonds and Max Planck Society for funding my project.

Of course, work would not have been nearly as enjoyable were it not for my wonderful colleagues and friends. I am thankful for the joy, laughter and great conversations and time I had with Michael, Aki, Neva, Betty, Irena, Raffa, Ole, Natalia, Michi, Cristina and Albena. I especially thank Michael for all help and support both professionally and personally. He is my live google translator and a very good friend. I thank Carlos for his support during the first year of my PhD and for very patiently answering all my non-stop questions. Aki and Neva are wonderful friends with whom I share a special bond. With my Indian company Namit, Nupur, Amitabh and Prajwal (almost Indian); I enjoyed Indian food, and conversations on broad topics. I also thank my lab members, especially the technical staff for their timely help and support. Working with them was a great pleasure and made everything smooth and easy. Special thanks also go to Dimitra, our secretary who helped me with the administrative work and made the process a lot more simple and comfortable.

I feel lucky to be a part of the IMPRS Molecular Biology program and take immense pleasure to thank our excellent coordinators Dr. Steffen Burkhardt and Kerstin Grüniger who made everything effortless in a different country from day one and also many thanks to fellow

MolBios who were highly enthusiastic and fun-loving and with whom I started my journey of doctoral studies.

Life in Göttingen became possible because of amazing friends I made outside my working place; with whom I shared some of the most important years of my life. Veena and Vinita, you are more than a friend to me. You stood by me all the time in my ups and downs, in my happiness and grief. Thank you for loving, caring, helping and supporting me all the time. Pawan, thank you very much for all the care you have given to me. It meant a lot. You are a wonderful friend. Sumir, you are the nicest person on earth. Because of your care and affection, everyone loves you. Ankit, I thank you for helping me with all German translations and for cooking nice different meals and also for playing guitar for us. You are a fun company. Avani, you are my moral support and partner who hates cooking and in some other opinions as well. Upasana, your time in Göttingen did not overlap so much with mine but still I found a very good friend in you. Thank you for making me comfortable during my initial days in Göttingen. Soham, my cutie pie, it is so much fun to listen to you whether you are discussing something serious or funny, whether you are angry or blushing. I always find it funny and can't stop laughing. Priyanka, thank you for your timely advices, they were very helpful. Anusha, you are a late entry to the group but still you have become a very good friend. I thank you for all your help in past and in future. Mayur, I also thank you for helping, guiding me during initial years in Göttingen and welcoming me in your group.

Now, comes my family. The most important person I met in Göttingen is my very soon to be husband, Kundan. You are my stress buster and staying with you makes me happy. Thank you for loving and supporting me in difficult times. I feel lucky to have you in my life. I also thank Mumma and Papa for their love, support and understanding. I thank all my cousins and relatives who directly or indirectly helped and assisted us in various facets of life. Chachi, I miss you.

My lifeline – my brother Aditya, Bhai, you have always been my strength and support. I am so carefree in your presence. Your advices in every aspect of my life have helped me to take decisions and because of your support I am here today, completing my Ph.D. in Germany. Mummy and Papa I know sending me to Germany was the most difficult decision in your life. I am aware that you had many sleepless nights and it continues even today. As I achieve the highest degree in education, I am sure it makes you feel proud and hopefully worth, at least to some extent, of staying away from you. My Ph.D. is dedicated to you and I love you more than anything in this world.

CURRICULUM VITAE

Heena Sharma

Max Planck Institute for Biophysical Chemistry

Am Fassberg 11

Göttingen 37077, Germany

Tel: +4917661340773

heena.sharma@mpibpc.mpg.de

Education

- | | |
|------|--|
| 2016 | Doctoral studies in Max Planck Institute for Biophysical Chemistry, Göttingen, Germany.
Supervisor: Prof. Marina V. Rodnina |
| 2012 | Masters studies in International Max Planck research School for Molecular Biology (IMPRS), Göttingen, Germany
<i>Grade of Master's examination: 1.25 =A (excellent)</i> |
| 2011 | Masters in Biochemistry, Department of Biochemistry, University of Delhi, India
<i>Grade of Master's examination: First division (highest grade)</i> |
| 2009 | Bachelors in Biochemistry, Department of Biochemistry, University of Delhi, India
<i>Grade of Bachelor's examination: First division (highest grade)</i> |

Publications

- **Sharma, H.**, Adio, S., Senyushkina, T., Belardinelli, R., Peske, F., and Rodnina, M.V. (2016). Kinetics of Spontaneous and EF-G-Accelerated Rotation of Ribosomal Subunits. *Cell Rep.* **16**, 2187-2196.
- Belardinelli, R., **Sharma, H.**, Caliskan, N., Cunha, C.E., Peske, F., Wintermeyer, W., and Rodnina, M.V. (2016). Choreography of molecular movements during ribosome progression along mRNA. *Nat. Struct. Mol. Biol.* **23**, 342-348.
- Belardinelli, R., **Sharma, H.**, Peske, F., Wintermeyer, W., and Rodnina, M.V. (2016). Translocation as continuous movement through the ribosome. *RNA Biol.*, **13**, 1197-1203.

Scholarships and awards

- | | |
|------|---|
| 2013 | Boehringer Ingelheim PhD fellowship |
| 2013 | GGNB Excellence Stipend |
| 2011 | Stipend of the Excellence Foundation for the Promotion of the Max Planck Society |
| 2011 | Gold Medal for 1 st rank in MSc. Biochemistry, University of Delhi, India. |

CURRICULUM VITAE

2011	Qualified Graduate Aptitude Test in Engineering (99 Percentile)
2010	Qualified the National Eligibility Test for CSIR – Junior Research Fellowship with rank 68 (all India rank)
2008	Monsanto Scholarship in MSc. for 2 years (given to the students with the highest grades in Masters)

Personal details

Date of Birth	20 th May, 1988
Place of Birth	New Delhi
Nationality	Indian